NTIA Report TR-05-429

Interference Potential of Ultrawideband Signals

Part 2: Measurement of Gated-Noise Interference to C-band Satellite Digital Television Receivers

Michael Cotton
Robert Achatz
Jeffery Wepman
Paul Runkle

report series

U.S. DEPARTMENT OF COMMERCE • National Telecommunications and Information Administration

NTIA Report TR-05-429

Interference Potential of Ultrawideband Signals

Part 2: Measurement of Gated-Noise Interference to C-Band Satellite Digital Television Receivers

Michael Cotton
Robert Achatz
Jeffery Wepman
Paul Runkle

U.S. DEPARTMENT OF COMMERCE
Carlos M. Gutierrez, Secretary

Michael D. Gallagher, Assistant Secretary
for Communications and Information

August 2005

DISCLAIMER

Certain commercial equipment, software, and materials are identified in this report to specify the technical aspects of the reported results. In no case does such identification imply recommendation or endorsement by the National Telecommunications and Information Administration, nor does it imply that the material or equipment identified is necessarily the best available for the purpose.

CONTENTS

Page

1. INTRODUCTION 1
1.1. Experiment 2
1.2. Organization of Report 3

2. DTV SUSCEPTIBILITY TO GN INTERFERENCE 4
2.1. Gating Parameters 4
2.2. Signal Powers and DTV Signal Quality Metrics 4
2.3. DTV Signal Quality as a Function of Interference Average Power 5
2.4. DTV Susceptibility and FEC Performance as a Function of Interference Fractional On-Time 10

3. CHARACTERIZATION OF GN SIGNALS 16
3.1. Temporal Analysis 16
3.2. Amplitude Analysis 18
3.3. Spectral Analysis 22

4. CONCLUSION 25

5. ACKNOWLEDGMENTS 28

6. REFERENCES 29

APPENDIX A: EXTENSION OF EXPERIMENT TO GN(MB) SIGNALS 31
A.1. DTV Susceptibility to GN(MB) Interference 32
A.2. Characterization of GN(MB) Signals 39

APPENDIX B: VERIFICATION OF SUSCEPTIBILITY RESULTS 42
B.1. Test System Overview 42
B.2. Signal Calibration 43
B.3. Measured DTV Signal Quality 45
B.4. Theoretical DTV Signal Quality for Gaussian Noise Degradation 48
B.5. Validation of Measured DTV Quality Metrics for Gaussian Noise Degradation 50

APPENDIX C: THEORETICAL ANALYSIS OF GATED GAUSSIAN NOISE 53
C.1. Amplitude Probability Distribution 53
C.2. Power Spectral Density 55

APPENDIX D: CHARACTERIZATION MEASUREMENTS 58
D.1. Measurement Setup 58
D.2. Results 59

FIGURES

Page

Figure 1. Simulated gated-noise signal, GN-10 4

Figure 2. *SNR*, *SNR'*, *INR*, *INR'*, *BER*, and *SER* reference points 5

Figure 3. *SER* versus *INR* for a DTV receiver operating at *SNR* = 9 dB and exposed to GN interference 7

Figure 4. *BER* versus *INR* for a DTV receiver operating at *SNR* = 9 dB and exposed to GN interference 7

Figure 5. *SER* versus *INR* for a DTV receiver operating at *SNR* = 12 dB and exposed to GN interference 8

Figure 6. *BER* versus *INR* for a DTV receiver operating at *SNR* = 12 dB and exposed to GN interference 8

Figure 7. *SER* versus *INR* for a DTV receiver operating at *SNR* = 15 dB and exposed to GN interference 9

Figure 8. *BER* versus *INR* for a DTV receiver operating at *SNR* = 15 dB and exposed to GN interference 9

Figure 9. Illustration of threshold-of-visibility metrics 10

Figure 10. INR_{TOV} versus 10log(1/ζ) for a DTV receiver operating at *SNR* = 9 dB and exposed to GN interference 12

Figure 11. BER_{TOV} versus 10log(1/ζ) for a DTV receiver operating at *SNR* = 9 dB and exposed to GN interference 12

Figure 12. INR_{TOV} versus 10log(1/ζ) for a DTV receiver operating at *SNR* = 12 dB and exposed to GN interference 13

Figure 13. BER_{TOV} versus 10log(1/ζ) for a DTV receiver operating at *SNR* = 12 dB and exposed to GN interference 13

Figure 14. INR_{TOV} versus 10log(1/ζ) for a DTV receiver operating at *SNR* = 15 dB and exposed to GN interference 14

Figure 15. BER_{TOV} versus 10log(1/ζ) for a DTV receiver operating at *SNR* = 15 dB and exposed to GN interference 14

Figure 16. Simulated gated-noise signals with the same average power 15

Figure 17. Illustration of pulse duration and pulse interval 16

Figure 18. Illustration of burst duration and burst interval 17

Figure 19. *APD*s of GN signals with τ_{on} = 10 ns band-limited to B_{DTV} 19

Figure 20. *APD*s of GN signals with τ_{on} = 100 ns band-limited to B_{DTV} 19

Figure 21. *APD*s of GN signals with τ_{on} = 1,000 ns band-limited to B_{DTV} 20

Figure 22. *APD*s of GN signals with τ_{on} = 10,000 ns band-limited to B_{DTV} 20

Figure 23. Illustration of *P/A* for GN-10 band-limited to B_{DTV} 21

Figure 24. *PSD*s of GN signals with τ_{on} = 10 ns 23

Figure 25. *PSD*s of GN signals with τ_{on} = 100 ns 23

Figure 26. *PSD*s of GN signals with τ_{on} = 1,000 ns 24

Figure 27. *PSD*s of GN signals with τ_{on} = 10,000 ns 24

Figure 28. INR_{TOV} versus *P/A* for a DTV receiver operating at *SNR* = 9 dB and exposed to GN interference 26

Figure 29. INR_{TOV} versus *P/A* for a DTV receiver operating at *SNR* = 12 dB and exposed to GN interference 26

Figure 30. INR_{TOV} versus *P/A* for a DTV receiver operating at *SNR* = 15 dB and exposed to GN interference 27

Figure A-1. Simulated gated-noise signal, GN(MB)-03 31

Figure A-2. *SER* versus *INR* for a DTV receiver operating at *SNR* = 9 dB and exposed to GN(MB) interference 33

Figure A-3. *BER* versus *INR* for a DTV receiver operating at *SNR* = 9 dB and exposed to GN(MB) interference 33

Figure A-4. *SER* versus *INR* for a DTV receiver operating at *SNR* = 12 dB and exposed to GN(MB) interference 34

Figure A-5. *BER* versus *INR* for a DTV receiver operating at *SNR* = 12 dB and exposed to GN(MB) interference 34

Figure A-6. *SER* versus *INR* for a DTV receiver operating at *SNR* = 15 dB and exposed to GN(MB) interference....35

Figure A-7. *BER* versus *INR* for a DTV receiver operating at *SNR* = 15 dB and exposed to GN(MB) interference....35

Figure A-8. INR_{TOV} versus 10log(1/ζ) for a DTV receiver operating at *SNR* = 9 dB and exposed to GN(MB) interference....36

Figure A-9. BER_{TOV} versus 10log(1/ζ) for a DTV receiver operating at *SNR* = 9 dB and exposed to GN(MB) interference....36

Figure A-10. INR_{TOV} versus 10log(1/ζ) for a DTV receiver operating at *SNR* = 12 dB and exposed to GN(MB) interference....37

Figure A-11. BER_{TOV} versus 10log(1/ζ) for a DTV receiver operating at *SNR* = 12 dB and exposed to GN(MB) interference....37

Figure A-12. INR_{TOV} versus 10log(1/ζ) for a DTV receiver operating at *SNR* = 15 dB and exposed to GN(MB) interference....38

Figure A-13. BER_{TOV} versus 10log(1/ζ) for a DTV receiver operating at *SNR* = 15 dB and exposed to GN(MB) interference....38

Figure A-14. *APD*s of single-dwell GN(MB) signals band-limited to B_{DTV}....40

Figure A-15. *APD*s of multi-dwell GN(MB) signals band-limited to B_{DTV}....40

Figure A-16. *PSD*s of single-dwell GN(MB) signals....41

Figure A-17. *PSD*s of multi-dwell GN(MB) signals....41

Figure B-1. Block diagram of DTV interference susceptibility test system....42

Figure B-2. Block diagrams for calibration measurements....44

Figure B-3. *BER* estimation circuit used by MPEG-2 stream monitor....46

Figure B-4. Simulation of *BER* estimation circuit used by MPEG-2 stream monitor....47

Figure B-5. Theoretical DTV receiver performance versus *SNR′*....49

Figure B-6. Theoretical versus measured bit error rate performance of a DTV receiver....50

Figure B-7. Theoretical and measured *BER* for Gaussian noise interference....52

Figure B-8. Theoretical and measured *SER* for Gaussian noise interference 52

Figure C-1. Theoretical *APD*s of gated noise in B_{UWB} 57

Figure C-2. Theoretical *P/A* of gated noise in B_{UWB}.....57

Figure D-1. Setup for RF signal characterization measurements.....58

Figure D-2. Simplified setup for IF signal characterization measurements.....59

Figure D-3. RF measurements of GN-01, Gaussian noise 62

Figure D-4. IF measurements of GN-01 at INR_{TOV} 63

Figure D-5. RF measurements of GN-02 (τ_{on} = 10 ns, ζ = 0.5000).....64

Figure D-6. IF measurements of GN-02 at INR_{TOV} 65

Figure D-7. RF measurements of GN-03 (τ_{on} = 10 ns, ζ = 0.2500).....66

Figure D-8. IF measurements of GN-03 at INR_{TOV} 67

Figure D-9. RF measurements of GN-04 (τ_{on} = 10 ns, ζ = 0.1250).....68

Figure D-10. IF measurements of GN-04 at INR_{TOV} 69

Figure D-11. RF measurements of GN-05 (τ_{on} = 10 ns, ζ = 0.0625).....70

Figure D-12. IF measurements of GN-05 at INR_{TOV} 71

Figure D-13. RF measurements of GN-06 (τ_{on} = 100 ns, ζ = 0.5000).....72

Figure D-14. IF measurements of GN-06 at INR_{TOV} 73

Figure D-15. RF measurements of GN-07 (τ_{on} = 100 ns, ζ = 0.2500).....74

Figure D-16. IF measurements of GN-07 at INR_{TOV} 75

Figure D-17. RF measurements of GN-08 (τ_{on} = 100 ns, ζ = 0.1250).....76

Figure D-18. IF measurements of GN-08 at INR_{TOV} 77

Figure D-19. RF measurements of GN-09 (τ_{on} = 100 ns, ζ = 0.0625).....78

Figure D-20. IF measurements of GN-09 at INR_{TOV} 79

Figure D-21. RF measurements of GN-10 (τ_{on} = 1000 ns, ζ = 0.5000) 80
Figure D-22. IF measurements of GN-10 at INR_{TOV} 81
Figure D-23. RF measurements of GN-11 (τ_{on} = 1000 ns, ζ = 0.2500) 82
Figure D-24. IF measurements of GN-11 at INR_{TOV} 83
Figure D-25. RF measurements of GN-12 (τ_{on} = 1000 ns, ζ = 0.1250) 84
Figure D-26. IF measurements of GN-12 at INR_{TOV} 85
Figure D-27. RF measurements of GN-13 (τ_{on} = 1000 ns, ζ = 0.0625) 86
Figure D-28. IF measurements of GN-13 at INR_{TOV} 87
Figure D-29. RF measurements of GN-14 (τ_{on} = 10,000 ns, ζ = 0.5000) 88
Figure D-30. IF measurements of GN-14 at INR_{TOV} 89
Figure D-31. RF measurements of GN-15 (τ_{on} = 10,000 ns, ζ = 0.2500) 90
Figure D-32. IF measurements of GN-15 at INR_{TOV} 91
Figure D-33. RF measurements of GN-16 (τ_{on} = 10,000 ns, ζ = 0.1250) 92
Figure D-34. IF measurements of GN-16 at INR_{TOV} 93
Figure D-35. RF measurements of GN-17 (τ_{on} = 10,000 ns, ζ = 0.0625) 94
Figure D-36. IF measurements of GN-17 at INR_{TOV} 95
Figure D-37. RF measurements of GN(MB)-01 (b = 1, d = 1) 96
Figure D-38. IF measurements of GN(MB)-01 at INR_{TOV} 97
Figure D-39. RF measurements of GN(MB)-02 (b = 3, d = 1) 98
Figure D-40. IF measurements of GN(MB)-02 at INR_{TOV} 99
Figure D-41. RF measurements of GN(MB)-03 (b = 3, d = 2) 100
Figure D-42. IF measurements of GN(MB)-03 at INR_{TOV} 101
Figure D-43. RF measurements of GN(MB)-04 (b = 7, d = 1) 102

Figure D-44. IF measurements of GN(MB)-04 at INR_{TOV} 103

Figure D-45. RF measurements of GN(MB)-05 (b = 7, d = 2) 104

Figure D-46. IF measurements of GN(MB)-05 at INR_{TOV} 105

Figure D-47. RF measurements of GN(MB)-06 (b = 7, d = 6) 106

Figure D-48. IF measurements of GN(MB)-06 at INR_{TOV} 107

Figure D-49. RF measurements of GN(MB)-07 (b = 13, d = 1) 108

Figure D-50. IF measurements of GN(MB)-07 at INR_{TOV} 109

Figure D-51. RF measurements of GN(MB)-08 (b = 13, d = 2) 110

Figure D-52. IF measurements of GN(MB)-08 at INR_{TOV} 111

Figure D-53. RF measurements of GN(MB)-09 (b = 13, d = 12) 112

Figure D-54. IF measurements of GN(MB)-09 at INR_{TOV} 113

TABLES

Page

Table 1. GN Gating Parameters 4

Table 2. Measured DTV Susceptibility and FEC Performance for GN Interference 11

Table 3. Temporal Characteristics of GN Signals Band-Limited to B_{DTV} 17

Table 4. Amplitude Characteristics of GN Signals Band-Limited to B_{DTV} 21

Table A-1. GN(MB) Gating Parameters 31

Table A-2. Measured DTV Susceptibility and FEC Performance for GN(MB) Interference 32

Table A-3. Temporal Characteristics of GN(MB) Signals Band-Limited to B_{DTV} 39

Table A-4. Amplitude Characteristics of GN(MB) Signals Band-Limited to B_{DTV} 39

Table B-1. Operational Scenario for DTV Interference Susceptibility Tests 43

Table B-2. Probability of Pre-Viterbi Bit Error and Post-RS Segment Error Near TOV 49

Table B-3. Signal Powers at the TOV for Gaussian Noise Interference 51

Table D-1. RF VSA Measurement Settings 58

Table D-2. RF *P/A* (dB) of GN and GN(MB) Signals Band-Limited to Different Bandwidths 60

Table D-3. IF *P/A* (dB) of GN and GN(MB) Signals at INR_{TOV} and Band-Limited to B_{DTV} 61

INTERFERENCE POTENTIAL OF ULTRAWIDEBAND SIGNALS

PART 2: MEASUREMENTS OF GATED-NOISE INTERFERENCE TO C-BAND SATELLITE DIGITAL TELEVISION RECEIVERS

Michael Cotton,[1] Robert Achatz,[1] Jeffery Wepman,[1] and Paul Runkle[2]

This report demonstrates that digital television (DTV) susceptibility to gated-noise interference cannot be predicted by interference power characteristics alone. It was found that DTV susceptibility is also dependent on temporal characteristics of the interfering signal and the bandwidth of the DTV receiver. A test system was developed to inject interference with known characteristics into a victim receiver and quantitatively measure susceptibility. In this experiment, a C-band satellite DTV victim receiver was exposed to gated-noise interference, whose temporal characteristics are defined by gating parameters such as on-time, fractional on-time, and off-time. The specific gating parameters considered in this report include on-times of 0.01, 0.10, 1.00, and 10.00 μs and fractional on-times of 1.00, 0.50, 0.25, 0.125, and 0.0625. Results showed that DTV susceptibility was strictly dependent on average power of the interfering signal only when off-times were less than the reciprocal bandwidth of the victim receiver. For longer off-times, however, susceptibility was dependent on the temporal characteristics of the interfering signal. Moreover, high correlation was observed between susceptibility and forward error correction performance of the receiver.

Key words: digital television; interference; satellite communications; ultrawideband

1. INTRODUCTION

In April 2002, the Federal Communications Commission (FCC) released *FCC 02-48* [1] legalizing intentional, low-power ultrawideband (UWB) emissions between 3.1 GHz and 10.6 GHz for communications devices operated indoors. UWB emissions were limited to -41 dBm average power in 1-MHz bandwidth and 0 dBm peak power in 50-MHz bandwidth, where average power is measured over a 1-millisecond integration time and peak power measurement duration is unspecified. The rules define a UWB device as one that emits signals with 10-dB bandwidth greater than 500 MHz or greater than 20% of the center frequency.

The FCC rules do not specify how the bandwidth requirement is achieved, consequently allowing industry considerable breadth in choosing a modulation. This breadth is exemplified by the development of Direct-Sequence Ultrawideband (DS-UWB) and Multi-band Orthogonal Frequency-Domain Multiplexing (MB-OFDM) ultrawideband technologies. Proponents of DS-UWB and MB-OFDM both seek standardization from IEEE (Institute of Electrical and Electronics Engineers) 802.15 working group 3a on high-rate (greater than 20 million bits per

[1] The authors are with the Institute for Telecommunication Sciences, National Telecommunications and Information Administration, U.S. Department of Commerce, Boulder, Colorado 80305.
[2] The author is with Signal Innovations Group, Inc., Durham, North Carolina 27713.

second) Wireless Personal Area Networks (WPAN). As the name implies, WPAN is intended for short-distance (nominally less than 10 meters) wireless networking of devices such as PCs, personal digital assistants, and mobile phones.

Both DS-UWB and MB-OFDM transmitters are based on state-of-the-art integrated circuitry. DS-UWB modulation controls pulse polarity and hence supports phase shifting modulations. It achieves its ultra-wide bandwidth by transmitting sufficiently narrow pulses. MB-OFDM simultaneously modulates 122 carriers spaced 4.125 MHz apart to achieve its ultra-wide bandwidth and frequency hops the modulated carriers between non-overlapping bands.

Since previous work performed at the Institute for Telecommunication Sciences (ITS) [2 – 5] did not specifically look at susceptibility of receivers to interference from DS-UWB or MB-OFDM signals, and since there is little published information on this subject, ITS entered into a Cooperative Research and Development Agreement (CRADA) with the Freescale subsidiary of Motorola, Inc. to study how susceptibility could be quantified in terms of interference signal characteristics.

1.1. Experiment

Interference potential is a general concept where performance degradation of a victim receiver is predicted from interference signal characteristics. Interference potential is derived from numerous susceptibility tests on receivers with a variety of bandwidths and signal demodulation techniques. This report describes one such test where C-band satellite digital television (DTV) is exposed to gated-noise interference. Development of the test system and procedure was described in Part 1 of this report series [6].

In this report, only continuous- and gated-noise signals are considered as interferers. While it is unlikely that these signals will be used in communications, their similarities to DS-UWB and MB-OFDM, respectively, are unmistakable and their analytic tractability is profoundly useful. More specifically, these signals emulate the noisy nature of DS-UWB and MB-OFDM as well as the gating characteristics of MB-OFDM caused by frequency hopping in and out of a victim receiver operational band. This emulation is accomplished without the mathematical complexities associated with actual UWB modulations. Comparisons between continuous noise and DS-UWB, and gated noise and MB-OFDM, will be discussed in Part 3 of this report series.

C-band satellite television was chosen as the victim receiver for the susceptibility tests because it demodulates signals transmitted in the 3.7 to 4.2 GHz frequency range, which lies within the band allocated for UWB operation. It also uses a variety of bandwidths and signal demodulation techniques, which makes it an ideal victim receiver for the study of interference potential. Additionally, instruments capable of providing quantitative signal quality data from various receiver subsystems are readily available.

1.2. Organization of Report

The main body of this report presents DTV susceptibility data and characterization measurements for gated-noise interference with the following gating parameters: on-time (τ_{on}) = {10, 100, 1000, 10000} ns and fractional on time (ζ) = {1.0, 0.5, 0.25, 0.125, 0.0625}. These signals are denoted by the acronym GN.

Section 2 provides DTV susceptibility test results plotted two different ways. First, post-Reed-Solomon segment error rate (*SER*) and pre-Viterbi bit error rate (*BER*) are plotted as a function of interference-to-noise ratio (*INR*) to demonstrate how susceptibility depends on average power of the interfering signals. Second, *INR* and *BER* at the threshold of visibility (TOV), i.e., INR_{TOV} and BER_{TOV}, are plotted as a function of ζ to demonstrate how DTV susceptibility and forward error correction (FEC) performance depend on the gating parameters of the interfering signals.

Section 3 provides temporal and amplitude analyses of measured GN signals to demonstrate the effects of band-limiting. The temporal analysis is based on crossing statistics. Burst duration (*BD*) and burst interval (*BI*) estimates of band-limited GN signals are compared to on- and off-times of the corresponding gating functions. The amplitude analysis is based on amplitude probability distributions (*APD*s). Peak-to-average ratio (*P/A*) estimates of the band-limited GN signals are compared to corresponding ultra-wide-bandwidth *P/A* limits. Also provided in Section 3 is a spectral analysis based on power spectral densities (*PSD*s) of measured GN signals.

Section 4 discusses how DTV susceptibility depends on the characteristics of interfering signals. It summarizes the important points of the test, describes findings, and evaluates the significance and scope of the findings.

Appendices to this report contain information supporting the main body. Appendix A provides DTV susceptibility test results and signal characterization measurements for gated-noise signals that emulate MB-OFDM. Appendix B gives an overview of the test system, provides precise measurement definitions for signal-to-noise ratio (*SNR*), *INR*, *SER*, and *BER*, and provides some degree of validation via comparison of theoretical and measured DTV signal quality metrics for Gaussian noise degradation. Appendix C develops theoretical expressions for the amplitude and spectral properties of gated Gaussian noise in an ultra-wide transmission bandwidth. Finally, Appendix D provides *APD*s of the gated-noise signals in a variety of bandwidths measured at the satellite radio frequency (RF) as well as *APD*s of the signals at the first intermediate frequency (IF) in the presence of low-noise block downconverter (LNB) noise for interference powers corresponding to INR_{TOV}.

2. DTV SUSCEPTIBILITY TO GN INTERFERENCE

Results of the DTV susceptibility tests for GN interference are described in this section. It presents gating parameters, discusses relevant signal powers and DTV signal quality metrics, and provides *SER* and *BER* versus *INR* plots and INR_{TOV} and BER_{TOV} versus ζ plots.

2.1. Gating Parameters

Table 1 gives on-time, fractional on-time, and off-time (τ_{off}) gating parameters of the periodically gated-noise interference signals considered in the main body of this report. The set of gated-noise signals in Table 1 is denoted by the acronym GN, and each individual signal is specified by identifiers in the first column. An illustration of the gating parameters is given in Figure 1. Appendix A extends the scope of this experiment to GN(MB) interference signals, which are gated-noise signals that emulate MB-OFDM.

Table 1. GN Gating Parameters

GN	τ_{on} (μs)	τ_{off} (μs)	ζ
01	∞	0.00	1.0000
02	0.01	0.01	0.5000
03	0.01	0.03	0.2500
04	0.01	0.07	0.1250
05	0.01	0.15	0.0625
06	0.10	0.10	0.5000
07	0.10	0.30	0.2500
08	0.10	0.70	0.1250
09	0.10	1.50	0.0625
10	1.00	1.00	0.5000
11	1.00	3.00	0.2500
12	1.00	7.00	0.1250
13	1.00	15.00	0.0625
14	10.00	10.00	0.5000
15	10.00	30.00	0.2500
16	10.00	70.00	0.1250
17	10.00	150.00	0.0625

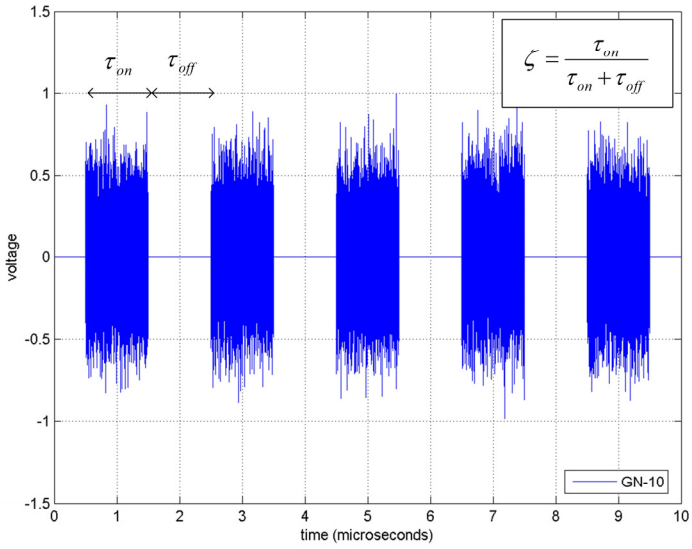

Figure 1. Simulated gated-noise signal, GN-10.

2.2. Signal Powers and DTV Signal Quality Metrics

Figure 2 illustrates reference points for the signal powers and DTV signal quality metrics acquired during the DTV susceptibility tests. *SNR* and *INR* define the average power of the DTV and interfering signals. These average power ratios were derived from vector signal analyzer data measured at IF and band-limited to B_{DTV} = 19.51 MHz in post-measurement processing by the same root-raised-cosine (RRC) filter found in the demodulator of the victim receiver. Figure B-1

provides a block diagram of the test hardware configuration and Section B.2 mathematically describes the power ratio measurements. DTV signal quality metrics *SER* and *BER* were acquired with the MPEG-2 transport stream monitor.[3] Section B.3 provides mathematical definitions of the DTV signal quality metrics.

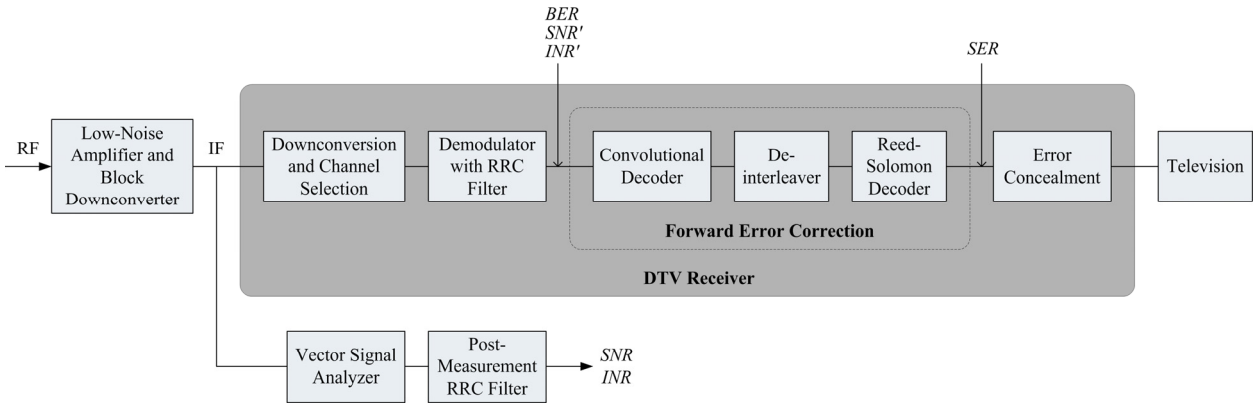

Figure 2. *SNR*, *SNR′*, *INR*, *INR′*, *BER*, and *SER* reference points.

It is important to note that *SNR* and *INR* were not measured at the same point as *BER*. Theoretical expressions for DTV signal quality metrics for Gaussian noise degradation are provided in Section B.4; these expressions use signal-to-noise ratio at the output of the demodulator (*SNR′*) as the dependent variable. Equation (B-1) was derived empirically to account for imperfect demodulation effects and compute *SNR′* from *SNR*. Using this model, *SNR′* = {8.2, 10.5, 12.5} dB was calculated from *SNR* = {9, 12, 15} dB. Note that this model was derived under Gaussian noise assumptions and cannot be generalized for gated-noise interference to obtain *INR′* from *INR* without further research. Therefore, test results are displayed as a function of the measurable dependent variables *SNR* and *INR*.

2.3. DTV Signal Quality as a Function of Interference Average Power

Figures 3 – 8 provide composite plots of measured *SER* and *BER* as a function of *INR* for *SNR* = {9, 12, 15} dB. Each page is dedicated to a single *SNR*, each plot is dedicated to a specific τ_{on}, and each curve represents a single ζ. Figures 3, 5, and 7 provide composite plots of *SER* while Figures 4, 6, and 8 provide composite plots of *BER*. The following are general comments regarding the shift, separation, and slope of these curves.

Both *SER* and *BER* shifted toward greater *INR* with increasing *SNR*. This occurred because more interference was needed to degrade stronger satellite signals.

[3] Modulation error ratio (*MER*) was also acquired with the MPEG-2 stream monitor. *MER* is an important DTV signal quality metric referenced to the output of the demodulator. Measured *MER*, however, was inconsistent with theory which prevented its use in this report.

SER curves with fixed *SNR* and τ_{on} show increased separation (from the continuous-noise case) with decreasing ζ. Likewise, all curves with fixed *SNR* and ζ exhibit increased separation with increasing τ_{on}. Hence, *SER* curves with τ_{on} = 10 ns and $\zeta \geq$ 0.25 lay close to the continuous-noise case, while those with τ_{on} = 10,000 ns and ζ = 0.0625 had the greatest separation. A notable anomaly to this trend occurred for GN-09 (τ_{on} = 100 ns, ζ = 0.0625), where the shallow slope of the *SER* curve caused it to cross higher-ζ *SER* curves.

SER curves were generally steeper than corresponding *BER* curves, which indicates that *SER* was more sensitive than *BER* to changes in average interference power. *SER* steepness was due to two stages of forward error correction (FEC), which were applied to post-Reed-Solomon segments but not to pre-Viterbi bits. Another trend was observed for sufficiently small ζ, i.e., ζ = 0.0625, where slopes of the *SER* curves were flatter compared to higher-ζ cases. This may be attributed to conditions more favorable to FEC performance or to longer off-times where errors were unlikely. In either case, DTV susceptibility to small-ζ gated-noise interference seemed to be more dependent on the temporal characteristics than on the power characteristics of the interference signal.

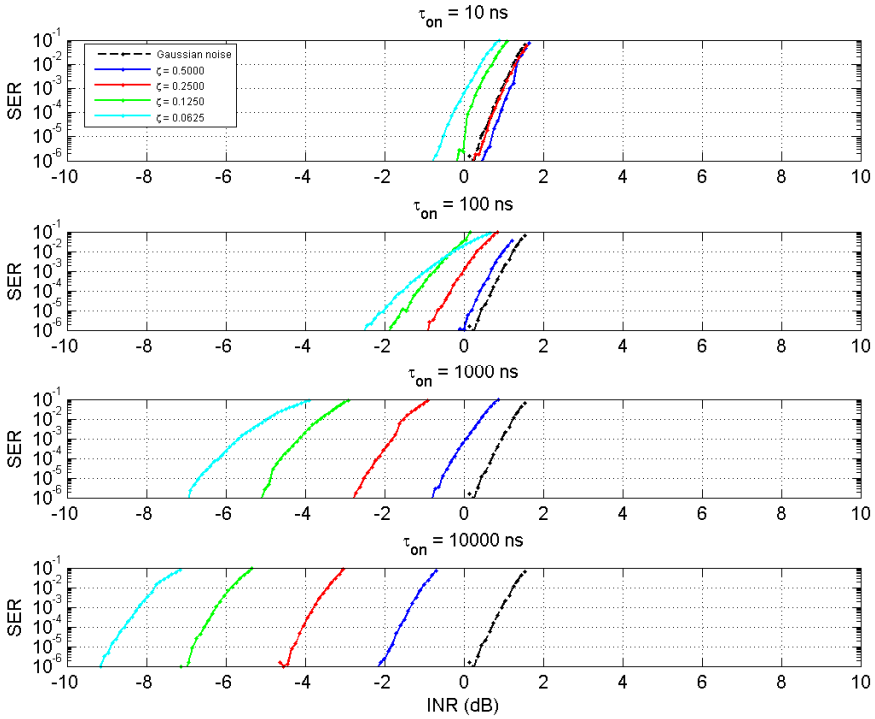

Figure 3. *SER* versus *INR* for a DTV receiver operating at *SNR* = 9 dB and exposed to GN interference.

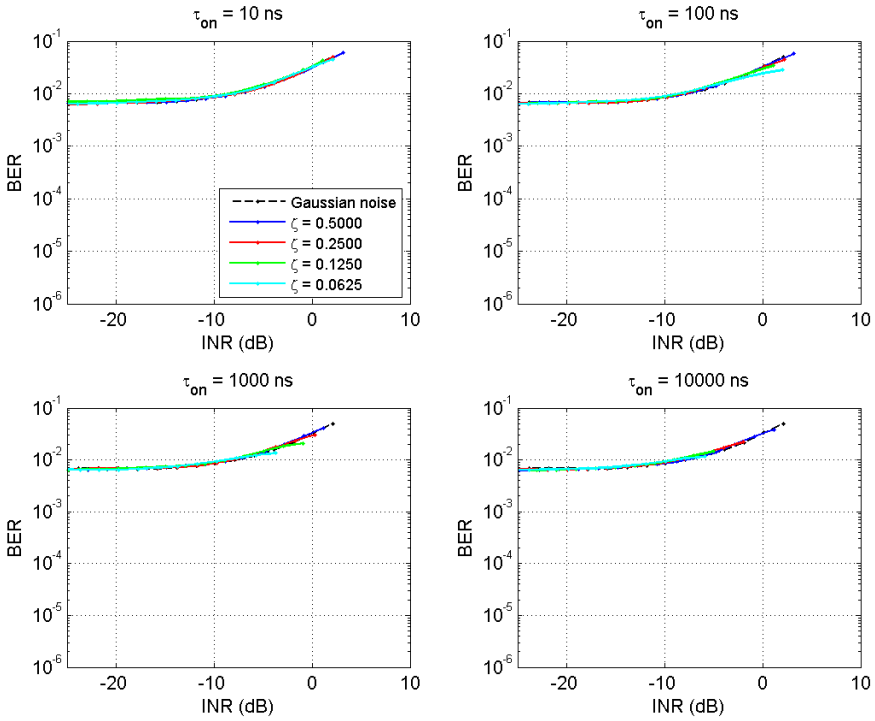

Figure 4. *BER* versus *INR* for a DTV receiver operating at *SNR* = 9 dB and exposed to GN interference.

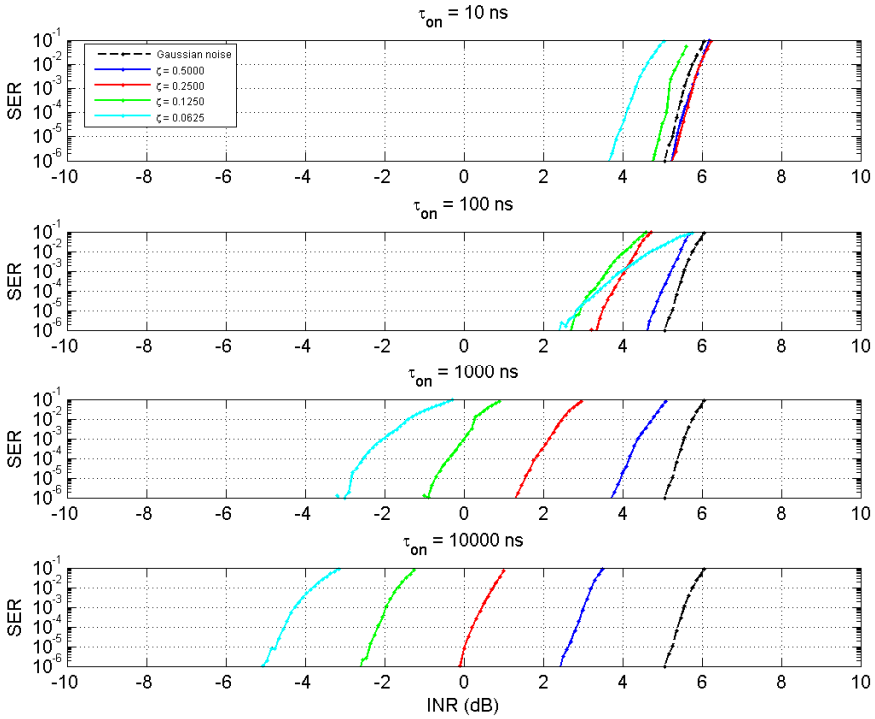

Figure 5. *SER* versus *INR* for a DTV receiver operating at *SNR* = 12 dB and exposed to GN interference.

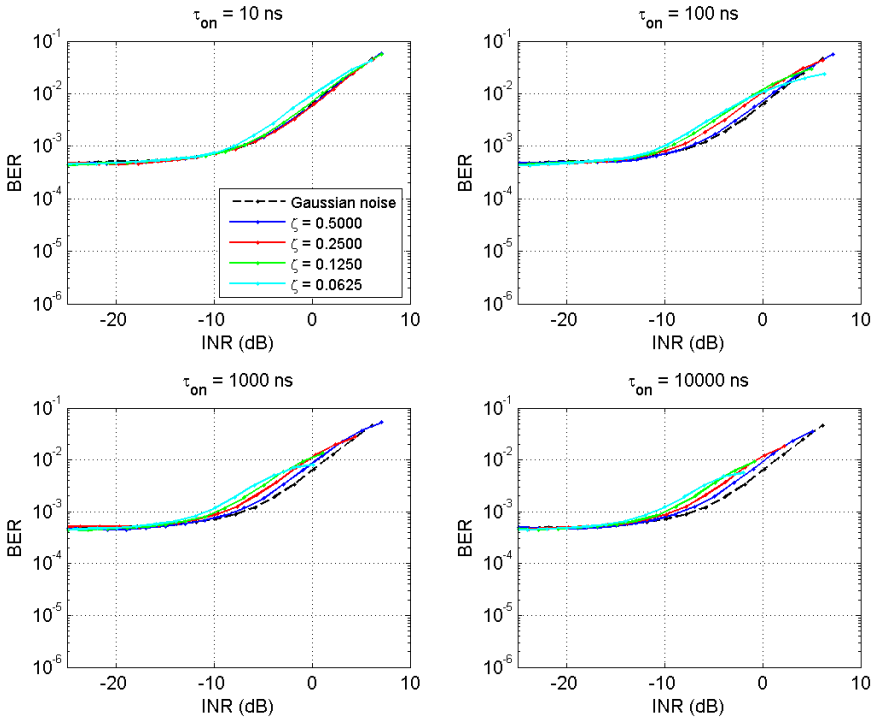

Figure 6. *BER* versus *INR* for a DTV receiver operating at *SNR* = 12 dB and exposed to GN interference.

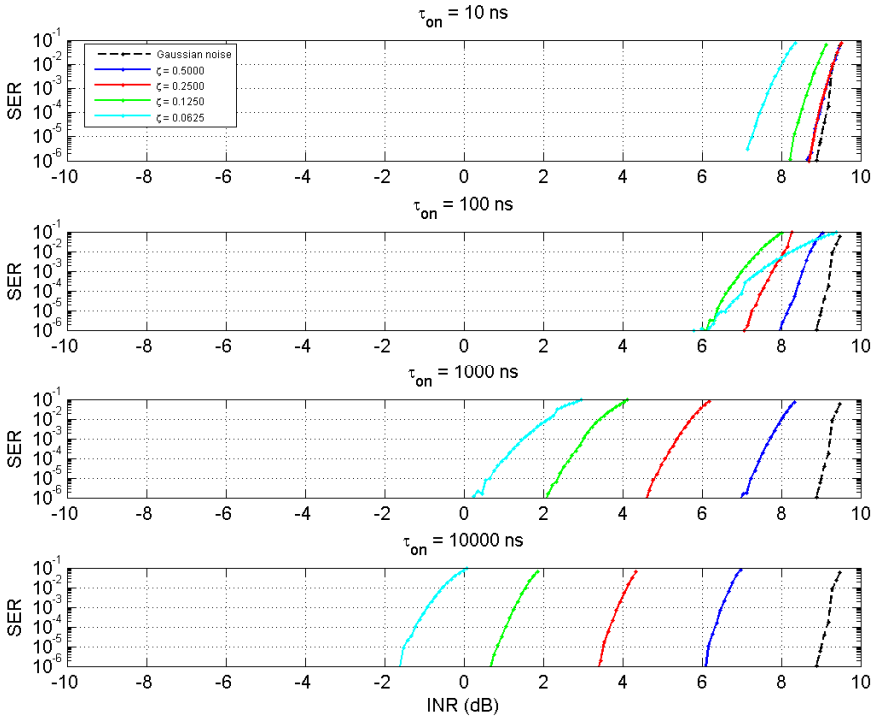

Figure 7. *SER* versus *INR* for a DTV receiver operating at *SNR* = 15 dB and exposed to GN interference.

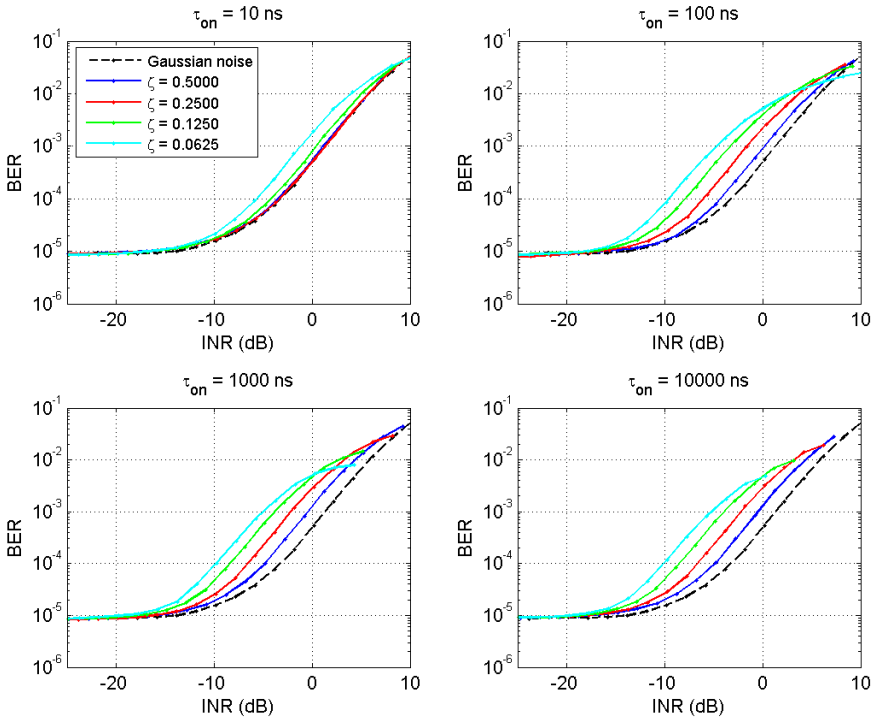

Figure 8. *BER* versus *INR* for a DTV receiver operating at *SNR* = 15 dB and exposed to GN interference.

2.4. DTV Susceptibility and FEC Performance as a Function of Interference Fractional On-Time

Figure 9 displays measured *SER* and *BER* curves for a DTV victim receiver operating at *SNR* = 15 dB and exposed to increasing levels of continuous-noise interference. This figure also identifies important DTV susceptibility and FEC performance metrics. Importantly, $SER_{TOV} = 10^{-4}$ is a level identified by video quality studies [7] as the threshold of visibility where video quality degradation is first evident.

INR that corresponds to SER_{TOV}, INR_{TOV}, is our primary DTV susceptibility metric. That is, receiver susceptibility increases as INR_{TOV} decreases. In Figure 9, INR_{TOV} is found vertically from the intersection of the measured *SER* curve and the SER_{TOV} horizontal line.

BER that corresponds to SER_{TOV}, BER_{TOV}, is our FEC performance metric. This metric quantifies the ability of the FEC to overcome bit errors caused by interference to achieve SER_{TOV}. In other words, larger BER_{TOV} indicates more corrected bits and better FEC performance. In Figure 9, BER_{TOV} is found horizontally from the intersection of INR_{TOV} and the measured *BER* curve.

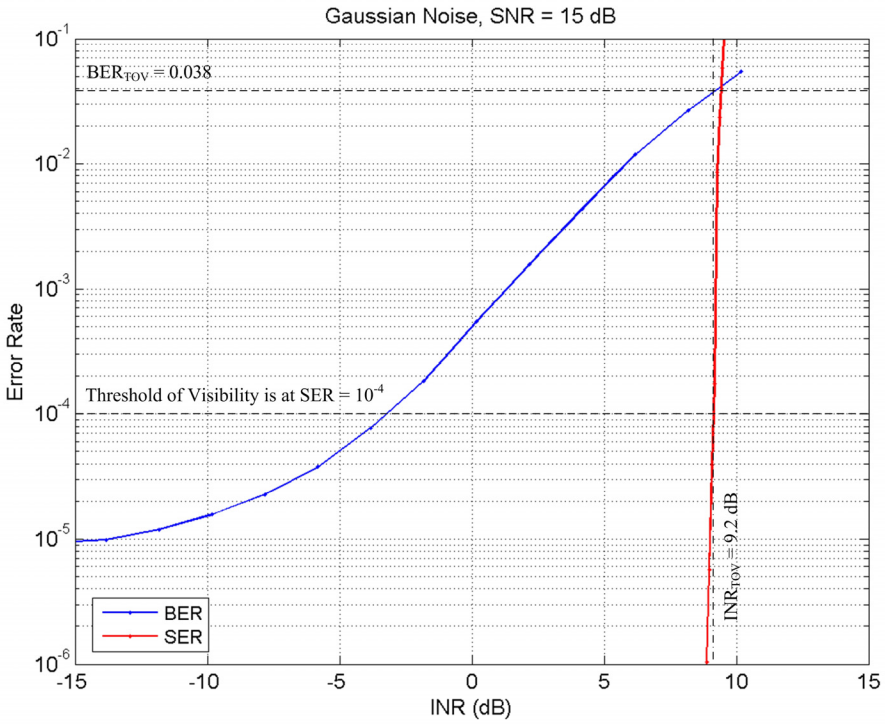

Figure 9. Illustration of threshold-of-visibility metrics.

Table 2 gives INR_{TOV} and BER_{TOV} metrics for all GN interference tests. A distinctive trend was the positive correlation between INR_{TOV} and BER_{TOV}. This demonstrates that DTV susceptibility was dependent on how effective the FEC was at overcoming bit errors caused by the interference. For example, the FEC was most effective at mitigating continuous-noise degradation and the receiver was least susceptible to continuous-noise interference.

Table 2. Measured DTV Susceptibility and FEC Performance for GN Interference

GN	Gating Parameters			SNR = 9 dB		SNR = 12 dB		SNR = 15 dB	
	τ_{on} (μs)	τ_{off} (μs)	ζ	INR_{TOV} (dB)	BER_{TOV}	INR_{TOV} (dB)	BER_{TOV}	INR_{TOV} (dB)	BER_{TOV}
01	∞	0.00	1.0000	0.7	0.038	5.4	0.038	9.2	0.038
02	0.01	0.01	0.5000	0.9	0.038	5.5	0.038	9.0	0.038
03	0.01	0.03	0.2500	0.7	0.038	5.6	0.038	9.0	0.038
04	0.01	0.07	0.1250	0.1	0.036	5.1	0.034	8.5	0.034
05	0.01	0.15	0.0625	-0.3	0.031	4.1	0.029	7.5	0.029
06	0.10	0.10	0.5000	0.4	0.035	5.0	0.033	8.4	0.033
07	0.10	0.30	0.2500	-0.3	0.030	3.8	0.028	7.5	0.028
08	0.10	0.70	0.1250	-1.2	0.025	3.2	0.023	6.7	0.023
09	0.10	1.50	0.0625	-1.5	0.021	3.4	0.018	7.0	0.018
10	1.00	1.00	0.5000	-0.3	0.032	4.2	0.030	7.5	0.030
11	1.00	3.00	0.2500	-2.2	0.022	1.8	0.018	5.1	0.018
12	1.00	7.00	0.1250	-4.6	0.015	-0.4	0.011	2.7	0.011
13	1.00	15.00	0.0625	-6.2	0.012	-2.5	0.007	1.1	0.007
14	10.00	10.00	0.5000	-1.6	0.025	2.8	0.022	6.3	0.022
15	10.00	30.00	0.2500	-4.1	0.017	0.2	0.012	3.7	0.012
16	10.00	70.00	0.1250	-6.5	0.013	-2.2	0.007	1.1	0.007
17	10.00	150.00	0.0625	-8.6	0.010	-4.5	0.004	-1.2	0.004

Figures 10 – 15 plot INR_{TOV} and BER_{TOV} as a function of $1/\zeta$ in dB, where $\zeta = \{1.00, 0.50, 0.25, 0.125, 0.0625\}$ correspond to $10\log(1/\zeta) = \{0.00, 3.01, 6.02, 9.03, 12.04\}$ dB. The horizontal dashed reference line in each INR_{TOV} plot corresponds to DTV susceptibility that is strictly dependent on average power of the interference signal. As an example, Figure 16 illustrates three gated-noise signals with different ζ but the same average power. If susceptibility were strictly dependent on average power, then the victim receiver would be equally susceptible to each of these signals.

For fixed SNR and τ_{on}, INR_{TOV} decreased (relative to the continuous-noise case) with decreasing ζ. Likewise, for fixed SNR and ζ, INR_{TOV} decreased with increasing τ_{on}. Hence, $INR_{TOV}(\tau_{on} = 10$ ns, $\zeta \geq 0.25)$ lay close to the horizontal reference line, while $INR_{TOV}(\tau_{on} = 10{,}000$ ns, $\zeta = 0.0625)$ deviated the furthest. A notable anomaly to this trend occurred when $INR_{TOV}(\tau_{on} = 100$ ns, $\zeta = 0.0625)$ was greater than $INR_{TOV}(\tau_{on} = 100$ ns, $\zeta = 0.125)$.

These observations demonstrate that DTV susceptibility was dependent on temporal parameters of the interfering signal, i.e., τ_{on} and τ_{off}. If τ_{off} was less than or comparable to the reciprocal bandwidth of the victim receiver RRC filter, i.e., approximately $1/B_{DTV} = 51.3$ ns, then INR_{TOV} clustered near the horizontal reference line and DTV susceptibility was strictly dependent on average power of the interference signal (independent of τ_{on} and ζ). However, if τ_{off} was significantly greater than the reciprocal bandwidth of the victim receiver, then DTV susceptibility was clearly dependent on τ_{on} and ζ.

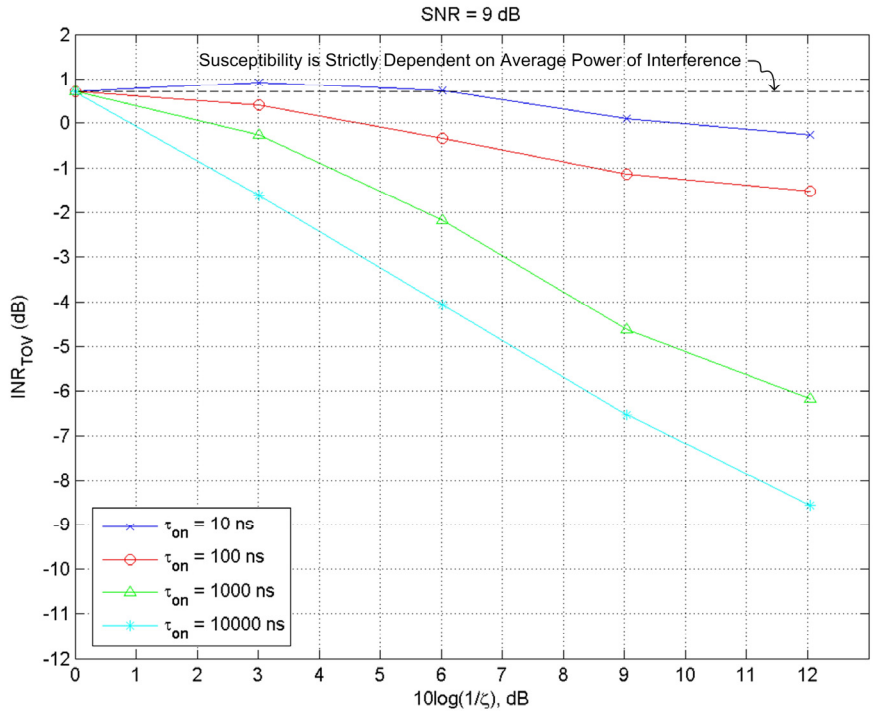

Figure 10. INR_{TOV} versus 10log(1/ζ) for a DTV receiver operating at SNR = 9 dB and exposed to GN interference.

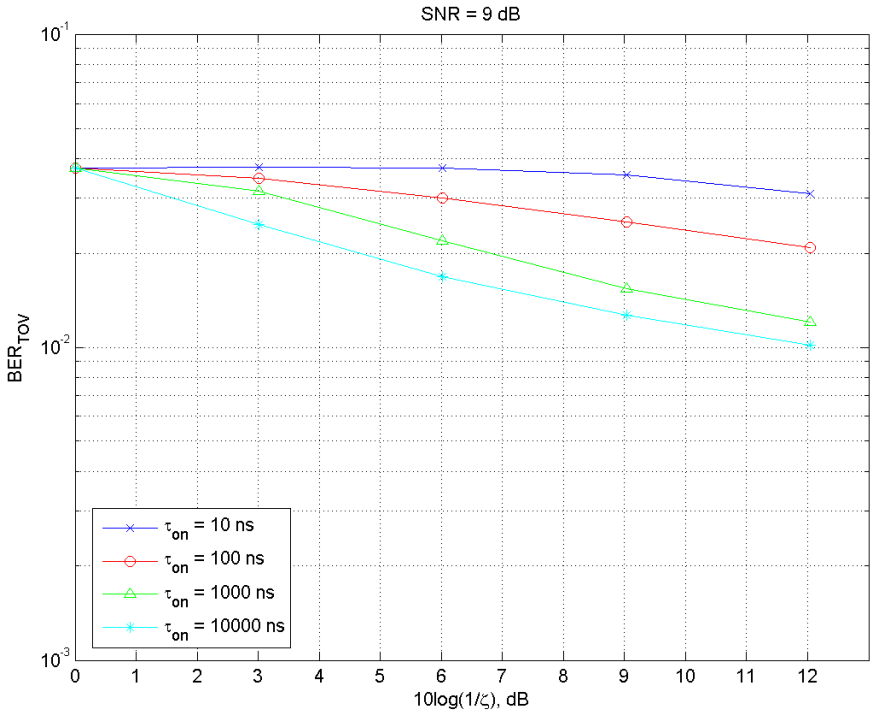

Figure 11. BER_{TOV} versus 10log(1/ζ) for a DTV receiver operating at SNR = 9 dB and exposed to GN interference.

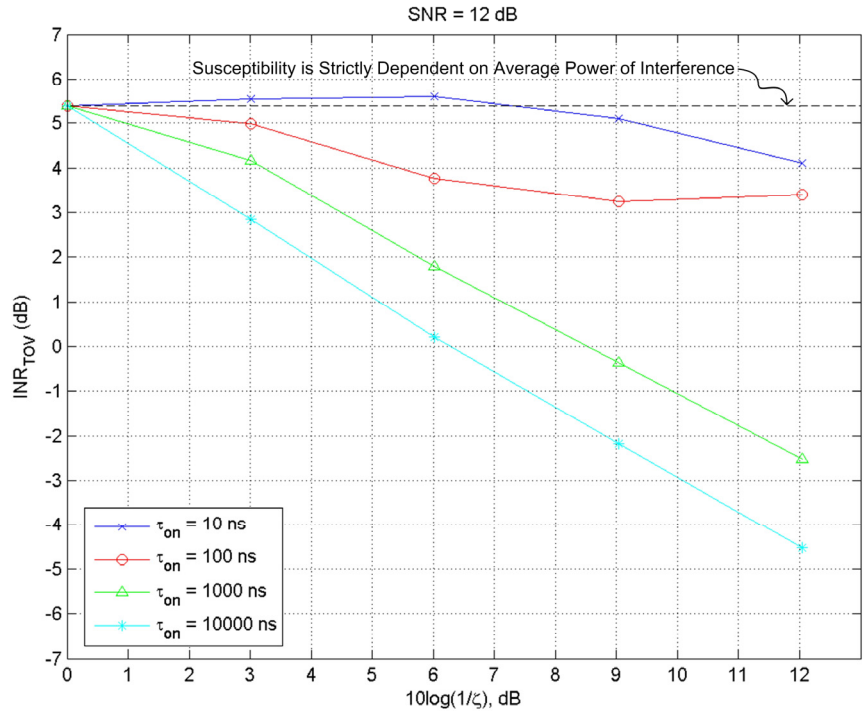

Figure 12. INR_{TOV} versus 10log(1/ζ) for a DTV receiver operating at SNR = 12 dB and exposed to GN interference.

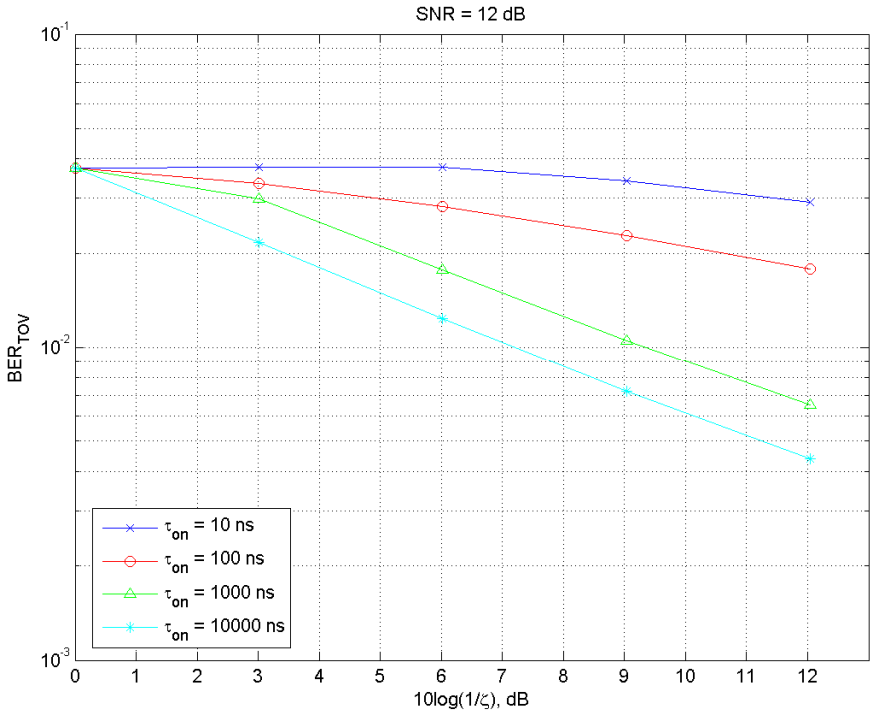

Figure 13. BER_{TOV} versus 10log(1/ζ) for a DTV receiver operating at SNR = 12 dB and exposed to GN interference.

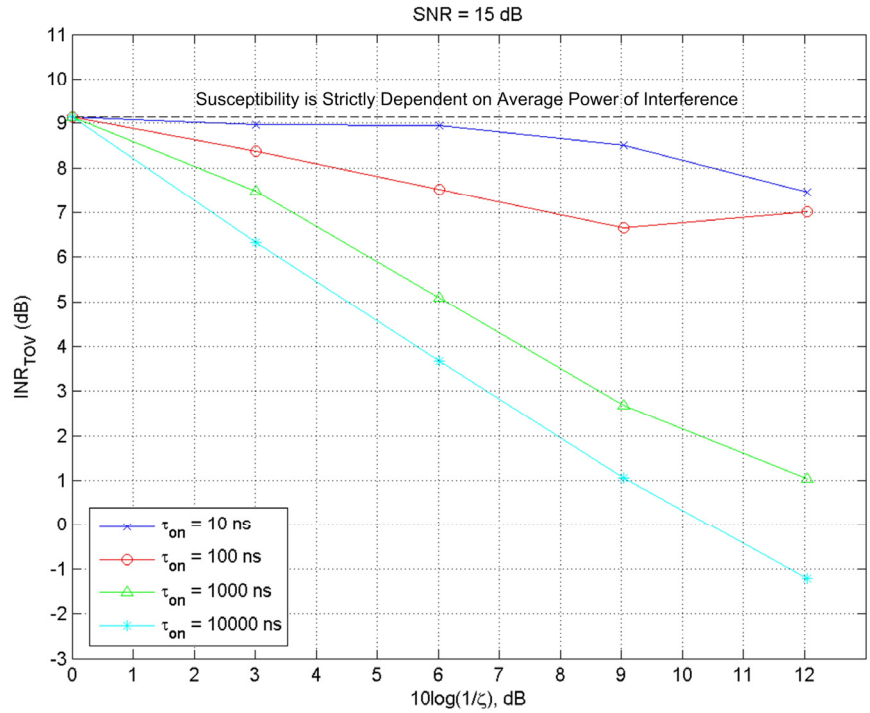

Figure 14. INR_{TOV} versus 10log(1/ζ) for a DTV receiver operating at SNR = 15 dB and exposed to GN interference.

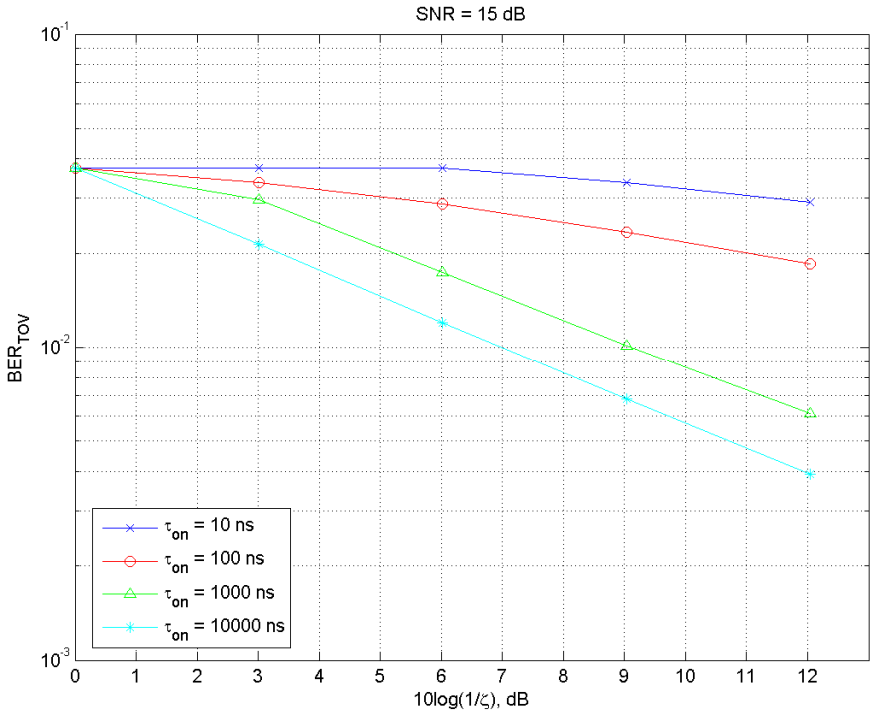

Figure 15. BER_{TOV} versus 10log(1/ζ) for a DTV receiver operating at SNR = 15 dB and exposed to GN interference.

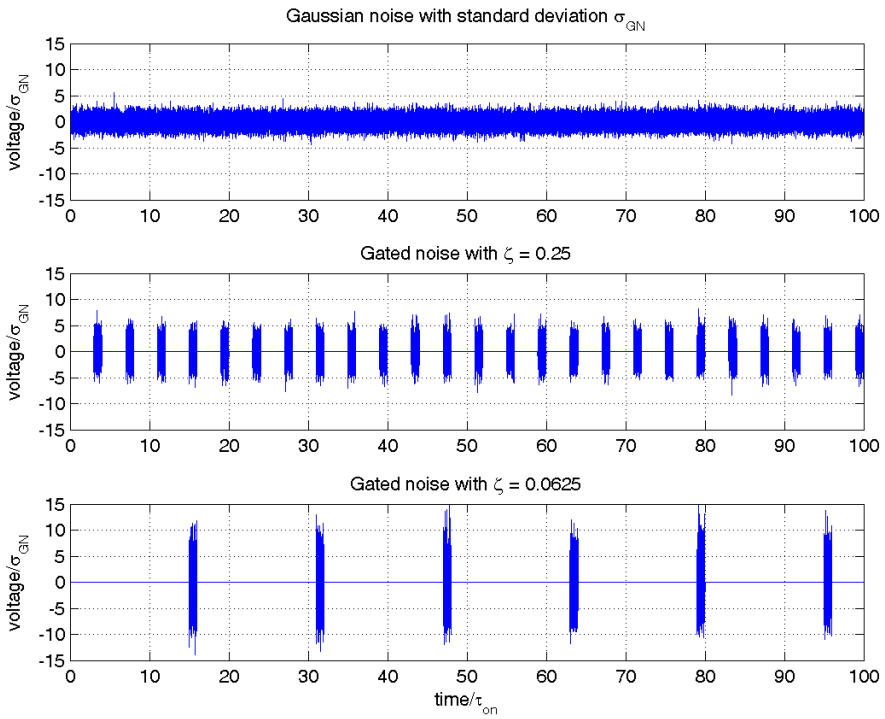

Figure 16. Simulated gated-noise signals with the same average power.

3. CHARACTERIZATION OF GN SIGNALS

Signal characterization of the complex-baseband (CBB) gated-noise signals was accomplished via temporal, amplitude, and spectral analyses. Appendix C provides a theoretical evaluation of the corresponding amplitude and spectral characteristics of gated-noise signals in an ultra-wide transmission bandwidth. To evaluate the effects of band-limiting, the GN signals were measured with the vector signal analyzer (VSA) under optimal measurement conditions at the RF output of the vector signal generator (VSG) and under TOV operational conditions at the IF. Appendix D provides a description of the measurement setup, RF measurement results in various bandwidths, i.e., 36, 10, 1, and 0.1 MHz, and IF measurement results at the three different *SNR*s. Unless otherwise noted, analyses in this section use RF measurements sampled at f_s = 46.08 MSps (corresponding to VSA span = 36 MHz) and band-limited to B_{DTV} with the victim receiver RRC filter applied in post-measurement processing.

3.1. Temporal Analysis

Temporal characteristics of GN signals were evaluated with crossing statistics, which provide probabilities of the time a signal crosses an amplitude threshold and stays either above or below that threshold. Historically, this type of analysis has been used to study pulse statistics of noise [8], hence the terms pulse duration and pulse interval depicted in Figure 17. In this analysis of gated noise, their utility has been extended to the temporal statistics of noise bursts; accordingly, the terminology was changed to burst duration (*BD*) and burst interval (*BI*) as illustrated in Figure 18. For our purposes, the 10th percentile of the cumulative distribution function (*CDF*) of *BD* and *BI* using a threshold equal to -70 dBm was optimal for quantifying the effects of band-limiting on temporal characteristics of the GN signals.

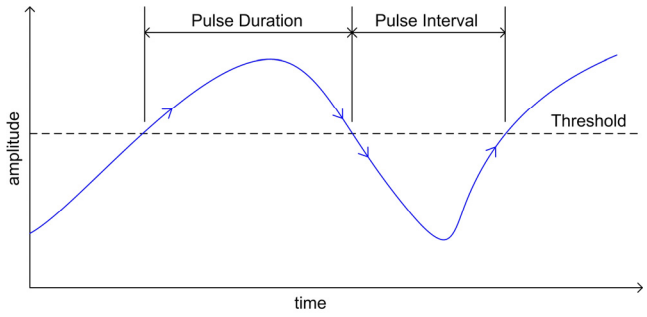

Figure 17. Illustration of pulse duration and pulse interval.

Table 3 summarizes the effects of band-limiting the GN signals to B_{DTV}. Note that *BD* and *BI* are given only when gating was resolved and the *CDF*s provided meaningful estimates of the band-limited on- and off-times, respectively. The band-limited fractional on-time, ζ_{DTV}, was computed as $BD/(BD + BI)$. As expected, band-limiting lengthened on-times, shortened off-times, and increased fractional on-times. Band-limited metrics approached the gating parameters only when τ_{on} and τ_{off} were significantly larger than $1/B_{DTV}$.

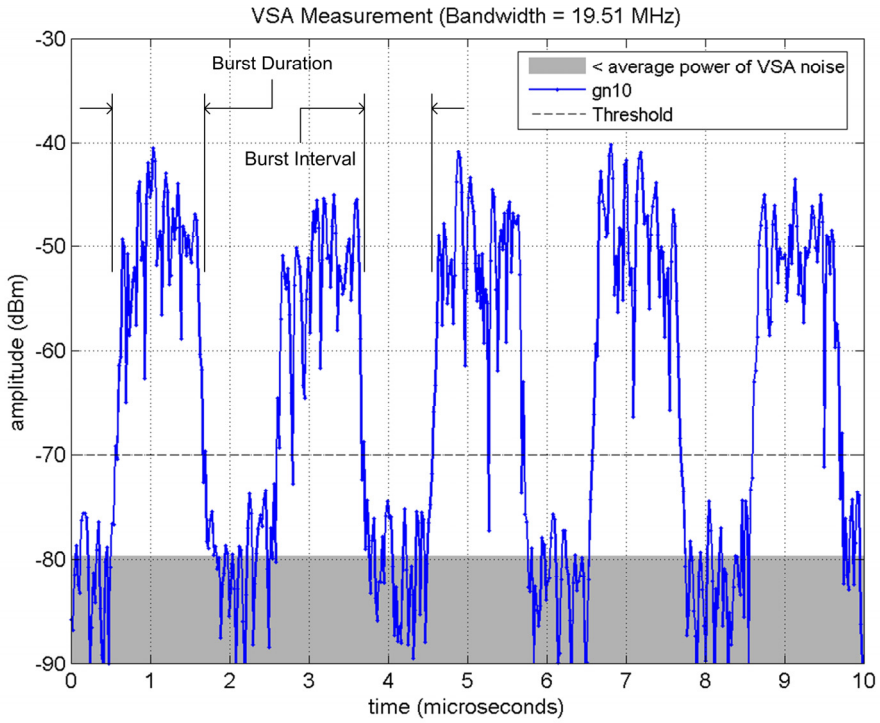

Figure 18. Illustration of burst duration and burst interval.

Table 3. Temporal Characteristics of GN Signals Band-Limited to B_{DTV}

GN	Gating Parameters			Band-Limited Metrics		
	τ_{on} (μs)	τ_{off} (μs)	ζ	BD (μs)	BI (μs)	ζ_{DTV}
01	∞	0.00	1.0000			1.00
02	0.01	0.01	0.5000			1.00
03	0.01	0.03	0.2500			1.00
04	0.01	0.07	0.1250			
05	0.01	0.15	0.0625			
06	0.10	0.10	0.5000			
07	0.10	0.30	0.2500	0.2	0.2	0.50
08	0.10	0.70	0.1250	0.2	0.6	0.25
09	0.10	1.50	0.0625	0.2	1.4	0.13
10	1.00	1.00	0.5000	1.1	0.9	0.55
11	1.00	3.00	0.2500	1.1	2.9	0.28
12	1.00	7.00	0.1250	1.1	6.9	0.14
13	1.00	15.00	0.0625	1.1	14.9	0.07
14	10.00	10.00	0.5000	10.1	9.9	0.51
15	10.00	30.00	0.2500	10.1	29.9	0.253
16	10.00	70.00	0.1250	10.1	69.9	0.126
17	10.00	150.00	0.0625	10.1	149.9	0.063

3.2. Amplitude Analysis

Random amplitudes of the gated-noise signals were characterized with the amplitude probability distribution, which describes the probability that signal amplitude exceeds a certain value. In this report, *APD*s are plotted on Rayleigh graphs where Rayleigh-distributed amplitudes of complex-Gaussian noise appear as a negatively-sloped, straight line. The sorting method, documented in Appendix D of Part 1, was used to estimate and plot *APD*s of 2^{17} = 131,072 samples that are free of correlation introduced by the measurement system and post-measurement band-limiting.

Figures 19 – 22 provide composite *APD* plots of the measured GN signals. Each plot represents a specific τ_{on}, and each curve within a plot represents a different ζ. Dashed lines represent the *APD* of the continuous-noise signal, GN-01. The upper bound of the shaded region is the average power of the VSA noise, approximately -79.7 dBm in B_{DTV}.

Band-limiting had profound effects on the *APD*s of the GN signals. If τ_{off} exceeded $1/B_{DTV}$ a step-like *APD* occurred, where higher amplitudes primarily corresponded to elongated on-times and lower amplitudes to the shortened off-times. This was most pronounced for GN-17 (τ_{on} = 10,000 ns, ζ = 0.0625). If τ_{off} was less than or comparable to $1/B_{DTV}$ a negatively-sloped, straight *APD* occurred, corresponding to Rayleigh-distributed amplitudes due to elongated noise bursts overlapping each other. This was most pronounced for GN-02 (τ_{on} = 10 ns, ζ = 0.50).

Peak-to-average ratio is a metric derived from the *APD* as illustrated in Figure 23 for GN-10. When interpreting *P/A* results, it is important to understand the bandwidth that peak and average powers were measured in, the duration or number of samples, and the statistical definition of peak in terms of percentage of samples. In this study, peak and average powers were measured in the same bandwidth to compute a single *P/A*. Also, peak power is defined as the amplitude exceeded 0.01% of the time, which corresponds to 13 of 131,072 samples. Figure C-2 shows how *P/A* changes with various peak definitions.

Table 4 summarizes measured *P/A* and *APD* characteristics for the band-limited GN signals. Also included are ultra-wide bandwidth limits to *P/A* derived in Section C.1. *APD* characteristics are labeled RAYL for Rayleigh-distributed amplitudes or RG for resolved gating, i.e., step-like *APD* whose amplitude falls below VSA average noise power at least 10% of the time.

Band-limiting affected *P/A*. If τ_{off} far exceeded $1/B_{DTV}$, then *P/A* approached the ultra-wide transmission bandwidth limit. If τ_{off} was less than $1/B_{DTV}$, then *P/A* approached the 9.6-dB value for Rayleigh-distributed amplitudes. When τ_{off} was between these extremes, *P/A* transitioned between the limits.

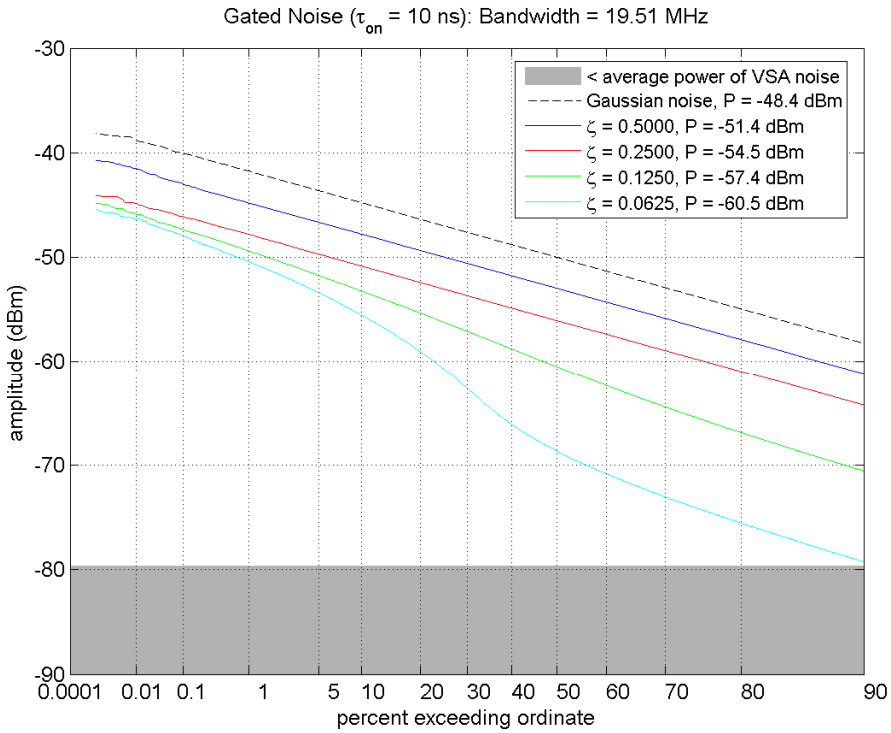

Figure 19. *APD*s of GN signals with τ_{on} = 10 ns band-limited to B_{DTV}.

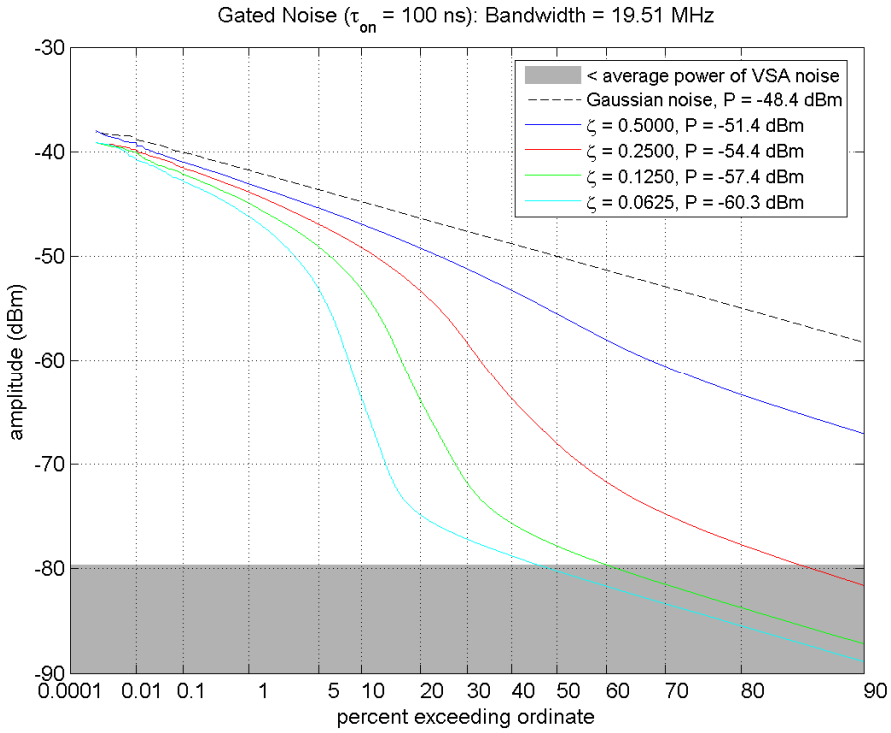

Figure 20. *APD*s of GN signals with τ_{on} = 100 ns band-limited to B_{DTV}.

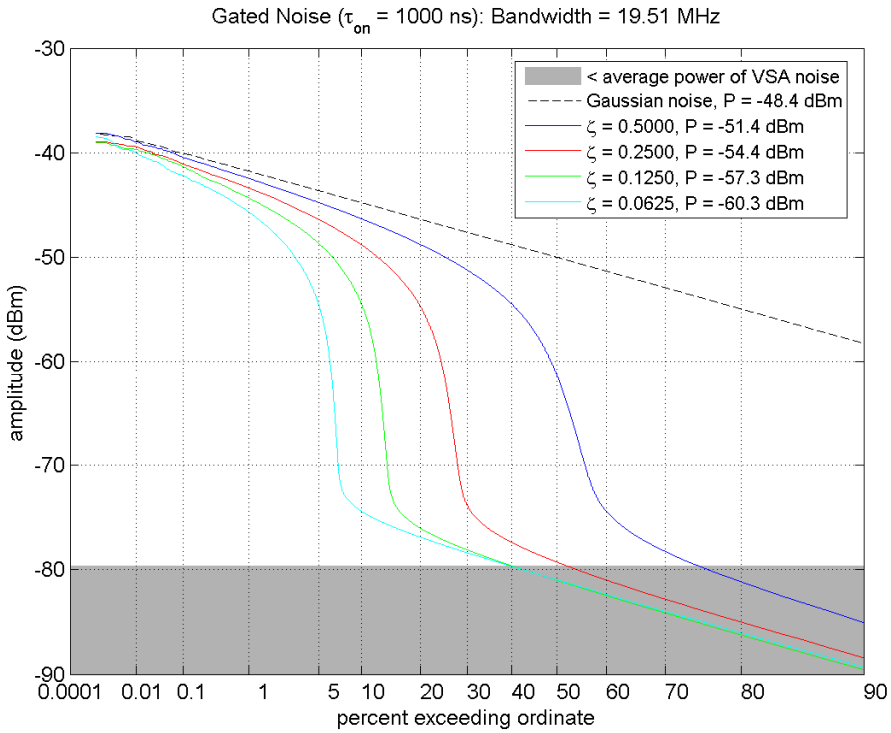

Figure 21. *APD*s of GN signals with τ_{on} = 1,000 ns band-limited to B_{DTV}.

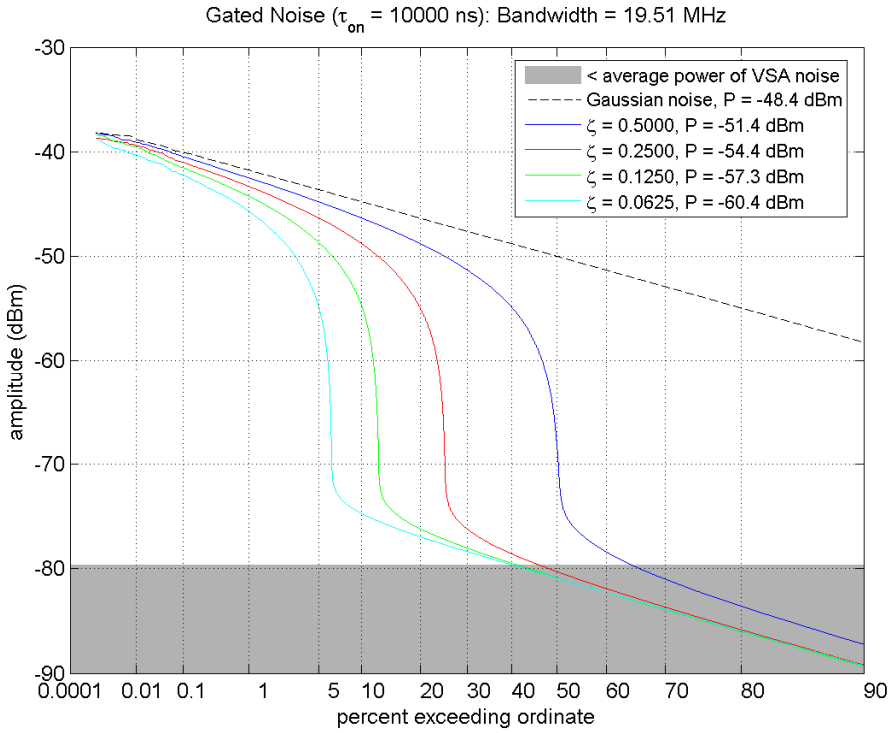

Figure 22. *APD*s of GN signals with τ_{on} = 10,000 ns band-limited to B_{DTV}.

Table 4. Amplitude Characteristics of GN Signals Band-Limited to B_{DTV}

GN	Ultra-wide Bandwidth Limits		Band-Limited Metrics	
	P/A (dB)	*APD*	*P/A* (dB)	*APD*
01	9.6	RAYL	9.6	RAYL
02	12.3	RG	9.9	RAYL
03	14.9	RG	9.7	RAYL
04	17.5	RG	11.5	
05	20.1	RG	14.2	
06	12.3	RG	12.2	
07	14.9	RG	14.6	RG
08	17.5	RG	17.3	RG
09	20.1	RG	19.6	RG
10	12.3	RG	12.4	RG
11	14.9	RG	15.0	RG
12	17.5	RG	17.6	RG
13	20.1	RG	20.3	RG
14	12.3	RG	12.3	RG
15	14.9	RG	15.1	RG
16	17.5	RG	17.8	RG
17	20.1	RG	20.1	RG

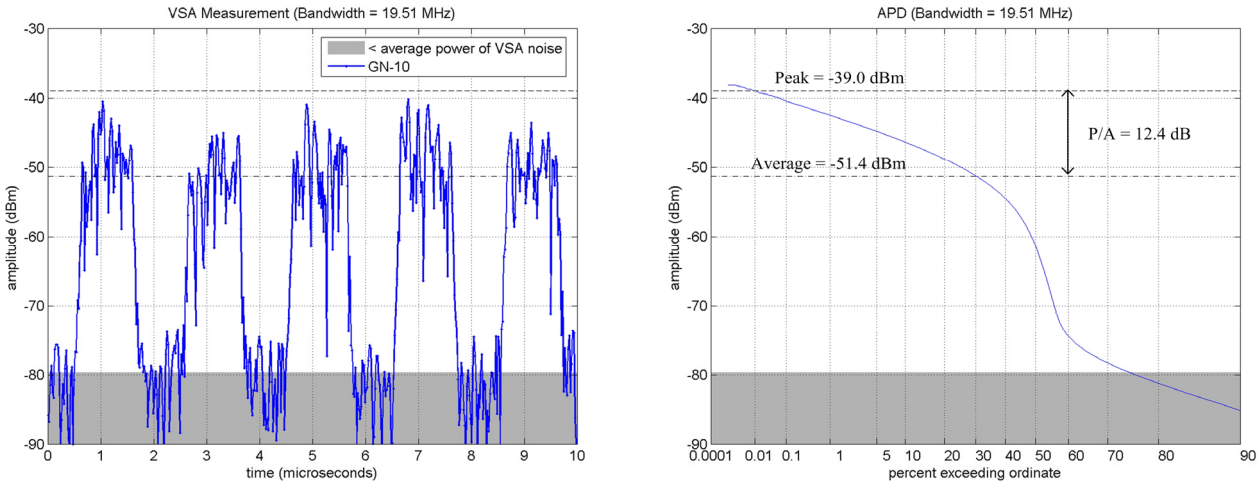

Figure 23. Illustration of *P/A* for GN-10 band-limited to B_{DTV}.

3.3. Spectral Analysis

Spectral characteristics of the gated-noise signals were characterized with the power spectral density, which represents the average power present per unit bandwidth as a function of frequency. Section C.2 provides a theoretical analysis of the *PSD* for gated Gaussian noise. In short, it can be considered to be constant over the bandwidth of interest.

Figures 24 – 27 provide *PSD*s of the GN signals over the entire VSA bandwidth, i.e., the victim receiver RRC filter was not applied to the data in post-measurement processing. *PSD*s were calculated by averaging squared spectrum magnitudes of rectangular-windowed, non-overlapping blocks of signal data. The periodic nature of the GN signals required that the block size be an integer multiple of the gating period. To have the same Δf for all *PSD*s, the block size must also be a common integer multiple of all gating periods. For the GN signals, these requirements were satisfied with a block size of 160 μs, which corresponds to Δf = 6.2 kHz. This allowed 500 blocks to be averaged, given the 4 million samples available in the acquired data sets.

The figures show that the power density of the gated signals decreased in proportion to ζ. In addition, the spectral spike at 0 Hz was due to VSG local-oscillator feed-through. The influence of the VSG local-oscillator feed-through to test results was discussed in Appendix C of Part 1.

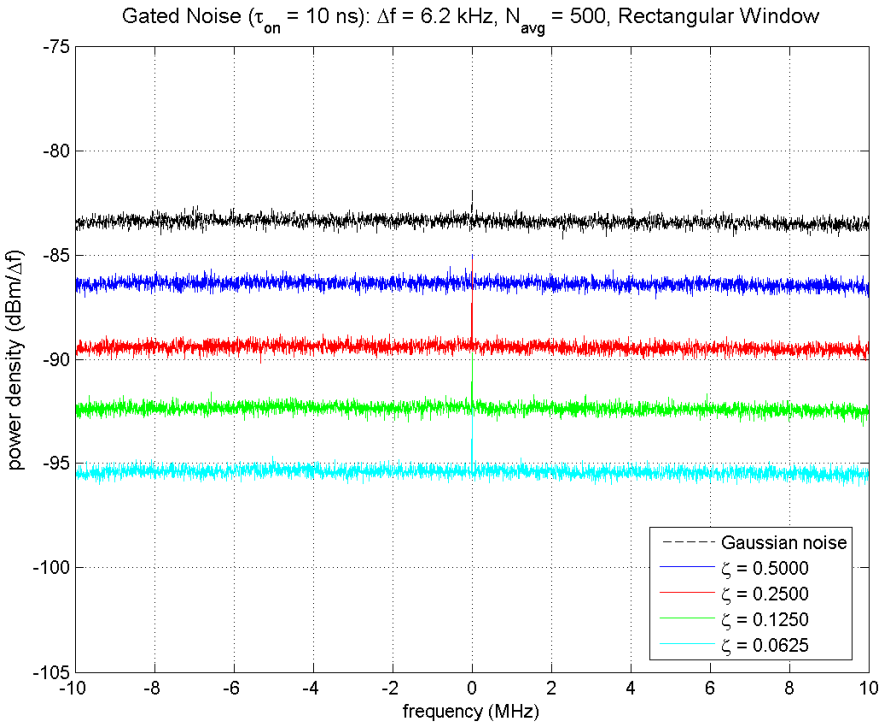

Figure 24. *PSD*s of GN signals with τ_{on} = 10 ns.

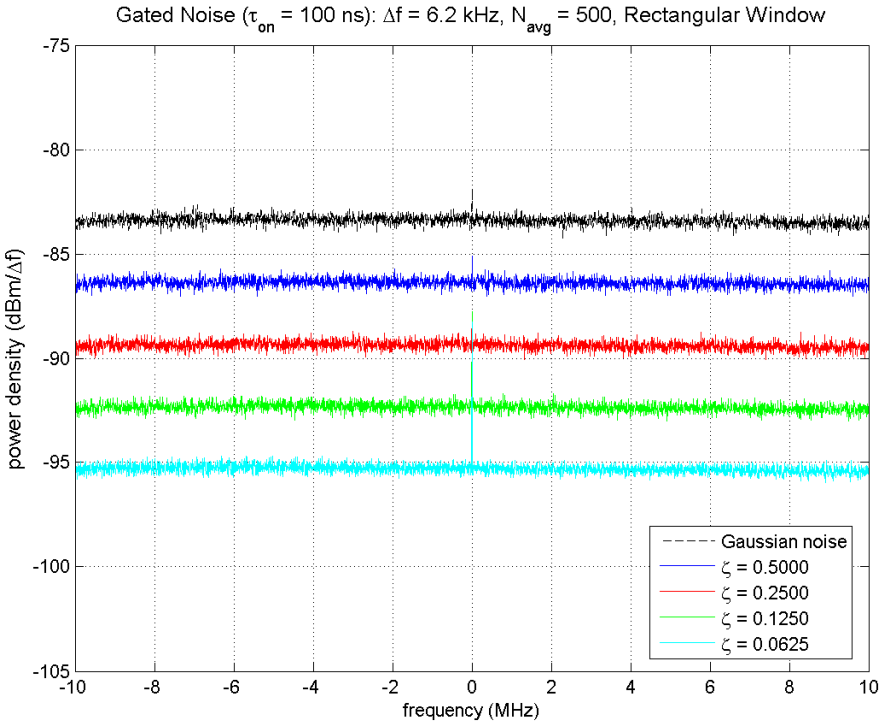

Figure 25. *PSD*s of GN signals with τ_{on} = 100 ns.

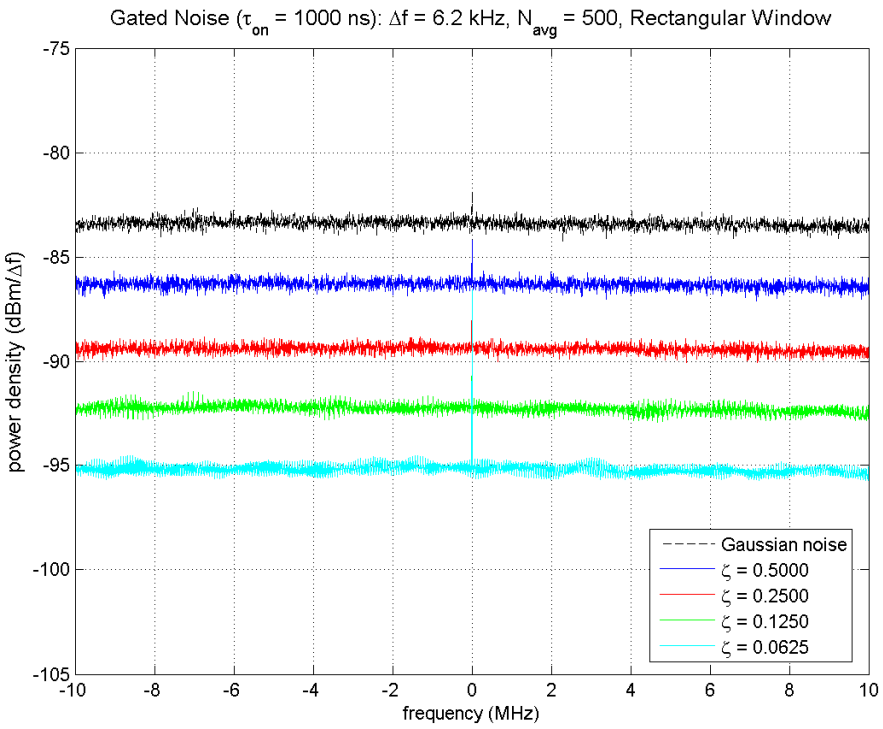

Figure 26. *PSD*s of GN signals with τ_{on} = 1,000 ns.

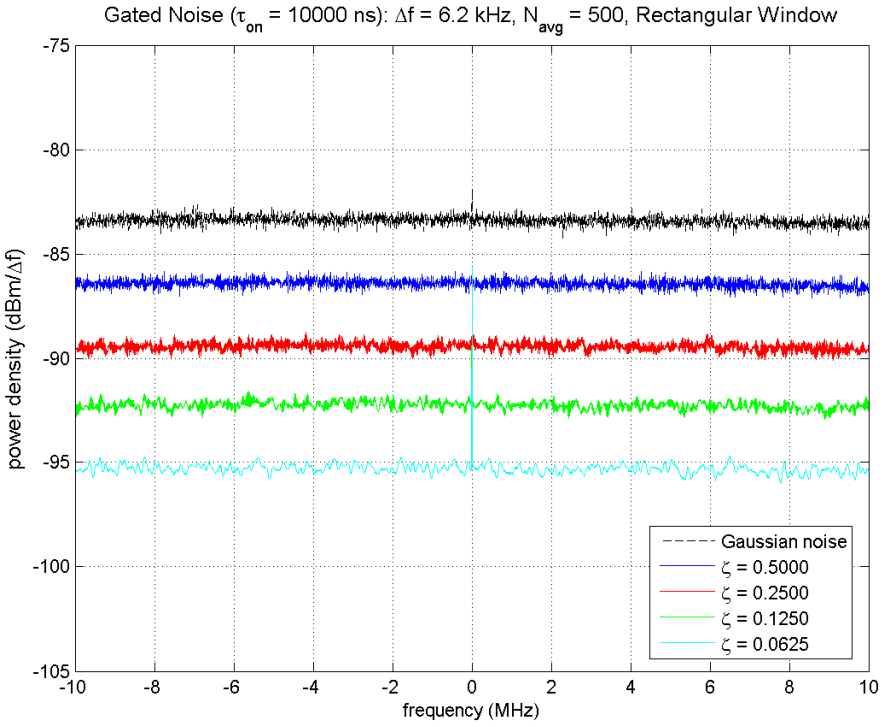

Figure 27. *PSD*s of GN signals with τ_{on} = 10,000 ns.

4. CONCLUSION

The objective of this experiment was to measure and evaluate the susceptibility of a C-band satellite DTV receiver to gated-noise interference. Results in this report have been measured with a reliable test system and repeatable procedures. Validation against theory is demonstrated in Appendix B. Results are expected to be fundamental in understanding interference caused by DS-UWB and MB-OFDM signals. In these concluding remarks, findings are summarized and their significance explained.

Temporal analyses showed that band-limiting the GN interference signals elongated on-times and shortened off-times, which had profound effects on corresponding *APD*s. When τ_{off} was less than or comparable to the receiver reciprocal bandwidth, the elongated on-times overlapped, producing Rayleigh amplitude statistics. When τ_{off} was several times greater than the reciprocal bandwidth, the elongated on-times remained distinct, producing gated-noise amplitude statistics.

These temporal and amplitude observations help explain the susceptibility results. When τ_{off} was less than or comparable to the reciprocal bandwidth, DTV susceptibility results were strictly dependent on average power of the band-limited interference. This is because Rayleigh-distributed amplitudes correspond to zero-mean Gaussian noise, which is completely characterized by its variance or average power. Moreover, the DTV receiver was least susceptible to signals that resembled continuous noise after band-limiting. Conversely, when τ_{off} was several times greater than the reciprocal bandwidth, gating was resolved and susceptibility results were clearly dependent on the gating parameters τ_{on} and ζ. The DTV receiver was more susceptible to the gated-noise signals that maintained some semblance of a gated signal after band-limiting. More specifically, DTV susceptibility increased with increasing τ_{on} and decreasing ζ.

Interestingly, peak-to-average ratios of the band-limited GN signals were also dependent on τ_{on} and ζ. In fact, as demonstrated in Figures 28 – 30, there was some correlation between measured DTV susceptibility and *P/A*, i.e., DTV was more susceptible to GN interference with higher *P/A*. However, these figures also show distinct separation between τ_{on} curves, which indicates that *P/A* alone cannot serve as a sole predictor of DTV interference susceptibility.

In summary, DTV susceptibility to gated-noise interference cannot be predicted by interference power characteristics alone. Indeed, it is essential to consider the temporal parameters of the interfering signal as well as the bandwidth of the victim receiver. Additionally, FEC performance trends, characterized by BER_{TOV}, behaved similar to DTV susceptibility trends, leading to the conclusion that DTV susceptibility is determined largely by FEC performance.

Caution is advised when extending these results to small ζ. For example, it is entirely likely that low susceptibility could be achieved for each τ_{on} provided ζ is sufficiently small, which may create conditions more favorable to FEC performance or simply provide longer off-times where errors are unlikely. Determination of these conditions is beyond the scope of this report.

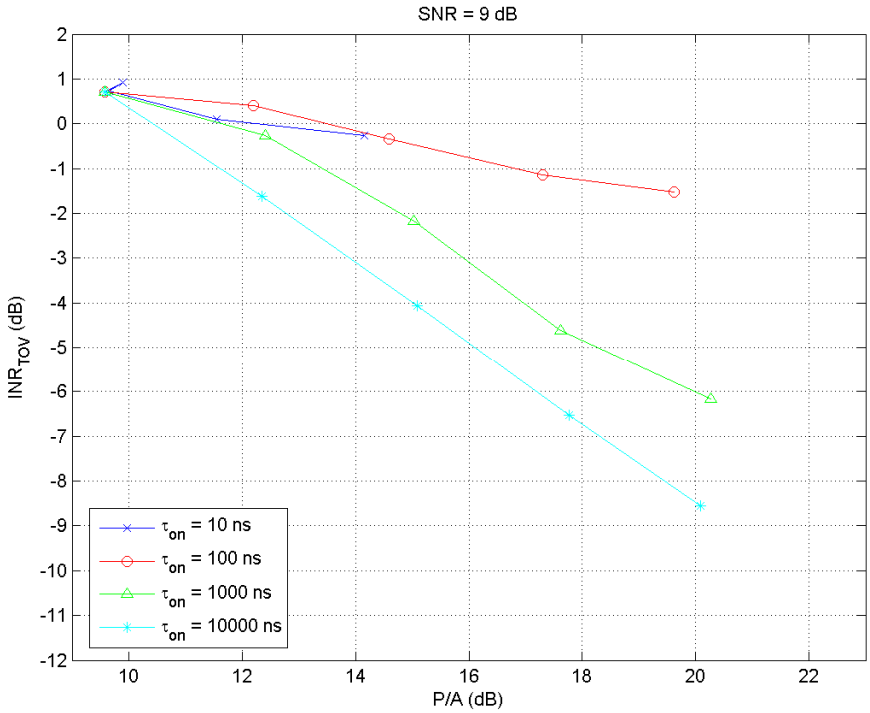

Figure 28. *INR*$_{TOV}$ versus *P/A* for a DTV receiver operating at *SNR* = 9 dB and exposed to GN interference.

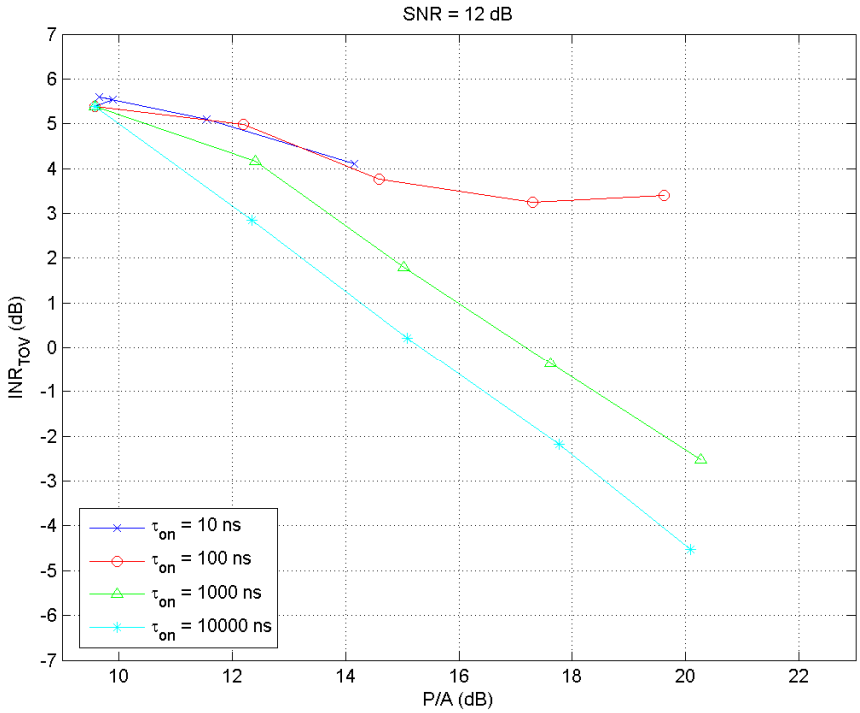

Figure 29. *INR*$_{TOV}$ versus *P/A* for a DTV receiver operating at *SNR* = 12 dB and exposed to GN interference.

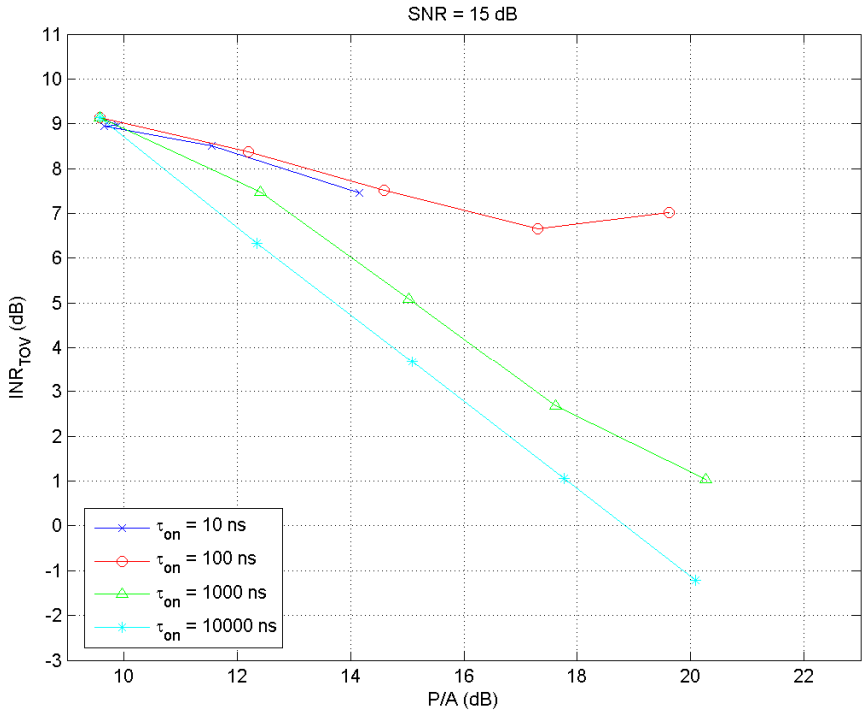

Figure 30. *INR_{TOV}* versus *P/A* for a DTV receiver operating at *SNR* = 15 dB and exposed to GN interference.

5. ACKNOWLEDGMENTS

The authors recognize John McCorkle of Freescale, Inc. for his leadership, insight, and insistence on the highest quality. We learned a great deal from working with John in all relevant technical areas.

This investigation required the services of a number of ITS engineers with a broad range of expertise, some of whom are not included in the list of authors. The authors recognize Brent Bedford for his expertise in test and measurement equipment and techniques; Randy Hoffman, Richard Statz, and Steve Engelking for developing much of the low level software routines needed to automate the experiment via software control; Stephen Wolf for his expertise in video quality assessment; Frank Sanders for sharing knowledge learned in previous interference tests on C-band earth station receivers [9]; Dr. Roger Dalke for his knowledge of random processes and experimental uncertainty analyses; Andrew Rogers and Michael Mitchell for their attention to detail in hardware production and signal characterization measurements; and Dr. William Kissick for his support and leadership.

6. REFERENCES

[1] "First Report and Order in the matter of ET Docket 98-153 (Revision of Part 15 of the Commission's Rules Regarding Ultra-Wideband Transmission Systems)," *FCC 02-48*, adopted Feb. 14, 2002, released Apr. 22, 2002.

[2] W.A. Kissick, Ed., "The temporal and spectral characteristics of ultrawideband signals," NTIA Report 01-383, Jan. 2001.

[3] J.R. Hoffman, M.G. Cotton, R.J. Achatz, R.N. Statz, and R.A. Dalke, "Measurements to determine potential interference to GPS receivers from ultrawideband transmission systems," NTIA Report 01-384, Feb. 2001.

[4] J.R. Hoffman, M.G. Cotton, R.J. Achatz, and R.N. Statz, "Addendum to NTIA Report 01-384: Measurements to determine potential interference to GPS receivers from ultrawideband transmission systems," NTIA Report 01-389, Sep. 2001.

[5] J.R. Hoffman, E.J. Haakinson, and Y. Lo, "Measurements to determine potential interference to public safety radio receivers from ultrawideband transmission systems," NTIA Report 03-396, Apr. 2003.

[6] M. Cotton, R. Achatz, J. Wepman, B. Bedford, "Ultrawideband interference potential: Part 1 – Procedures to characterize ultrawideband emissions and characterize interference susceptibility of C-band satellite digital television receivers," NTIA Report TR-05-419, Feb. 2005.

[7] J.C. Whitaker, "Digital television transmission systems," Ch. 13 in *Standard Handbook of Video and Television Engineering*, J.C. Whitaker, Ed., New York, NY: McGraw-Hill, 2000.

[8] L.R. Espeland and A.D. Spaulding, "Amplitude and time statistics for atmospheric radio noise," ESSA Technical Memorandum, ERLTM-ITS 253, Sep. 1970.

[9] F. Sanders, "Measurements of pulsed co-channel interference in a 4-GHz digital earth station receiver," NTIA Report 02-393, May 2002.

[10] ETS 300 421: "Digital broadcasting systems for television, sound, and data services: Framing structure, channel coding, and modulation for 11/12 GHz satellite services," *European Telecommunications Standards Institute*, Dec. 1994.

[11] ETSI TR 101 290: "Digital Video Broadcasting (DVB); Measurement guidelines for DVB systems," *European Telecommunications Standards Institute*, v1.2.1, 2001.

APPENDIX A: EXTENSION OF EXPERIMENT TO GN(MB) SIGNALS

This appendix provides susceptibility and characterization measurements for gated-noise signals that emulate MB-OFDM, i.e., GN(MB) signals. Recall that MB-OFDM is an ultrawideband (UWB) signal that hops between 14 bands according to a specified time-frequency code; it is specified by the number of bands (b) it hops between and the number of consecutive dwells (d) the signal stays in a particular band. To a relatively narrowband victim receiver, MB-OFDM appears as gated interference. Table A-1 provides the MB-OFDM parameters, i.e., b and d, and corresponding gating parameters, i.e., on-time (τ_{on}), off-time (τ_{off}), and fractional on-time (ζ). Gating parameters are illustrated in Figure A-1 for GN(MB)-03.

Table A-1. GN(MB) Gating Parameters

GN (MB)	MB-OFDM Parameters		Gating Parameters		
	b	d	τ_{on} (μs)	τ_{off} (μs)	ζ
01	1	1	0.24	0.07	0.7758
02	3	1	0.24	0.70	0.2586
03	3	2	0.55	1.32	0.2586
04	7	1	0.24	1.95	0.1108
05	7	2	0.55	3.82	0.1108
06	7	6	1.80	11.32	0.1108
07	13	1	0.24	3.82	0.0597
08	13	2	0.55	7.57	0.0597
09	13	12	3.68	45.07	0.0597

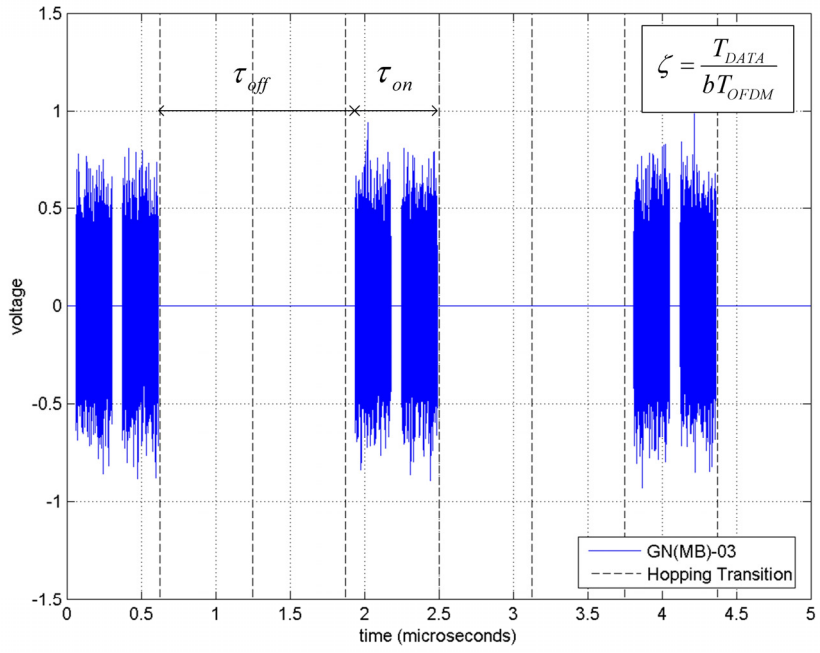

Figure A-1. Simulated gated-noise signal, GN(MB)-03.

From the perspective of a victim receiver, MB-OFDM has two gating processes associated with: (1) hopping and (2) insertion of zero-prefix and guard-intervals in each MB-OFDM symbol. Each MB-OFDM symbol is comprised of a zero-prefix, data block, and guard interval; the MB-OFDM symbol period is the sum of its constituents, i.e., $T_{OFDM} = T_{ZP} + T_{DATA} + T_{GI}$, where T_{ZP} = 60.6 ns, T_{DATA} = 242.4 ns, and T_{GI} = 9.5 ns. Fractional on-time is calculated as $\zeta = T_{DATA} / bT_{OFDM}$. τ_{on} is approximated by including the zero-prefix and guard interval between consecutive dwells and excluding those adjacent to hopping transitions,

$$\tau_{on} \approx dT_{OFDM} - T_{ZP} - T_{GI} \quad .$$

Accordingly, τ_{off} is approximated as

$$\tau_{off} \approx (b-1)dT_{OFDM} + T_{ZP} + T_{GI} \quad .$$

A.1. DTV Susceptibility to GN(MB) Interference

Figures A-2 – A-7 provide measured segment error rate (*SER*) and pre-Viterbi bit error rate (*BER*) versus interference-to-noise ratio (*INR*). These composite graphs for GN(MB) signals correspond to Figures 3 – 8 for GN signals in the main text.

Figures A-8 – A-13 plot INR_{TOV} and BER_{TOV} versus $1/\zeta$ in dB, where ζ = {0.78, 0.26, 0.11, 0.06} correspond to $10\log(1/\zeta)$ = {1.10, 5.87, 9.55, 12.24} dB. These composite graphs for GN(MB) signals correspond to Figures 10 – 15 for GN signals. Table A-2 provides INR_{TOV} and BER_{TOV} for GN(MB) signals as Table 2 does for GN signals.

There is no one-to-one correspondence for gating parameters between the two sets. For example, $\tau_{on} \approx$ {0.24, 0.55, 1.80, 3.68} μs for GN(MB) are different than τ_{on} = {0.01, 0.10, 1.00, 10.00} μs for GN and $10\log(1/\zeta)$ = {1.10, 5.87, 9.55, 12.24} dB for GN(MB) are different than $10\log(1/\zeta)$ = {0.00, 3.01, 6.02, 9.03, 12.04} dB for GN. In spite of these discrepancies, GN(MB) results lie where expected in the region bounded by 0.10- to 10.00-μs τ_{on} curves.

Table A-2. Measured DTV Susceptibility and FEC Performance for GN(MB) Interference

GN (MB)	Gating Parameters			*SNR* = 9 dB		*SNR* = 12 dB		*SNR* = 15 dB	
	τ_{on} (μs)	τ_{off} (μs)	ζ	INR_{TOV} (dB)	BER_{TOV}	INR_{TOV} (dB)	BER_{TOV}	INR_{TOV} (dB)	BER_{TOV}
01	0.24	0.07	0.7758	0.5	0.037	5.2	0.036	8.5	0.036
02	0.24	0.70	0.2586	-0.7	0.030	3.7	0.027	7.0	0.028
03	0.55	1.32	0.2586	-0.9	0.028	3.5	0.025	6.5	0.025
04	0.24	1.95	0.1108	-1.9	0.022	2.3	0.018	5.8	0.019
05	0.55	3.82	0.1108	-3.2	0.018	0.8	0.013	4.2	0.013
06	1.80	11.32	0.1108	-5.0	0.015	-1.2	0.009	2.3	0.009
07	0.24	3.82	0.0597	-3.3	0.016	0.7	0.012	4.3	0.011
08	0.55	7.57	0.0597	-5.1	0.014	-1.1	0.009	2.3	0.008
09	3.68	45.07	0.0597	-7.4	0.011	-3.3	0.005	-0.3	0.005

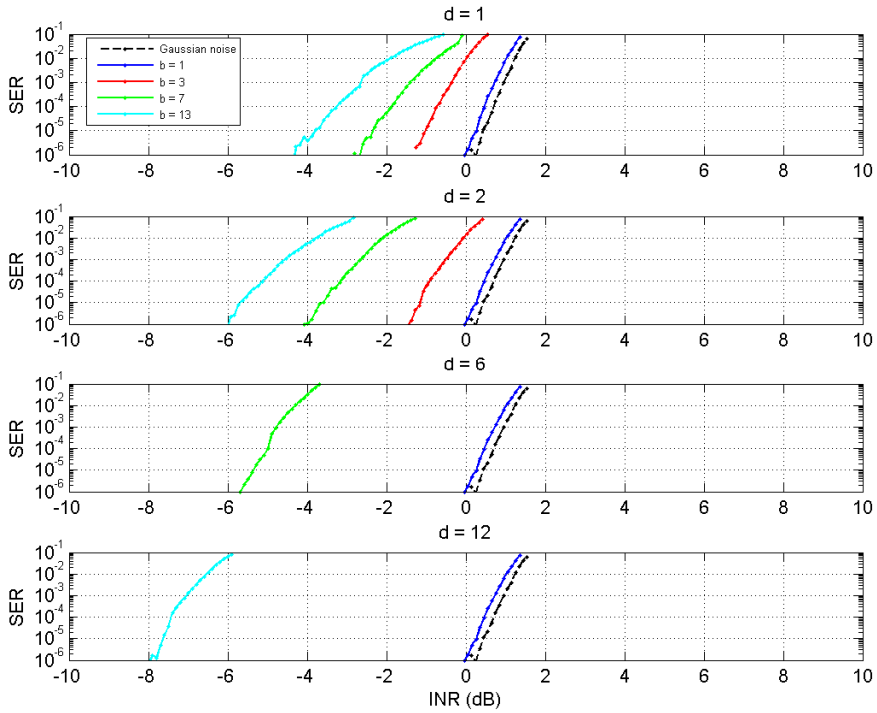

Figure A-2. *SER* versus *INR* for a DTV receiver operating at *SNR* = 9 dB and exposed to GN(MB) interference.

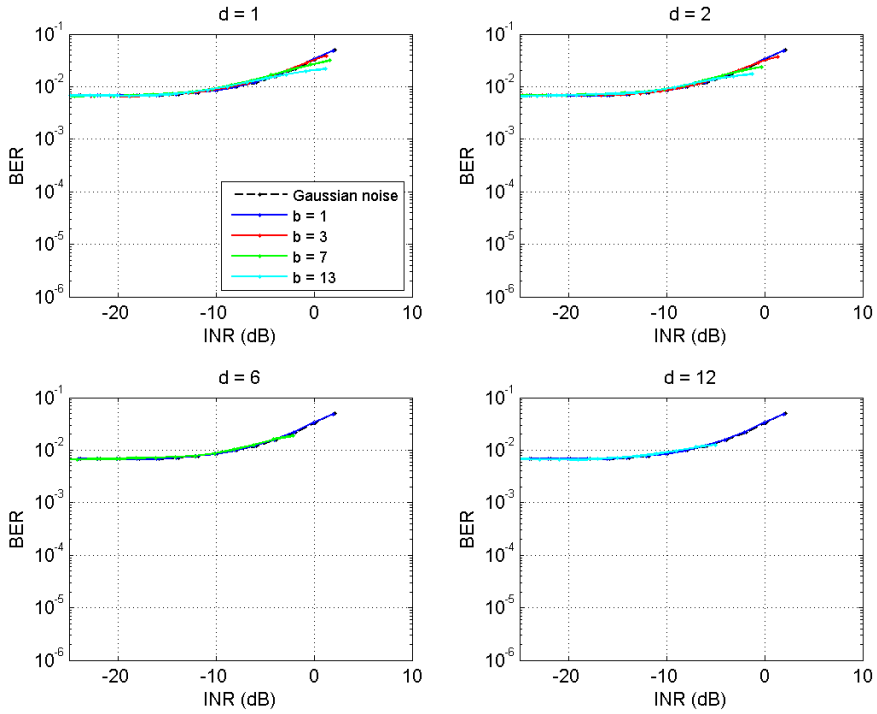

Figure A-3. *BER* versus *INR* for a DTV receiver operating at *SNR* = 9 dB and exposed to GN(MB) interference.

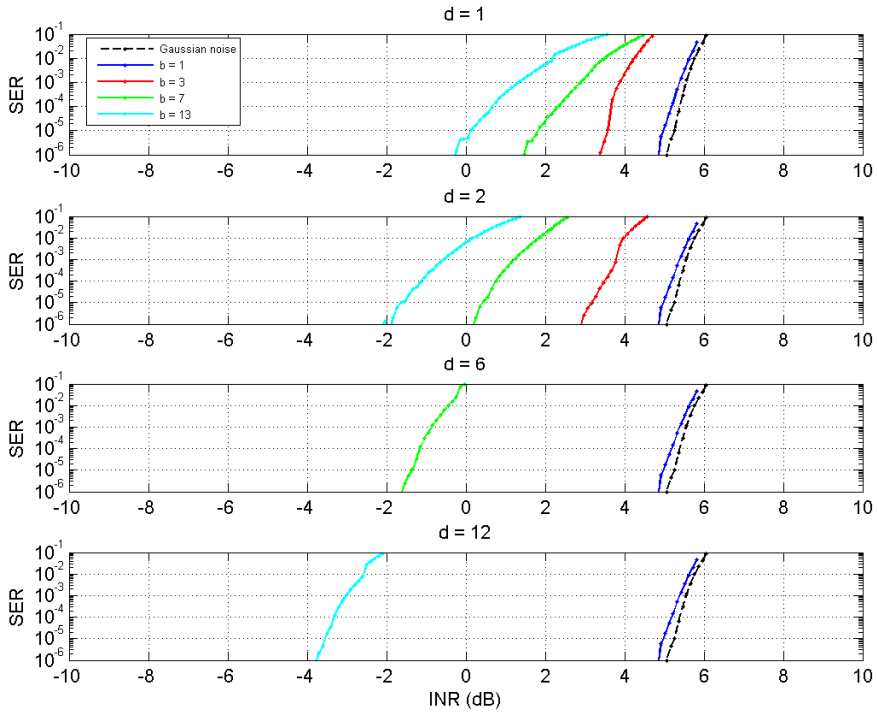

Figure A-4. *SER* versus *INR* for a DTV receiver operating at *SNR* = 12 dB and exposed to GN(MB) interference.

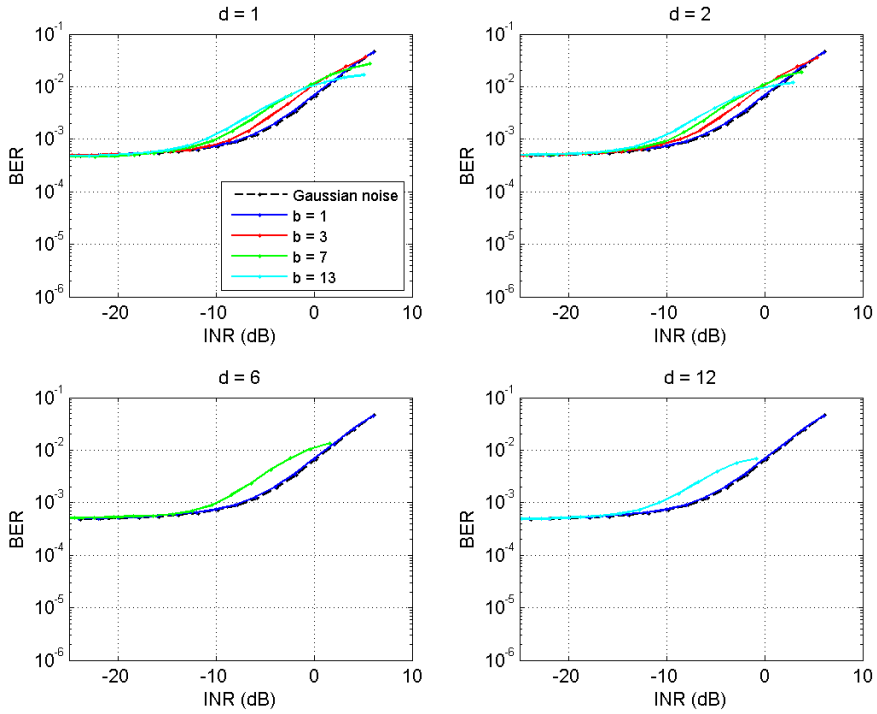

Figure A-5. *BER* versus *INR* for a DTV receiver operating at *SNR* = 12 dB and exposed to GN(MB) interference.

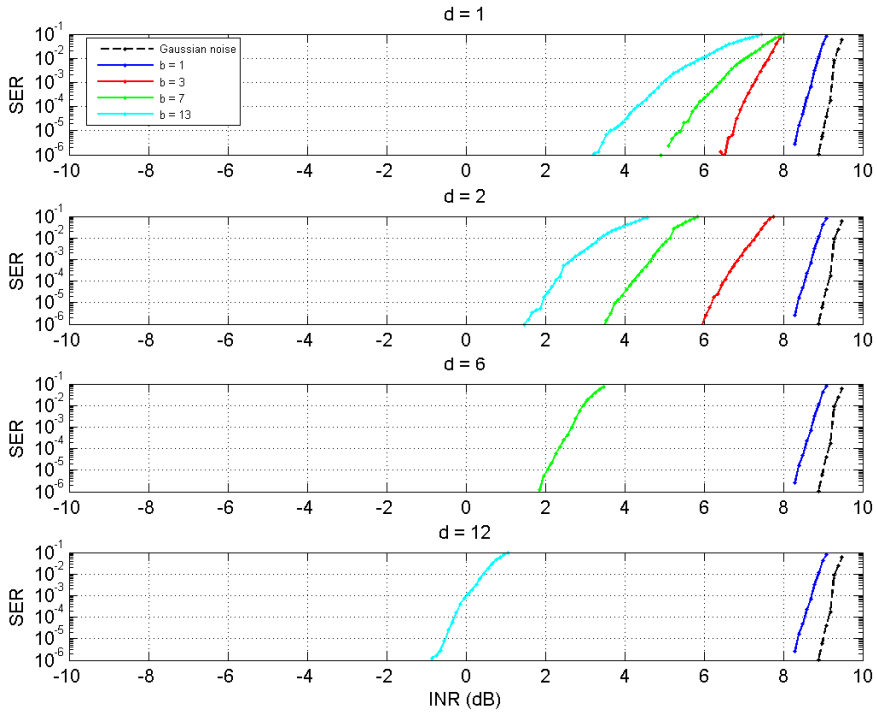

Figure A-6. *SER* versus *INR* for a DTV receiver operating at *SNR* = 15 dB and exposed to GN(MB) interference.

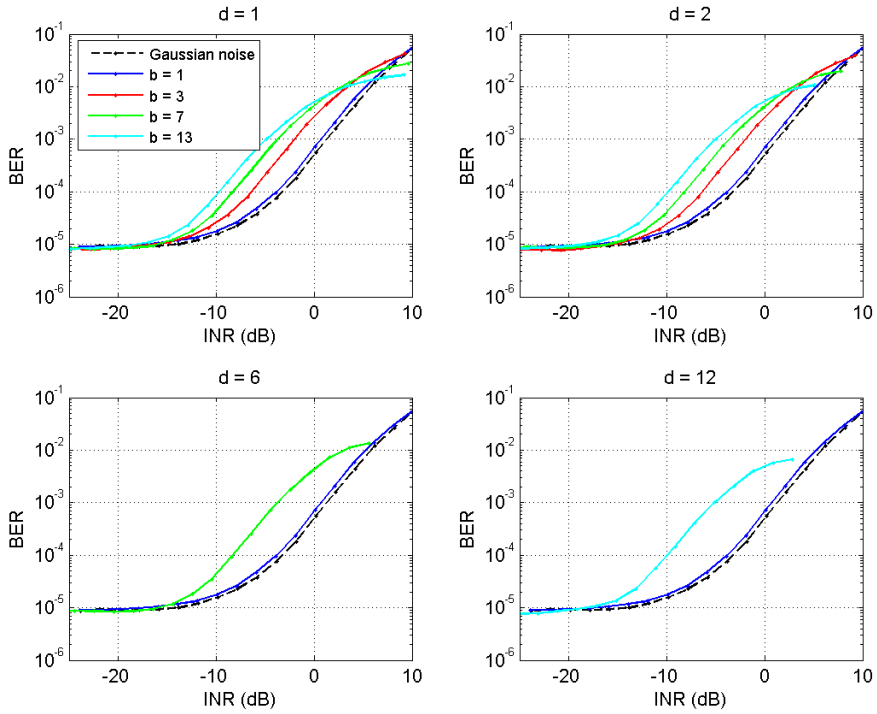

Figure A-7. *BER* versus *INR* for a DTV receiver operating at *SNR* = 15 dB and exposed to GN(MB) interference.

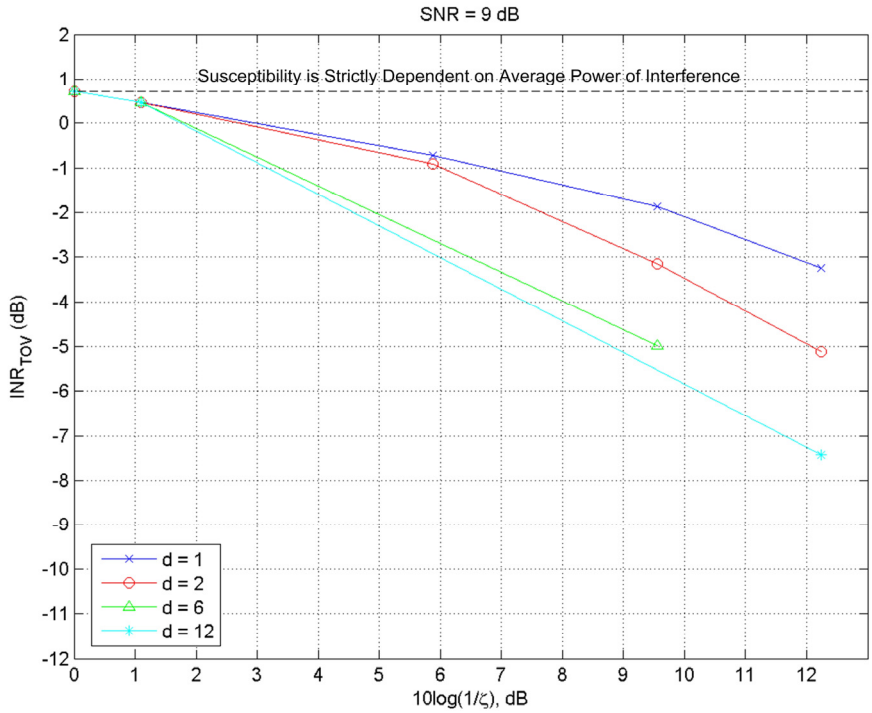

Figure A-8. INR_{TOV} versus 10log(1/ζ) for a DTV receiver operating at SNR = 9 dB and exposed to GN(MB) interference.

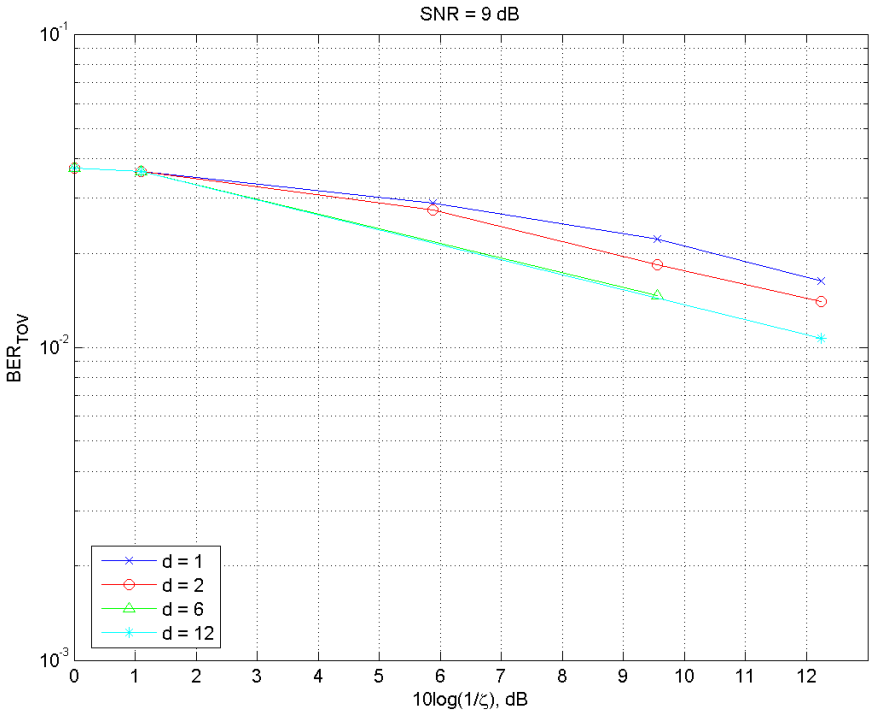

Figure A-9. BER_{TOV} versus 10log(1/ζ) for a DTV receiver operating at SNR = 9 dB and exposed to GN(MB) interference.

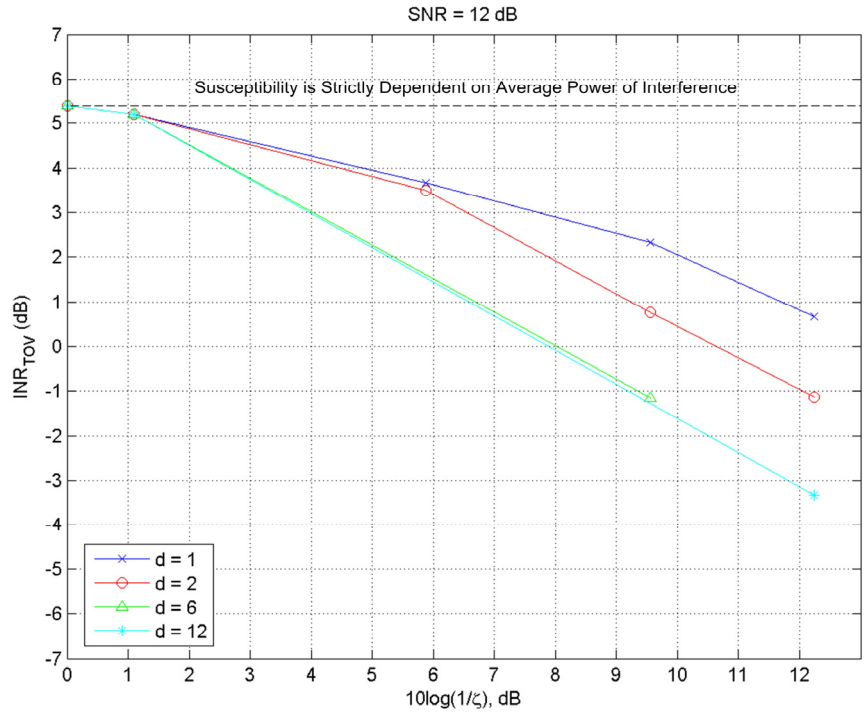

Figure A-10. INR_{TOV} versus 10log(1/ζ) for a DTV receiver operating at SNR = 12 dB and exposed to GN(MB) interference.

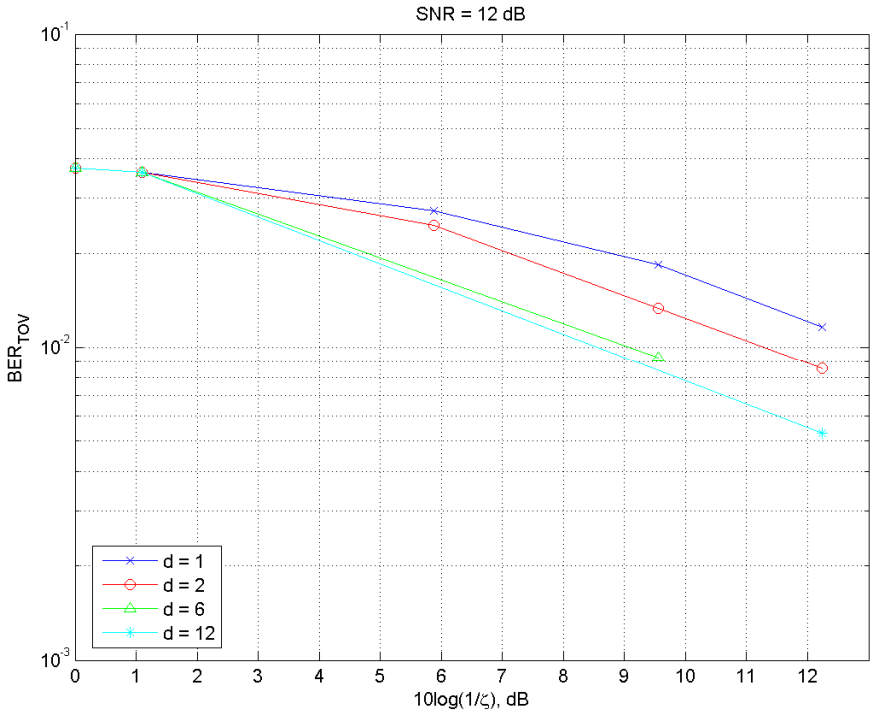

Figure A-11. BER_{TOV} versus 10log(1/ζ) for a DTV receiver operating at SNR = 12 dB and exposed to GN(MB) interference.

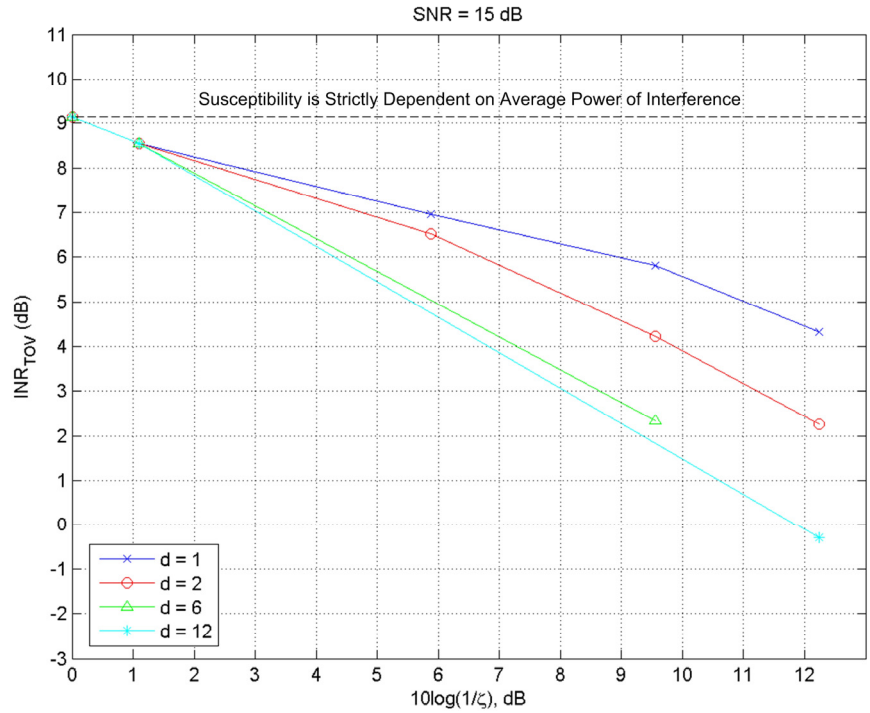

Figure A-12. INR_{TOV} versus 10log(1/ζ) for a DTV receiver operating at SNR = 15 dB and exposed to GN(MB) interference.

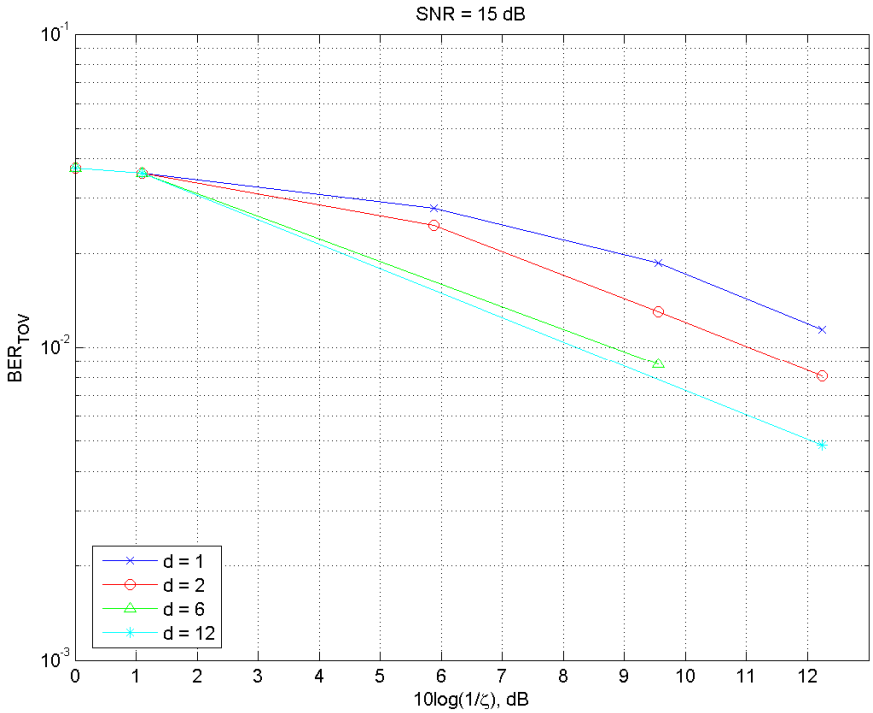

Figure A-13. BER_{TOV} versus 10log(1/ζ) for a DTV receiver operating at SNR = 15 dB and exposed to GN(MB) interference.

A.2. Characterization of GN(MB) Signals

Table A-3 provides band-limited temporal metrics compared to the approximate gating parameters of the GN(MB) signals. Table A-3 provides temporal characteristics of GN(MB) signals as Table 3 does for GN signals.

Table A-3. Temporal Characteristics of GN(MB) Signals Band-Limited to B_{DTV}

GN (MB)	Gating Parameters			Band-Limited Metrics		
	τ_{on} (μs)	τ_{off} (μs)	ζ	BD (μs)	BI (μs)	ζ_{DTV}
01	0.24	0.07	0.7758			
02	0.24	0.70	0.2586	0.4	0.6	0.40
03	0.55	1.32	0.2586	0.7	1.2	0.37
04	0.24	1.95	0.1108	0.4	1.8	0.18
05	0.55	3.82	0.1108	0.7	3.7	0.16
06	1.80	11.32	0.1108	1.9	11.2	0.15
07	0.24	3.82	0.0597	0.4	3.7	0.10
08	0.55	7.57	0.0597	0.7	7.4	0.09
09	3.68	45.07	0.0597	3.8	44.9	0.08

Figures A-14 and A-15 provide amplitude probability distributions (*APD*s) of single- and multi-dwell GN(MB) signals, respectively. Table A-4 provides band-limited amplitude metrics compared to the corresponding ultra-wide bandwidth limits. Table A-4 provides amplitude characteristics of GN(MB) signals as Table 4 does for GN signals.

Table A-4. Amplitude Characteristics of GN(MB) Signals Band-Limited to B_{DTV}

GN (MB)	Ultra-wide Bandwidth Limits		Band-Limited Metrics	
	P/A (dB)	*APD*	*P/A* (dB)	*APD*
01	10.6	RG	10.5	
02	14.8	RG	14.7	RG
03	14.8	RG	14.6	RG
04	18.0	RG	18.0	RG
05	18.0	RG	17.9	RG
06	18.0	RG	17.8	RG
07	20.3	RG	20.2	RG
08	20.3	RG	20.1	RG
09	20.3	RG	19.9	RG

Figures A-16 – A-17 provide power spectral densities (*PSD*s) for the GN(MB) signals. *PSD*s were calculated as described in Section 3.3. Block length was chosen as 170.6 μs (Δf = 5.9 kHz), which allowed 500 averages. The *PSD* of GN(MB)-09 (b = 13, d = 12) was excluded because it would have forced the number of averages to be less than 500. In Figure A-17, the *PSD* of GN(MB)-05 (b = 7, d = 2) is directly beneath GN(MB)-06 (b = 7, d = 6).

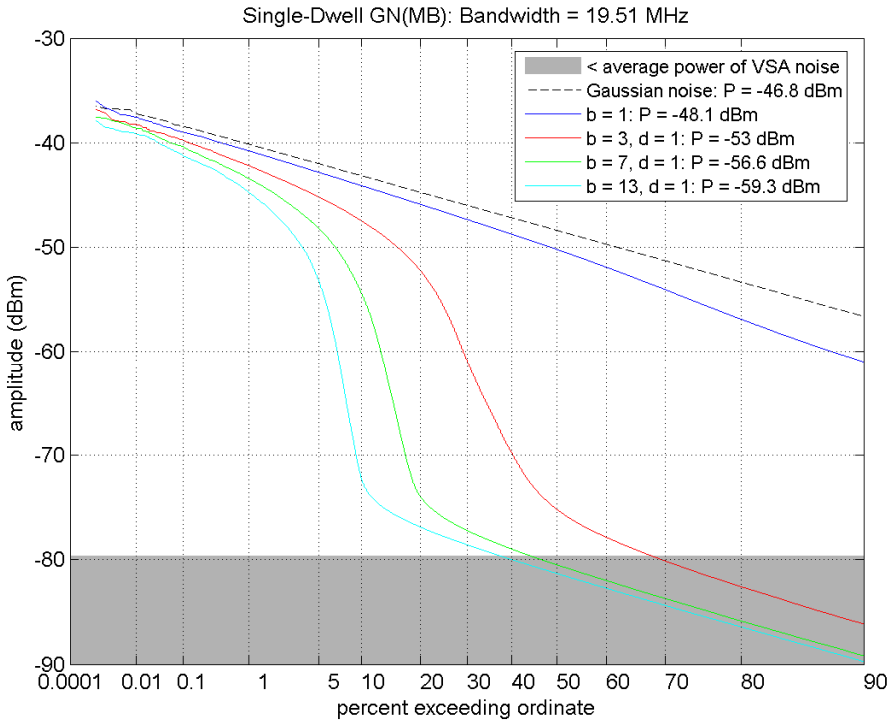

Figure A-14. *APD*s of single-dwell GN(MB) signals band-limited to B_{DTV}.

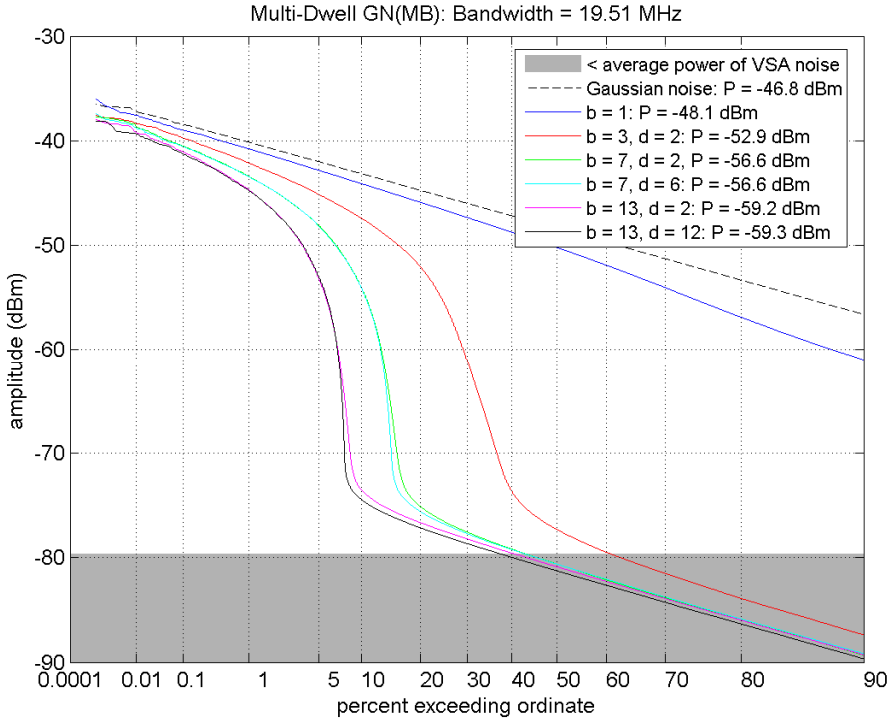

Figure A-15. *APD*s of multi-dwell GN(MB) signals band-limited to B_{DTV}.

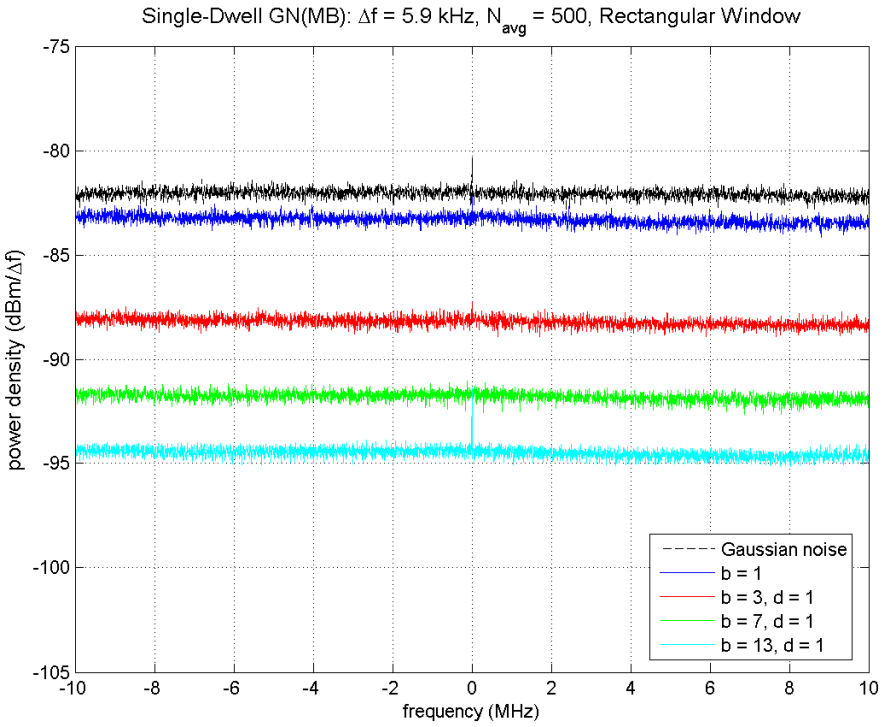

Figure A-16. *PSD*s of single-dwell GN(MB) signals.

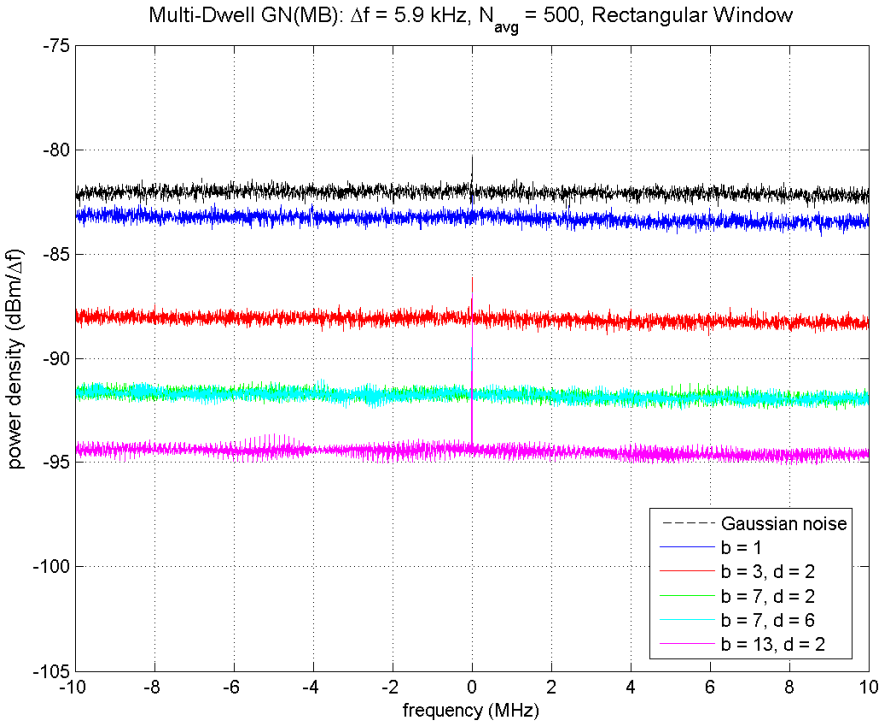

Figure A-17. *PSD*s of multi-dwell GN(MB) signals.

APPENDIX B: VERIFICATION OF SUSCEPTIBILITY RESULTS

Susceptibility of C-band satellite digital television (DTV) to gated-noise interference was measured with the test system and procedures described in Part 1 [6]. These tests measured effects on DTV signal quality due to increasing levels of interference. DTV signal quality metrics collected during the tests include modulation error ratio (*MER*), pre-Viterbi bit error rate (*BER*), and post-Reed-Solomon segment error rate (*SER*).

From the point of view of interference susceptibility tests, it is essential that signal power measurements and DTV signal quality metrics be precisely defined. This appendix gives an overview of the test system, provides precise measurement definitions for signal-to-noise ratio (*SNR*), interference-to-noise ratio (*INR*), *MER*, *BER*, and *SER*, and provides some degree of validation via comparison of theoretical and measured DTV signal quality metrics for Gaussian noise degradation.

B.1. Test System Overview

The test system was designed to inject carefully characterized interference into an operating satellite DTV receiver and measure susceptibility of the receiver with precisely defined DTV signal quality metrics. Figure B-1 is a block diagram of the test system hardware. In this figure BPF, LPF, and LNB correspond to bandpass filter, lowpass filter, and low-noise block downconverter.

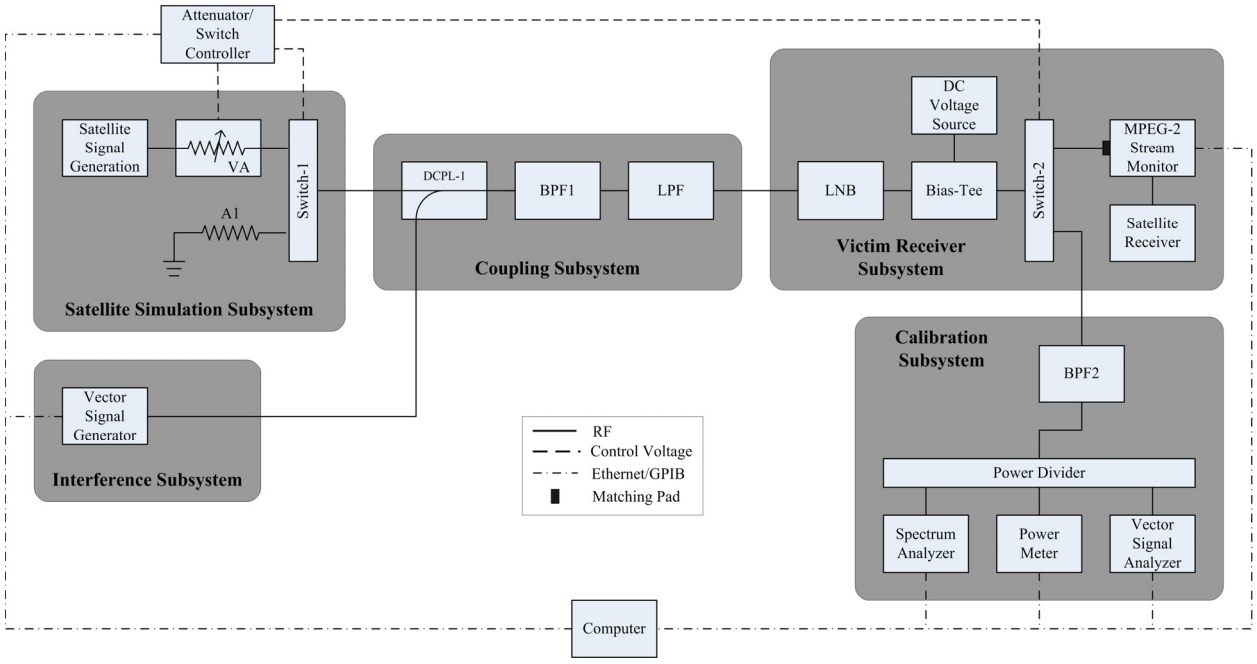

Figure B-1. Block diagram of DTV interference susceptibility test system.

The test system:

- simulated interference signals in software, so the widest range of UWB signal parameters were available for testing;
- generated interference signals with a vector signal generator (VSG), so *INR* was precisely controlled;
- characterized interference signals with a vector signal analyzer (VSA), which provided both amplitude and phase information for post-measurement analyses;
- simulated the satellite signal, so that scene content and *SNR* were controlled;
- conductively coupled signals to the satellite receiver, so uncertainties introduced by radio channel interference, attenuation, and distortion were eliminated;
- evaluated performance degradation objectively and quantitatively with DTV signal quality metrics from an MPEG-2 stream monitor;
- was completely characterized, so that its effects on the test were known;
- was under software control to eliminate procedural errors.

For this test, the operational scenario is summarized in Table B-1. Compression, modulation, and error correction schemes comply with digital video broadcast (DVB) recommendations described in *ETS 300 421* [10].

Table B-1. Operational Scenario for DTV Interference Susceptibility Tests

Transponder Center Frequency	3820 MHz
Modulation	QPSK with root-raised cosine filter ($\alpha = 0.35$)
Compression	MPEG-2
Data Rate	26.970353 Mbps
Symbol Rate	R_S = 19.510468 Mbaud
Segment Rate	R_{seg} = 17,932 segments/second
Reed-Solomon Error Correction	R_{RS} = 188/204
Convolutional Error Correction	R_{conv} = 3/4, K = 7
Interleaving	Depth = 12 bytes
Signal-to-Noise Ratio	{8.5, 11.5, 14.5} dB

B.2. Signal Calibration

At the beginning of each test, the system was calibrated to ensure that all hardware was operating properly and *SNR* and *INR* were correct. Figure B-2 provides a simplified model of the four calibration measurements: (m_1) VSA noise, (m_2) combined system noise and VSA noise, (m_3) combined DTV signal, system noise, and VSA noise, and (m_4) combined interference, system noise, and VSA noise. For these measurements, DTV signal power was set to a level corresponding to the appropriate *SNR*, the interfering signal power was set to a level that produced an accurate VSA measurement, and a 36-MHz VSA span was used. The satellite signal path (SSP) and interference signal path (ISP) were characterized in Appendix F of Part 1.

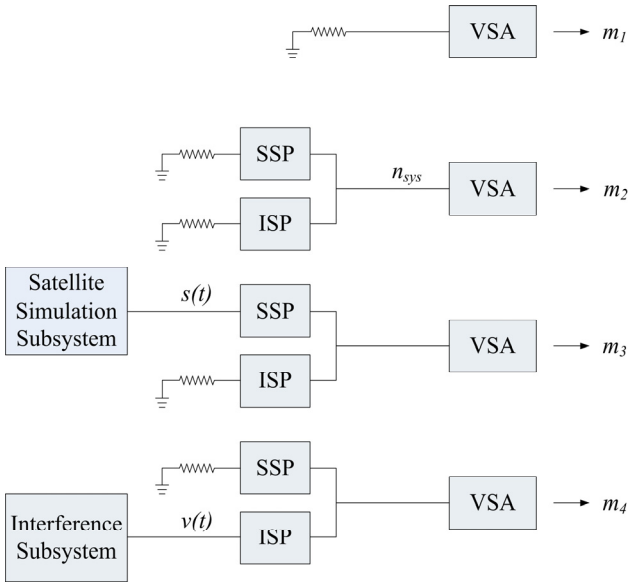

Figure B-2. Block diagrams for calibration measurements.

The following equations define these measurements

$$m_1(t) = n_{vsa}(t) + n_0(t)$$

$$m_2(t) = n_{sys}(t) + n_{vsa}(t)$$

$$m_3(t) = G_{SSP}\, s(t) + n_{sys}(t) + n_{vsa}(t)$$

$$m_4(t) = G_{ISP}\, v(t) + n_{sys}(t) + n_{vsa}(t)$$

where $n_{vsa}(t)$ is the internal noise of the VSA instrument, $n_0(t)$ is thermal noise, $n_{sys}(t)$ is the system noise, $s(t)$ is the satellite signal, $v(t)$ is the interference signal, and G_{SSP} and G_{ISP} are gains of SSP and ISP, respectively. The noise analysis was simplified by assuming the gain of the VSA to be one; this is justified because gain of the VSA is divided out in the power ratio calculations.

Measurement results were then band-limited in post-measurement processing by the victim receiver RRC filter

$$P_k = \left\langle \left| m_k(t) * h_{rrc}(t) \right|^2 \right\rangle$$

where k is the measurement index, $h_{rrc}(t)$ is the impulse response of the victim receiver RRC filter, $\langle\ \rangle$ is the time-average operator, and $*$ is the convolutional operator. Power estimates were derived from approximately 2.8 milliseconds of data, i.e., 2^{17} = 131,072 samples.

Power of the system noise (P_N), satellite signal (P_S), and interference signal (P_I) are calculated as

$$P_N \approx P_2 - P_1$$

$$P_S = P_3 - P_2$$

$$P_I = P_4 - P_2 \quad ,$$

where P_N is a good estimate because $n_{sys}(t) >> n_0(t)$.

Finally, *SNR* and *INR* are computed as

$$SNR = \frac{P_S}{P_N}$$

$$INR = \frac{P_I}{P_N} \quad .$$

Example calculations are provided in the validation portion of this appendix (see Table B-3).

B.3. Measured DTV Signal Quality

The MPEG-2 stream monitor was used to measure DTV signal quality. DTV signal quality metrics and their reference points within the receiver include *MER* and *BER* at the output of the quadrature demodulator, or equivalently at the input of the Viterbi decoder, and *SER* at the output of the Reed-Solomon (RS) decoder.

During the test, the following procedure was followed at each discrete interference level:

1. Interference was turned off and the receiver was allowed to acquire and demodulate the desired satellite signal in the absence of interference for 20 seconds.
2. Interference was applied for approximately 200 seconds.
3. *MER*, *BER*, cumulative transport error flag (*TEF*), and UTC time were sampled during the time of interference exposure at about 3 times per second and written to a data file.

DTV signal quality metrics were acquired with coarse and fine interference-level resolution. For coarse resolution, interference level was increased in 2-dB steps, beginning at a level that had negligible effect on DTV signal quality and ending where *SER* was in excess of 0.1. Fine-resolution acquisition began 2 dB below the level where the first *TEF* occurred during coarse-resolution acquisition and interference was incremented in 0.1-dB steps until 0.1 *SER* was again achieved.

B.3.1. *MER*

Measured *MER* is defined as

$$MER = 10\log_{10}\left(\frac{\sum_{n=1}^{N}\left(I_n^{\,2} + Q_n^{\,2}\right)}{\sum_{n=1}^{N}\left(\delta I_n^{\,2} + \delta Q_n^{\,2}\right)}\right) \quad ,$$

where I_n and Q_n are the ideal in- and quadrature-phase samples of the demodulated signal, δI and δQ are the error between actual and ideal samples, and N is the number of samples used for estimation. The MPEG-2 stream monitor utilized in this experiment derives *MER* from 512 samples collected at a rate of approximately 25 Hz.

B.3.2. *BER*

Measured pre-Viterbi bit error rate is defined as

$$BER = \frac{bit\ error\ count}{bit\ count} \quad .$$

The MPEG-2 stream monitor estimates *BER* with the circuit illustrated in Figure B-3. This circuit compares received bits to the estimated transmit bits. *BER* measurements use $2^{26} = 67{,}108{,}864$ bits which provide good precision to approximately $7 \cdot 10^{-5}$ *BER* assuming 100 errors are needed.

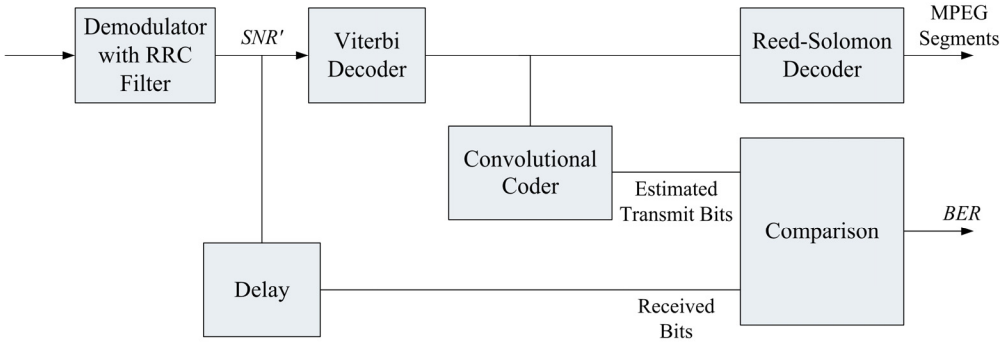

Figure B-3. *BER* estimation circuit used by MPEG-2 stream monitor.

Figure B-4 displays simulation results for the *BER* estimation circuit, where no interference was present. Good agreement was found for $SNR' > 4.5$ dB corresponding to $BER < 0.05$, where SNR' is referenced to the output of the demodulator. Poor agreement at lower SNR' was due to errors in the estimated transmit bits.

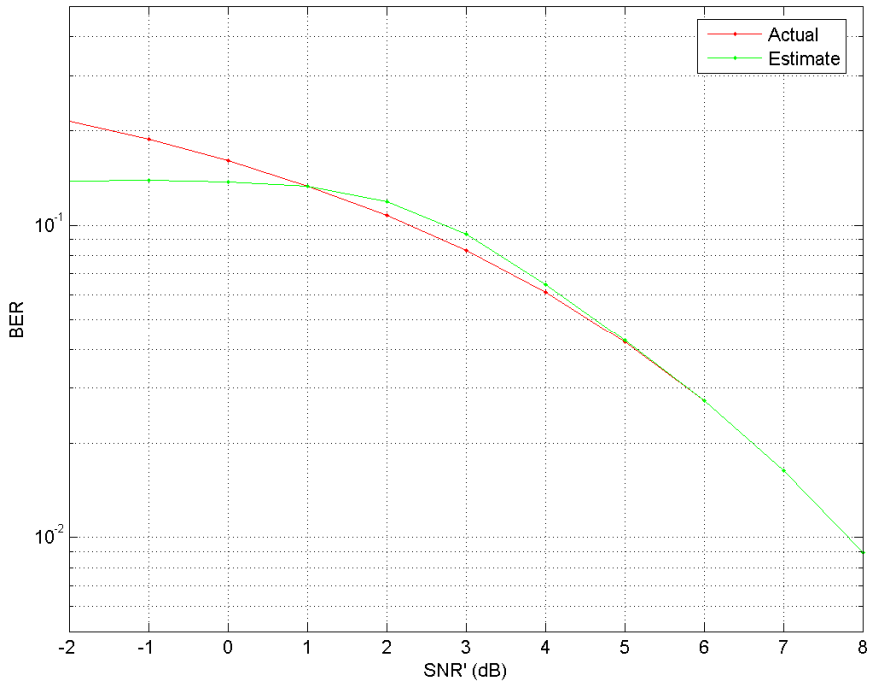

Figure B-4. Simulation of *BER* estimation circuit used by MPEG-2 stream monitor.

B.3.3. *SER*

Measured *SER* is defined by

$$SER = \frac{segment\ error\ count}{segment\ count} = \frac{TEF(t_2) - TEF(t_1)}{(t_2 - t_1)R_{seg}} \quad ,$$

where $TEF(t_k)$ is the cumulative number of segment errors at UTC time t_k and R_{seg} is the number of segments per second specified by the DTV operational scenario. Measured *SER* was computed from approximately 200 seconds of data. During this time period, approximately 3.6 million segments were transmitted. Each segment is considered to be an independent susceptibility trial.

Satellite and interference signals were not without systematic uncertainty. More specifically, sinusoidal variations of approximately 0.1-dB peak-to-peak with periods of 20 – 50 minutes were measured in signal amplitudes with a power meter after the LNB. Subsequent *SER* fluctuations were approximately an order of magnitude, which is explained by the high sensitivity of *SER* to change in signal-to-noise ratio (see Table B-2). This *SER* fluctuation is only evident during long measurement periods when interference is either absent or has negligible effect on *SER*. For the interference tests considered in this report, the 0.1-dB increase in interference power every 220 seconds increased *SER* at a rate that rendered the *SER* systematic fluctuations indistinguishable.

B.4. Theoretical DTV Signal Quality for Gaussian Noise Degradation

This section provides theoretical expressions of *MER*, *BER*, and *SER* for Gaussian noise degradation. For a Gaussian noise radio environment, degradation is predictable from the signal-to-noise ratio at the output of the demodulator (SNR').

B.4.1. *MER*

For Gaussian noise degradation, theoretical *MER* is equivalent to SNR' in dB, that is

$$MER = 10\log(SNR') \quad .$$

B.4.2. *BER*

Theoretical probability of a bit error for QPSK, comparable to measured *BER*, is computed as

$$P_{QPSK} = Q\left(\sqrt{SNR'}\right) \quad ,$$

where Q represents the Q-function defined as

$$Q(z) = \frac{1}{2\pi}\int_{z}^{\infty} \exp\left(\frac{-\xi^2}{2}\right) d\xi \quad .$$

B.4.3. *SER*

Probability of post-Viterbi bit error for QPSK is upper bounded by

$$P_{conv} \le \frac{1}{K}\sum_{d=d_{free}}^{\infty} w(d)Q\left(\sqrt{d \cdot SNR'}\right) \quad ,$$

where constraint length K is specified by the operational scenario, d_{free} is the free distance of the code, and $w(d)$ are the code weights.

Theoretical calculation of *SER* requires converting P_{conv} to P_{byte}, i.e., the probability of a byte error. The conversion factor can be determined mathematically with the assumption of independent bit errors [11]; however, if more accuracy is desired the effects of correlated bit errors, caused by the Viterbi algorithm, can be simulated. Simulations of Gaussian noise degradation near the SNR' required for $P_{RS} = 10^{-4}$ have shown a probability of a byte error approximately equal to three times the probability of a bit error, i.e., $P_{byte} \approx 3P_{conv}$.

For the RS scheme specified in Table B-1, a segment error occurs when more than (204 –188)/2 or 8 byte errors occur in a single segment. Hence, if post-Viterbi byte errors are independent, P_{byte} is small, and the number of bytes per segment is large, then the upper bound of the probability of a post RS segment error can be estimated by

$$P_{RS} = P(m > M) \le 1 - \sum_{l=0}^{M} \frac{\lambda^l}{l!} e^{-\lambda} \quad ,$$

where $M = 8$ and $\lambda = 204 P_{byte}$ for the RS(204,188) code.

Figure B-5 shows P_{QPSK}, P_{conv}, and P_{RS} as a function of SNR'. Table B-2 provides P_{QPSK} and P_{RS} at various SNR' near the threshold of visibility, i.e., $P_{RS} = 10^{-4}$. Notice that P_{RS} is sensitive to changes in SNR', varying as much as an order of magnitude for each 0.1-dB increment in SNR'. In contrast, P_{QPSK} is relatively insensitive. Such differences between P_{QPSK} and P_{RS} are attributed to the forward error correction (FEC).

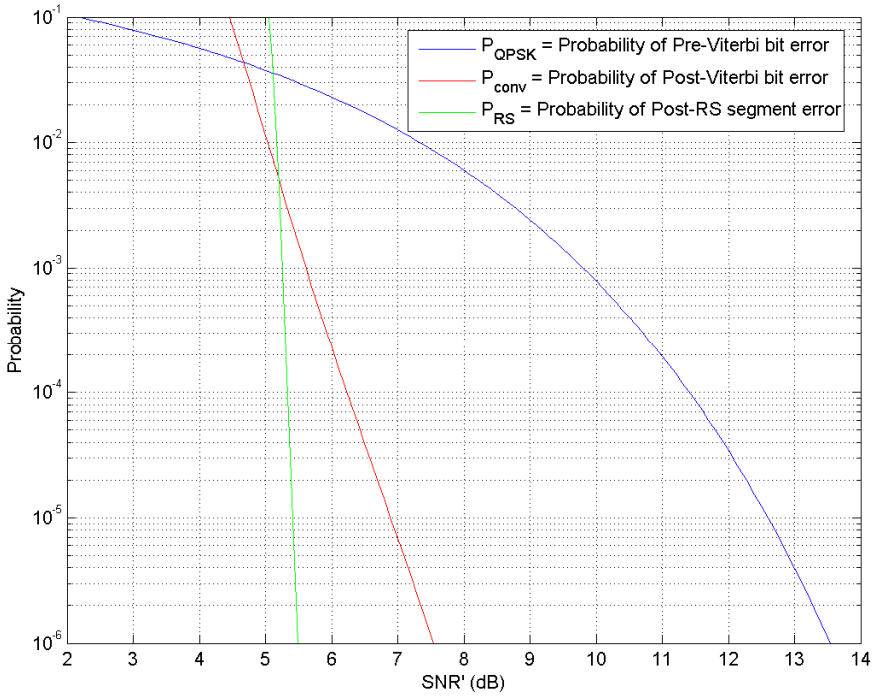

Figure B-5. Theoretical DTV receiver performance versus SNR'.

Table B-2. Probability of Pre-Viterbi Bit Error and Post-RS Segment Error Near TOV

SNR' (dB)	P_{QPSK}	P_{RS}
5.0	0.038	0.27
5.1	0.036	0.046
5.2	0.034	0.0045
5.3	0.033	0.00029
5.4	0.031	0.000014

B.5. Validation of Measured DTV Quality Metrics for Gaussian Noise Degradation

In this section, some degree of validation is accomplished by comparing theoretical predictions to measured DTV quality metrics for Gaussian noise degradation. Two scenarios are evaluated: (1) *BER* versus *SNR* in the absence of interference, and (2) *BER* and *SER* versus *INR* for a DTV receiver exposed to continuous noise interference. It is important to understand that results in this subsection relate to Gaussian noise degradation and cannot be generalized without further research.

B.5.1. *BER* as a Function of *SNR* in the Absence of Interference

The test system was set up as shown in Figure B-1, except the interference signal path was terminated. *SNR*, *BER*, and *SER* were measured (as described in Sections B.2 and B.3) at various satellite signal powers. Figure B-6 shows measured *BER* and theoretical P_{QPSK} versus *SNR*.

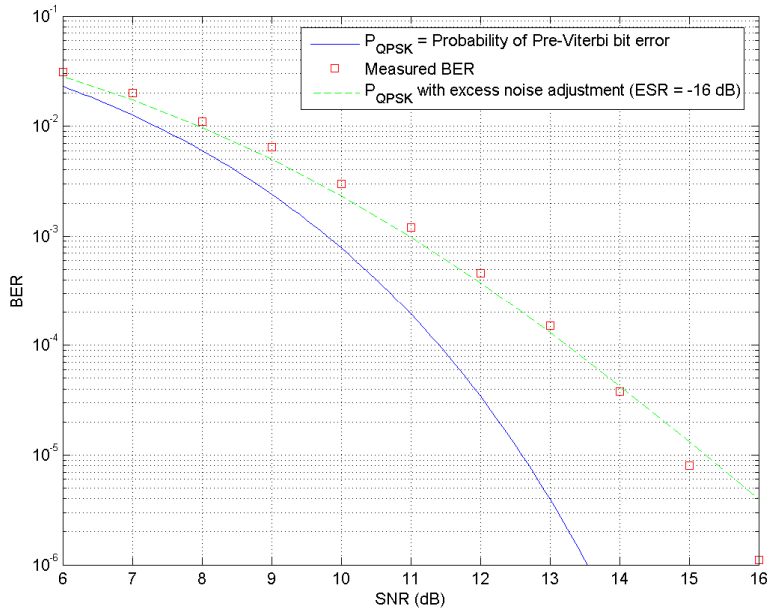

Figure B-6. Theoretical versus measured bit error rate performance of a DTV receiver.

Presumably, the primary difference between theory and measurement was due to distortions introduced by imperfect demodulation that effectively reduced the signal-to-noise ratio. Good agreement with measured *BER* was achieved when an excess noise term, proportional to the average power of the satellite signal, was used to model demodulator imperfections. More specifically, at the output of the demodulator

$$SNR' = \frac{P_S}{P_N + P_\varepsilon} = \frac{SNR}{1 + ESR \cdot SNR} \quad , \tag{B-1}$$

where P_ε is the average power of the excess noise and excess-noise-to-signal ratio was determined empirically as $ESR = P_\varepsilon / P_S = -16$ dB. Using this model, SNR = {9, 12, 15} dB measured during the DTV susceptibility test corresponds to SNR' = {8.2, 10.5, 12.5} dB.

B.5.2. *BER* and *SER* as a Function of *INR* for Gaussian-Noise Interference

In this subsection, an "effective signal-to-noise ratio" concept is developed to validate the GN-01 measurements. This concept is based on the assumption that receiver noise, excess noise, and GN-01 interference are all Gaussian noise processes. Theoretical expressions provided in Section B.4 are applicable since the addition of these noise processes results in a Gaussian noise process with an average power equal to the sum of its constituents. Hence, in the case of GN-01, the effective signal-to-noise ratio at the output of the demodulator is expressed as

$$SNR'_{eff} = \frac{P_S}{P_N + P_I + P_\varepsilon} = \frac{SNR}{1 + INR + ESR \cdot SNR} \quad .$$

Figures B-7 and B-8 provide theoretical versus measured *BER* and *SER*, respectively, for a DTV receiver operating at the different *SNR*s and exposed to a range of Gaussian noise interference levels. Table B-3 provides theoretical and measured test results for Gaussian noise interference that caused degradation at the TOV. Calibration measurements with the VSA provided P_1, P_2, P_3, and P_4. These measurements were used to compute P_S , P_I , SNR, and INR. Interestingly, P_S / P_4 , which corresponds to the ratio of signal power to the combined power of interference and system noise, was approximately 5.5 dB in all cases. In general, theoretical results using the SNR'_{eff} model demonstrated good agreement with measured data.

Table B-3. Signal Powers at the TOV for Gaussian Noise Interference

Calibration Measurements			Susceptibility Test Results					Theoretical Results
P_2 (dBm)	P_3 (dBm)	P_4 (dBm)	P_S (dBm)	P_I (dBm)	P_S / P_4 (dB)	SNR (dB)	INR_{TOV} (dB)	INR_{TOV} (dB)
-47.8	-38.4	-44.4	-38.9	-47.1	5.5	8.9	0.7	0.5
-47.7	-35.4	-41.2	-35.7	-42.3	5.5	12.0	5.4	5.1
-47.8	-32.6	-38.1	-32.7	-38.6	5.4	15.0	9.2	8.7

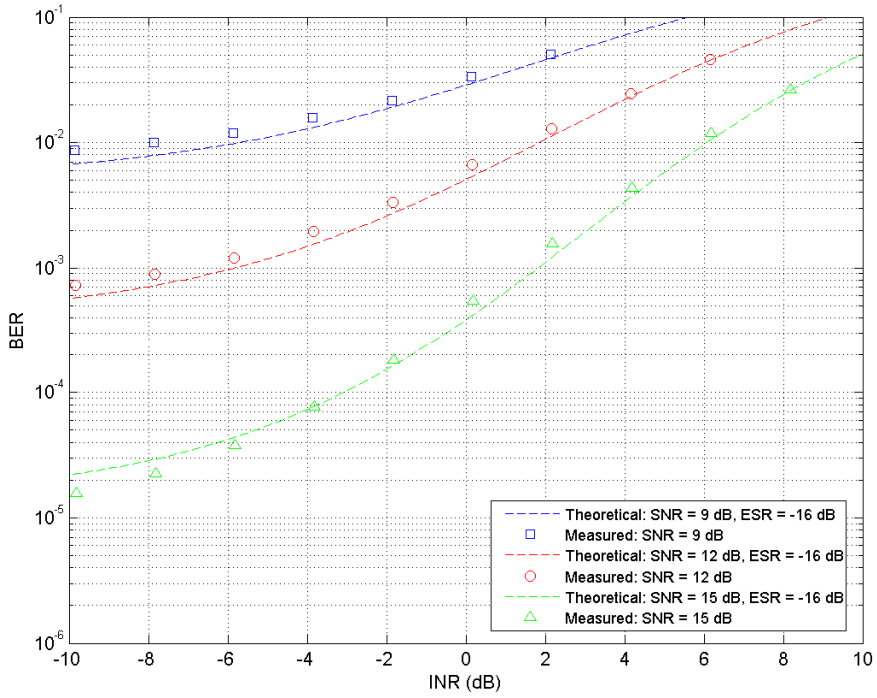

Figure B-7. Theoretical and measured *BER* for Gaussian noise interference.

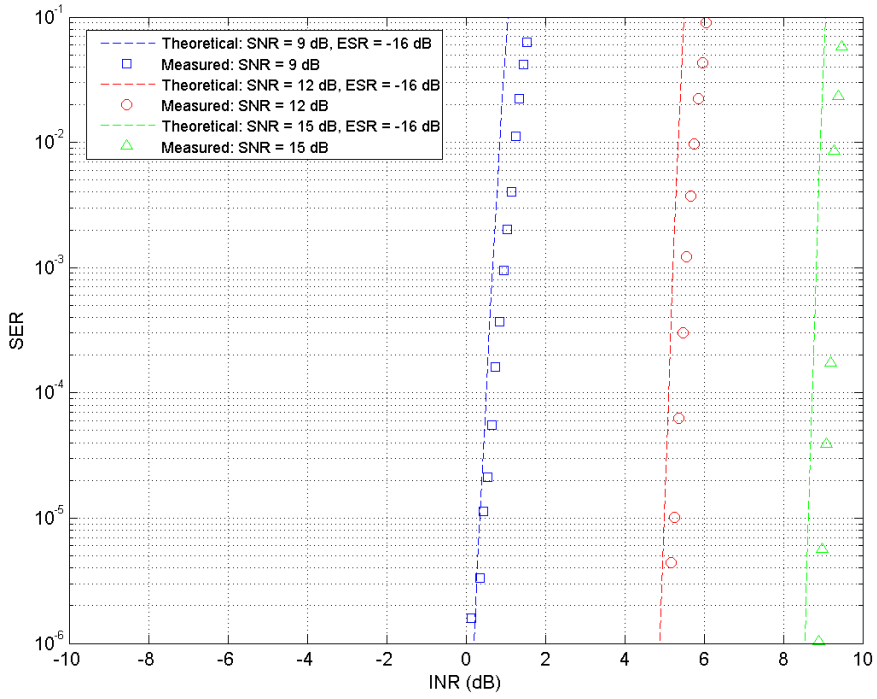

Figure B-8. Theoretical and measured *SER* for Gaussian noise interference.

APPENDIX C: THEORETICAL ANALYSIS OF GATED GAUSSIAN NOISE

This appendix provides theoretical analyses of gated Gaussian noise expressed mathematically as

$$u(t) = z(t)g(t;T,\tau_{on}) = \big(n(t) * h_{BPF}(t)\big)g(t;T,\tau_{on}) \quad ,$$

where $z(t)$ is a Gaussian noise random process with an ultra-wide transmission bandwidth (B_{UWB}) much greater than the victim receiver bandwidth (B_{DTV}), $n(t)$ is a zero-mean white Gaussian noise random process, $h_{BPF}(t)$ is the impulse response of a band-pass filter that defines B_{UWB} , and * is the convolutional operator. The ideal gating function is described mathematically as

$$g(t;T,\tau_{on}) = \sum_{k=-\infty}^{\infty} R(t-kT;\tau_{on}) \quad , \quad \text{where} \quad R(t;\tau_{on}) = \begin{cases} 1 & (S_1: \quad 0 \le t < \tau_{on}) \\ 0 & (S_2: \quad \tau_{on} \le t < T) \end{cases}$$

and S_1 and S_2 refer to gated-on and gated-off states, respectively. The complex-baseband (CBB) representation, denoted by ˆ, of $u(t)$ is modeled as

$$\hat{u}(t) = \hat{z}(t)g(t;T,\tau_{on}) \quad ,$$

where $\hat{z}(t)$ is a complex Gaussian-distributed random variable with zero-mean. The variance of $\hat{z}(t)$ is $\sigma_{\hat{z}}^{\,2} = 2\sigma^2$, where σ^2 is the variance of the real and imaginary parts. The following amplitude probability distribution (*APD*) and power spectral density (*PSD*) expressions are derived in terms of $\hat{u}(t)$.

C.1. Amplitude Probability Distribution

Computation of the *APD* for gated Gaussian noise begins with the total probability expression

$$\wp(A \le a) = \wp(A \le a \mid S_1)\wp(S_1) + \wp(A \le a \mid S_2)\wp(S_2) \quad , \qquad \text{(C-1)}$$

where $\wp$ represents probability, $A = |\hat{u}(t)|$ is the amplitude random variable which takes on values of a ranging from 0 to ∞ , $\wp(S_k)$ represents the probability of being in state S_k , and $\wp(A \le a \mid S_k)$ represents the conditional probability of $A \le a$ given the state S_k .

Amplitudes are Rayleigh distributed in state S_1 giving the probability density function (*PDF*)

$$q(a \mid S_1) = \frac{a}{\sigma^2}\exp\left(\frac{-a^2}{2\sigma^2}\right) \quad .$$

The corresponding cumulative distribution function (*CDF*) is

$$\wp(A \le a \mid S_1) = 1 - \exp\left(\frac{-a^2}{2\sigma^2}\right) \quad .$$

Similarly, the amplitude is always 0 in state S_2 giving the *PDF*

$$q(a \mid S_2) = \delta(a) \quad ,$$

where $\delta(a)$ is the delta function. The corresponding *CDF* is acquired by integrating the *PDF* over all amplitudes which yields the step function $U(a)$. Recall that $a \geq 0$, hence $U(a) = 1$ yielding

$$\wp(A \le a \mid S_2) = 1 \quad .$$

Probabilities of being in each state are expressed in terms of the fractional on-time (ζ)

$$\wp(S_1) = \zeta \quad ; \qquad \wp(S_2) = (1 - \zeta) \quad .$$

Substituting these expressions into the total probability expression (C-1) yields the *CDF*

$$\wp(A \le a) = 1 - \zeta \exp\left(\frac{-a^2}{2\sigma^2}\right) \quad .$$

The corresponding *APD* is obtained by subtracting the *CDF* from 1

$$\wp(A > a) = \zeta \exp\left(\frac{-a^2}{2\sigma^2}\right) \quad . \qquad \text{(C-2)}$$

Figure C-1 provides *APD*s of normalized ($\sigma^2 = 1$) gated Gaussian noise with $\zeta = \{1, 0.5, 0.25, 0.125, 0.0625\}$ in an ultra-wide transmission bandwidth.

Peak-to-average ratio (*P/A*) is computed from the peak and root-mean-square (rms) amplitudes. Peak amplitude (a_{pk}) is defined by the percentile ρ. Replacing $\wp(A > a)$ with ρ and a with a_{pk} in equation (C-2) and solving for a_{pk} yields

$$a_{pk} = \sigma\sqrt{\ln(\zeta/\rho)} \quad .$$

This expression is only valid when $\zeta \geq \rho$.

Rms amplitude is found by substituting the probability densities given previously into the derivative of (C-1) with respect to *a* to obtain

$$q(a) = q(a \mid S_1)\wp(S_1) + q(a \mid S_2)\wp(S_2) = \zeta \frac{a}{\sigma^2} \exp\left(\frac{-a^2}{2\sigma^2}\right) + (1-\zeta)\delta(a) \quad ,$$

and using this *PDF* to calculate rms amplitude

$$a_{rms} = \sqrt{\int_0^\infty a^2 q(a) da} = \sigma\sqrt{\zeta} \quad .$$

Finally, the expression for *P/A* is

$$P/A = \left(\frac{a_{pk}}{a_{rms}}\right)^2 = \frac{\ln(\zeta/\rho)}{\zeta} \quad .$$

Figure C-2 provides *P/A* as a function of ζ for gated noise in the ultra-wide transmission bandwidth; peak definitions considered in Figure C-2 are ρ = {0.001, 0.01, 0.1, 1.0} %.

C.2. Power Spectral Density

Derivation of the *PSD* for gated Gaussian noise begins with the autocorrelation function

$$R_{\hat{u}\hat{u}}(t, t+\tau) = E\left\{\hat{u}(t)\hat{u}^*(t+\tau)\right\} \quad ,$$

where $E\{\ \}$ denotes expectation and * denotes conjugation. Pulling the deterministic gating function out of the expectation gives

$$R_{\hat{u}\hat{u}}(t, t+\tau) = g(t)g^*(t+\tau)R_{\hat{z}\hat{z}}(\tau) \quad .$$

Expressing the gating function as a Fourier series

$$g(t) = \sum_{k=-\infty}^{\infty} c_k \exp(j2\pi kt/T) \quad , \qquad c_k = \frac{1}{T}\int_0^T g(t)\exp(-j2\pi kt/T)dt$$

yields

$$R_{\hat{u}\hat{u}}(t, t+\tau) = \sum_{l=-\infty}^{\infty}\sum_{k=-\infty}^{\infty} c_l c_k^* \exp(j2\pi(l-k)t/T)\exp(-j2\pi k\tau/T)R_{\hat{z}\hat{z}}(\tau) \quad .$$

The first complex-exponential term causes the autocorrelation to be time-varying. This variation is periodic, in that

$$R_{\hat{u}\hat{u}}(t,t+\tau) = R_{\hat{u}\hat{u}}(t+T,t+\tau+T) \quad ,$$

and is removed by averaging over the gating period. The resulting time-averaged autocorrelation function is

$$\left\langle R_{\hat{u}\hat{u}}(\tau)\right\rangle = \frac{1}{T}\int_0^T R_{\hat{u}\hat{u}}(t,t+\tau)dt = \sum_{l=-\infty}^{\infty}\sum_{k=-\infty}^{\infty} c_l c_k^* \exp\left(-j2\pi k\tau/T\right) R_{\hat{z}\hat{z}}(\tau)\frac{1}{T}\int_0^T \exp\left(j2\pi(l-k)t/T\right)dt \quad ,$$

which evaluates to

$$\left\langle R_{\hat{u}\hat{u}}(\tau)\right\rangle = \begin{cases} \sum_{k=-\infty}^{\infty}\left|c_k\right|^2 \exp\left(-j2\pi k\tau/T\right) R_{\hat{z}\hat{z}}(\tau) & (l=k) \\ 0 & (l\neq k) \end{cases} \quad .$$

The *PSD* is derived from the Fourier transform of the time-averaged autocorrelation function

$$\left\langle S_{\hat{u}\hat{u}}(f)\right\rangle = \int_{-\infty}^{\infty}\left\langle R_{\hat{u}\hat{u}}(\tau)\right\rangle \exp\left(-j2\pi f\tau\right)d\tau \quad .$$

Substitution yields the following expression for the *PSD* of gated Gaussian noise

$$\left\langle S_{\hat{u}\hat{u}}(f)\right\rangle = \sum_{k=-\infty}^{\infty}\left|c_k\right|^2 \delta(f+\frac{k}{T}) * S_{\hat{z}\hat{z}}(f) \quad .$$

Note that $S_{nn}(f)$ is constant, yielding

$$S_{\hat{z}\hat{z}}(f) = n_0\left|H_{LPF}(f)\right|^2 \quad ,$$

where n_0 is the power density of the underlying white Gaussian process and $H_{LPF}(f)$ is the CBB representation of $H_{BPF}(f)$. This simplifies the *PSD* expression

$$\left\langle S_{\hat{u}\hat{u}}(f)\right\rangle = n_0\sum_{k=-\infty}^{\infty}\left|c_k\right|^2 \delta(f+\frac{k}{T}) * \left|H_{LPF}(f)\right|^2 \quad .$$

In this experiment we assume the transmission filter, $H_{LPF}(f)$, is constant over the bandwidth of the victim receiver. Hence, the *PSD* of gated noise is constant for all frequencies considered.

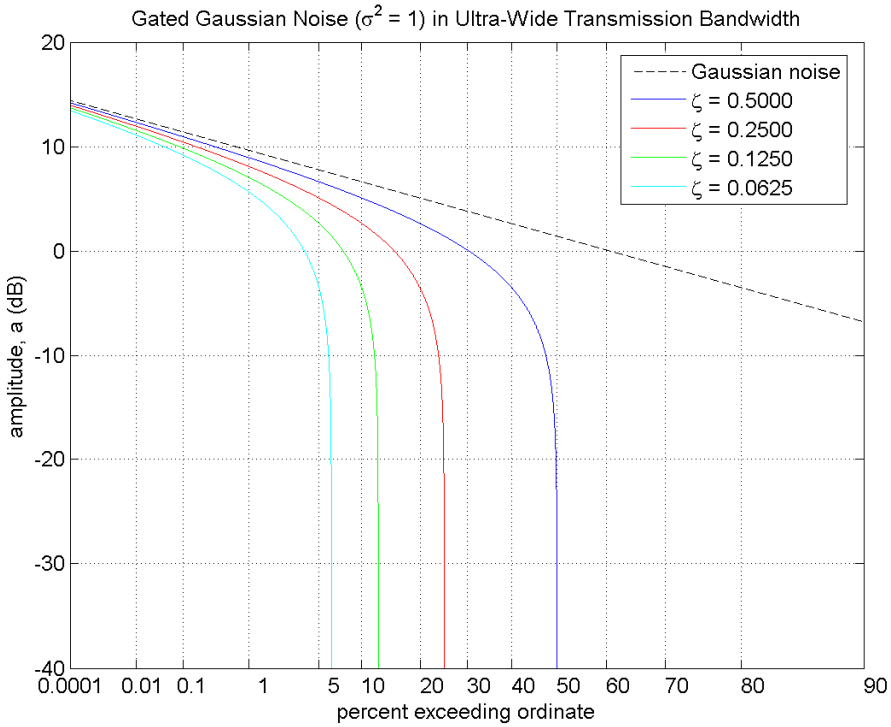

Figure C-1. Theoretical *APD*s of gated noise in B_{UWB}.

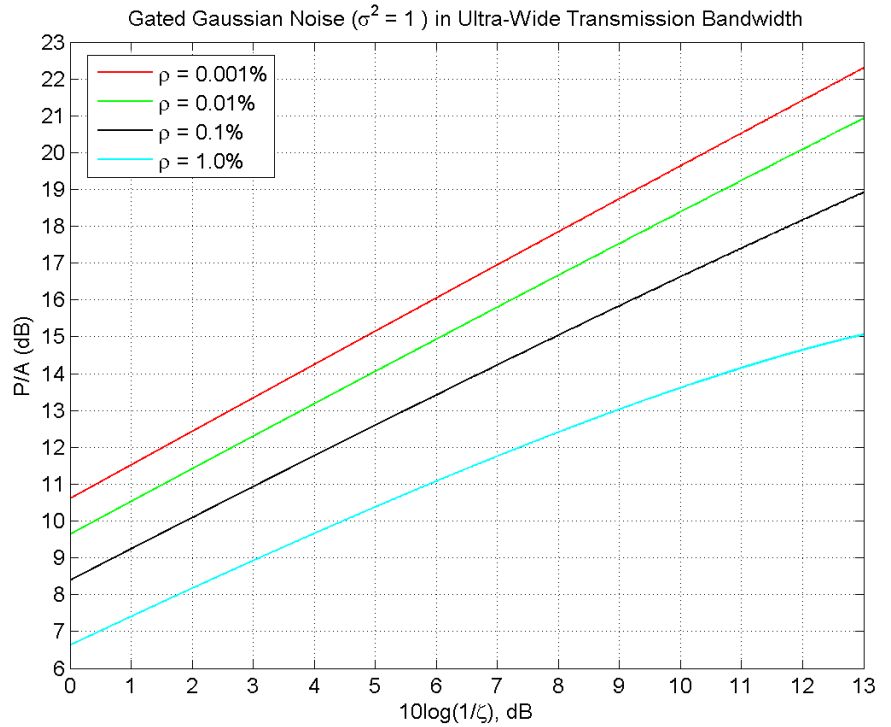

Figure C-2. Theoretical *P/A* of gated noise in B_{UWB}.

APPENDIX D: CHARACTERIZATION MEASUREMENTS

This appendix provides a description of measurement setup and signal characterization measurements that complement those in Section 3.

D.1. Measurement Setup

Interference signals were measured under optimal conditions at the radio frequency (RF) output of the vector signal generator (VSG) as described in Figure D-1. The VSG was set up with the procedures described in Appendix B of Part 1 [6]. Measurements at RF were made with the vector signal analyzer (VSA) and digital oscilloscope (DO).

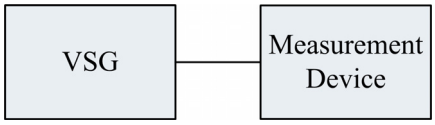

Figure D-1. Setup for RF signal characterization measurements.

The gated-noise signals, GN-02 – GN-17, were simulated by applying different gating signals to the continuous-noise signal, GN-01. This ensured that voltages of all signals were identical when gated on. Gated-noise signals, generated in hardware with the setup described by Figure C-2 in Part 1, were also measured to verify corresponding VSG-generated signals. Characteristics of the hardware-generated signals matched those of the VSG-generated signals and therefore are not included in this report.

For VSA characterization measurements at RF, the VSG output level was set to -28.19 dBm for GN-01 through GN-17 and -27.17 dBm for GN(MB)-01 through GN(MB)-09. At these levels, the VSG generated the "continuous" signals, GN-01 and GN(MB)-01, at an average power of approximately -45 dBm in a 36-MHz bandwidth at the output of the cable. This optimally utilized the dynamic range of the VSA as discussed in Appendix E of Part 1. VSA instrument settings are summarized in Table D-1.

Table D-1. RF VSA Measurement Settings

Post-Processing Bandwidths (MHz)	Span (MHz)	Number of Samples	Center Frequency (MHz)	Input Range (dBm)
36, 19.51, 10 1 0.1	36 4.5 0.5625	> 360,000 > 450,000 > 562,500	3820	-30

DO measurements at the maximum sample rate, i.e., 20 GSps, provided real time-domain representations of RF signals. DO measurements were made with the VSG output level set to a higher value, i.e., 0 dBm, to compensate for low DO sensitivity at the maximum sample rate.

Interference signals were measured under TOV operational conditions at the IF output of the low-noise block downconverter (LNB) with the setup described in Figure 20 of Part 1. The simplified block diagram of those components that affect the IF signal characterization measurements are shown in Figure D-2. Bandpass filter BPF1 has a 1-dB bandwidth equal to 40 MHz. The VSG output level was set to INR_{TOV}. Measurements at IF were made with the VSA only. VSA settings for IF measurements were the same as those used for RF measurements described in Table D-1, except the center frequency was set to 1330 MHz.

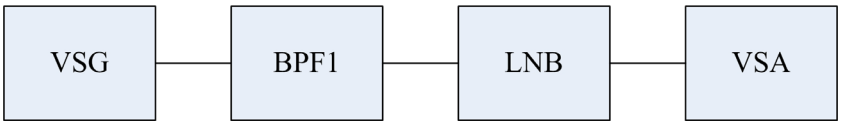

Figure D-2. Simplified setup for IF signal characterization measurements.

D.2. Results

This subsection provides amplitude statistics and time series of the gated-noise signals. Odd numbered plots in Figures D-3 – D-54 provide RF measurement results organized as:

(a) Real time series measured with DO and amplitude time series measured with the VSA and band-limited to B_{DTV} = 19.51 MHz.
(b) *APD*s measured with a VSA and band-limited to 36, 10, 1, and 0.1 MHz as well as B_{DTV}.

Even numbered plots in Figures D-3 – D-54 provide IF measurement results organized as:

(a) Amplitude time series measured with the VSA and band-limited to B_{DTV}.
(b) *APD*s measured with the VSA and band-limited to B_{DTV}.

Table D-2 provides peak-to-average (*P/A*) values for the gated-noise signals measured at RF and band-limited to various bandwidths in post-measurement processing. The shaded cells highlight signals with Rayleigh-distributed amplitudes. Ultra-wide transmission bandwidth (B_{UWB}) limits for *P/A* were derived in Appendix C.

Table D-3 provides *P/A* values for gated-noise signals measured at IF under TOV operational conditions and band-limited to B_{DTV} in post-measurement processing.

Table D-2. RF *P/A* (dB) of GN and GN(MB) Signals Band-Limited to Different Bandwidths

Type	Index	B_{UWB}	36.0 MHz	B_{DTV}	10.0 MHz	1.0 MHz	0.1 MHz
GN	01	9.6	9.6	9.6	9.8	9.8	9.0
	02	12.3	9.7	9.9	9.5	9.7	9.6
	03	14.9	11.0	9.7	9.8	9.5	8.9
	04	17.5	13.1	11.5	9.4	9.5	10.1
	05	20.1	15.9	14.2	11.7	9.8	9.1
	06	12.3	11.8	12.2	11.2	9.5	9.3
	07	14.9	14.4	14.6	13.9	9.6	9.9
	08	17.5	16.8	17.3	16.5	9.7	9.4
	09	20.1	19.8	19.6	18.9	11.7	9.2
	10	12.3	12.5	12.4	12.5	11.1	10.1
	11	14.9	15.1	15.0	14.8	13.6	9.8
	12	17.5	17.9	17.6	17.6	16.3	9.4
	13	20.1	20.3	20.3	20.0	18.8	11.0
	14	12.3	12.6	12.3	12.2	12.3	10.3
	15	14.9	15.3	15.1	14.8	14.8	14.1
	16	17.5	17.4	17.8	17.9	17.6	15.7
	17	20.1	19.9	20.1	20.0	19.9	16.4
GN (MB)	01	10.6	10.5	10.5	10.1	9.6	9.7
	02	14.8	14.4	14.7	14.6	9.8	9.5
	03	14.8	14.7	14.6	14.5	11.6	9.5
	04	18.0	17.5	18.0	17.6	12.7	9.7
	05	18.0	17.6	17.9	17.5	14.7	9.5
	06	18.0	17.6	17.8	17.6	16.5	10.6
	07	20.3	20.1	20.2	19.7	15.0	9.4
	08	20.3	20.0	20.1	19.8	16.8	9.0
	09	20.3	20.1	19.9	19.5	19.0	15.0

*Shaded cells highlight Rayleigh-amplitude statistics.

Table D-3. IF *P/A* (dB) of GN and GN(MB) Signals at INR_{TOV} and Band-Limited to B_{DTV}

Type	Index	*SNR* ≈ 9 dB	*SNR* ≈ 12 dB	*SNR* ≈ 15 dB
GN	01	9.6	9.6	9.4
	02	9.8	9.8	9.9
	03	9.6	9.5	9.5
	04	10.4	11.1	11.1
	05	12.0	13.2	13.6
	06	10.8	11.1	11.7
	07	12.1	13.2	13.8
	08	14.1	15.2	16.4
	09	16.1	17.8	18.8
	10	11.2	11.4	11.8
	11	11.9	13.1	13.7
	12	13.0	14.6	15.8
	13	13.5	16.2	17.5
	14	10.7	11.5	12.0
	15	11.4	12.8	13.6
	16	12.0	13.8	15.3
	17	11.9	14.3	16.6
GN (MB)	01	10.2	10.2	10.3
	02	12.1	13.3	14.3
	03	12.0	13.4	13.9
	04	14.0	16.2	16.7
	05	13.5	15.4	16.4
	06	12.6	14.6	15.8
	07	15.0	17.8	18.7
	08	14.3	16.5	17.9
	09	12.7	15.2	17.4

*Shaded cells highlight Rayleigh-amplitude statistics.

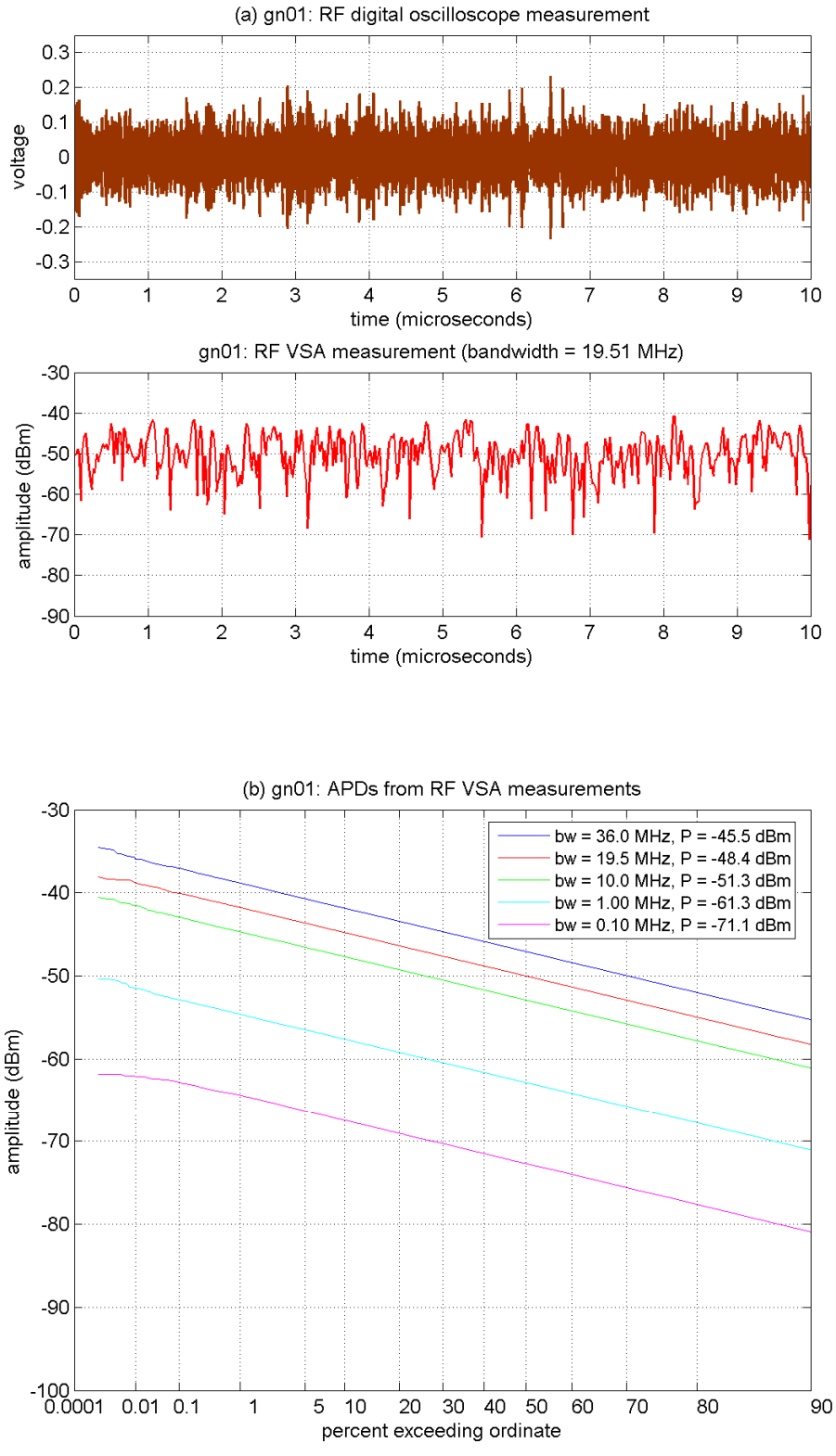

Figure D-3. RF measurements of GN-01, Gaussian noise.

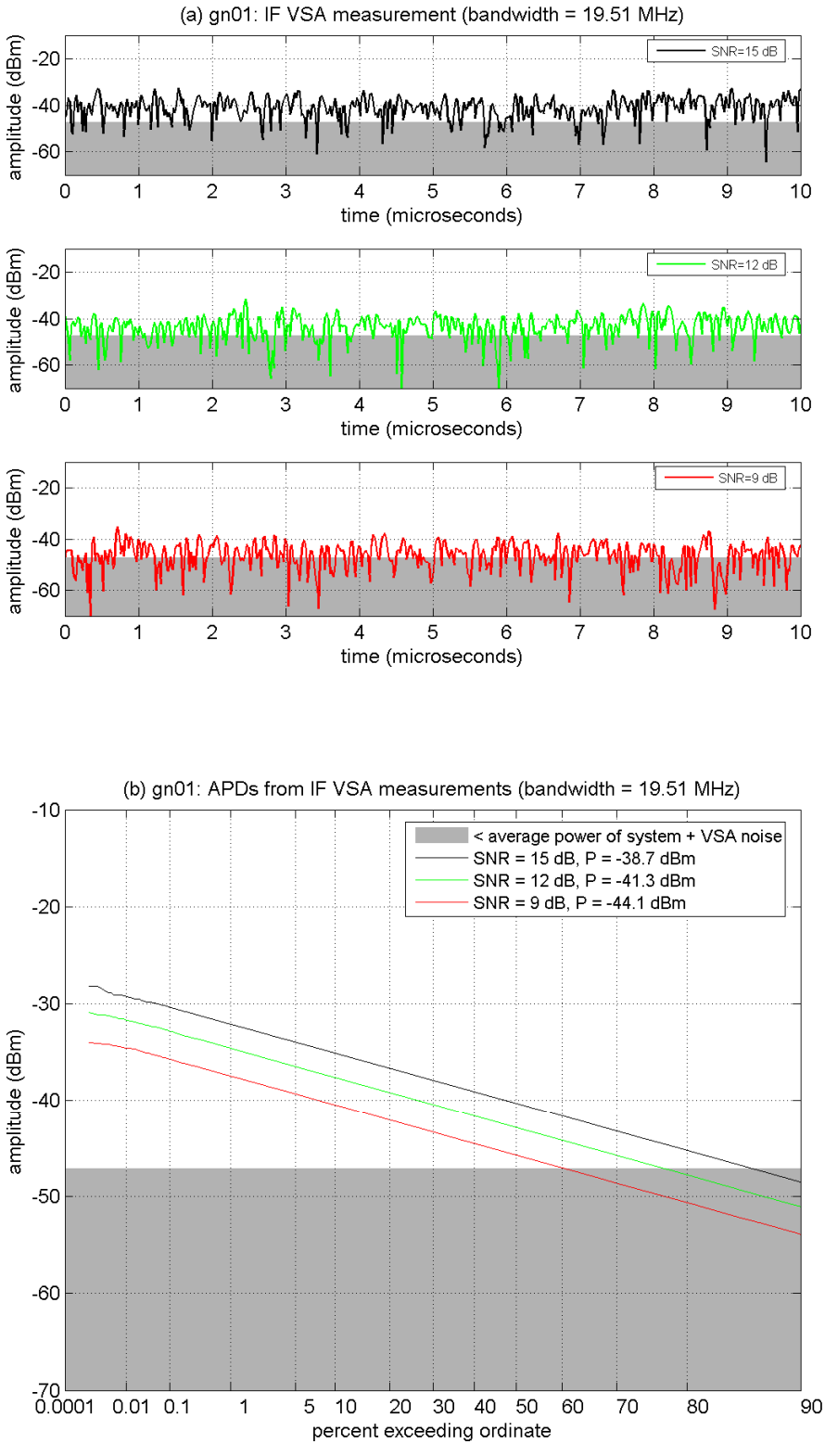

Figure D-4. IF measurements of GN-01 at INR_{TOV}.

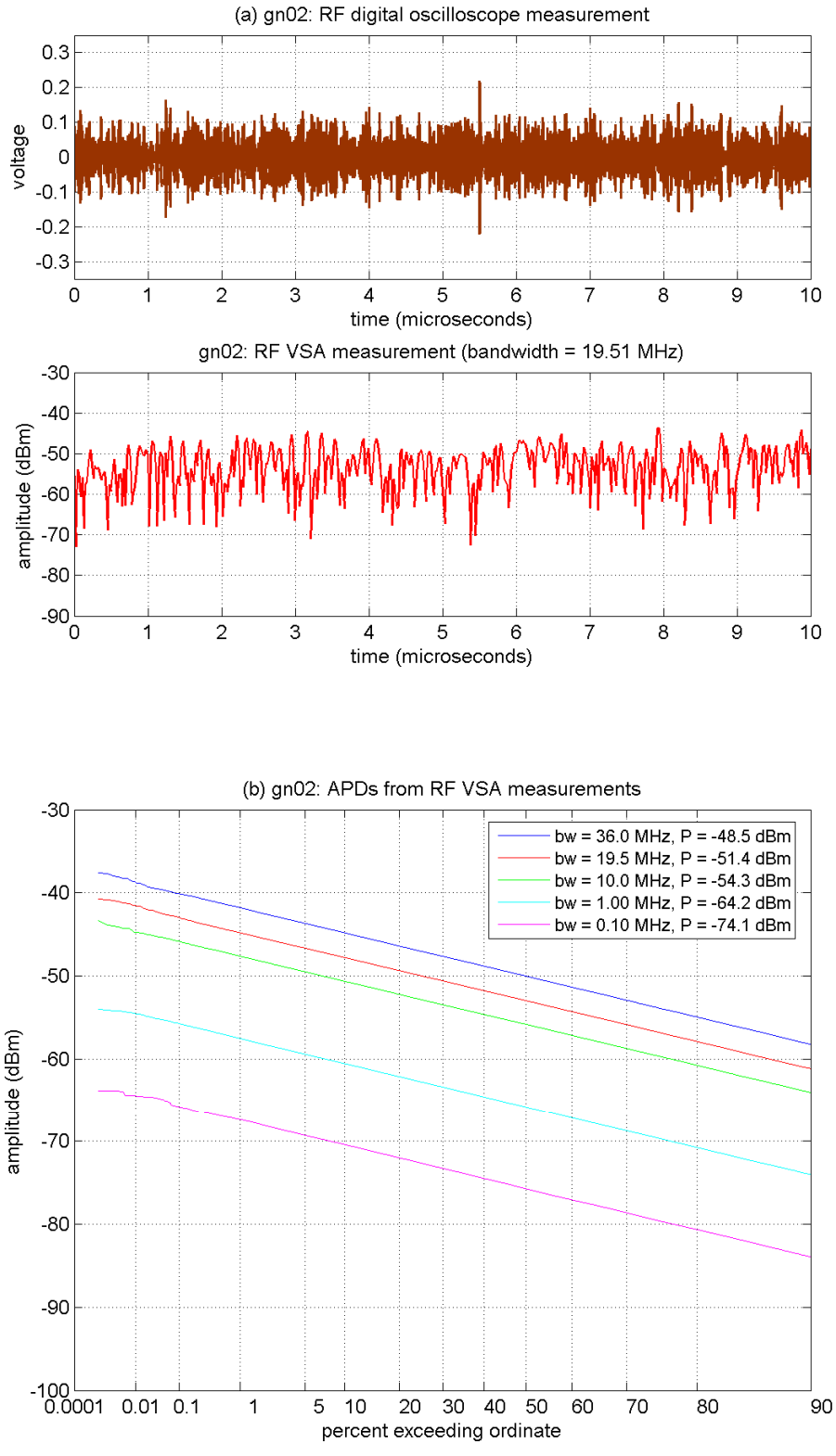

Figure D-5. RF measurements of GN-02 (τ_{on} = 10 ns, ζ = 0.5000).

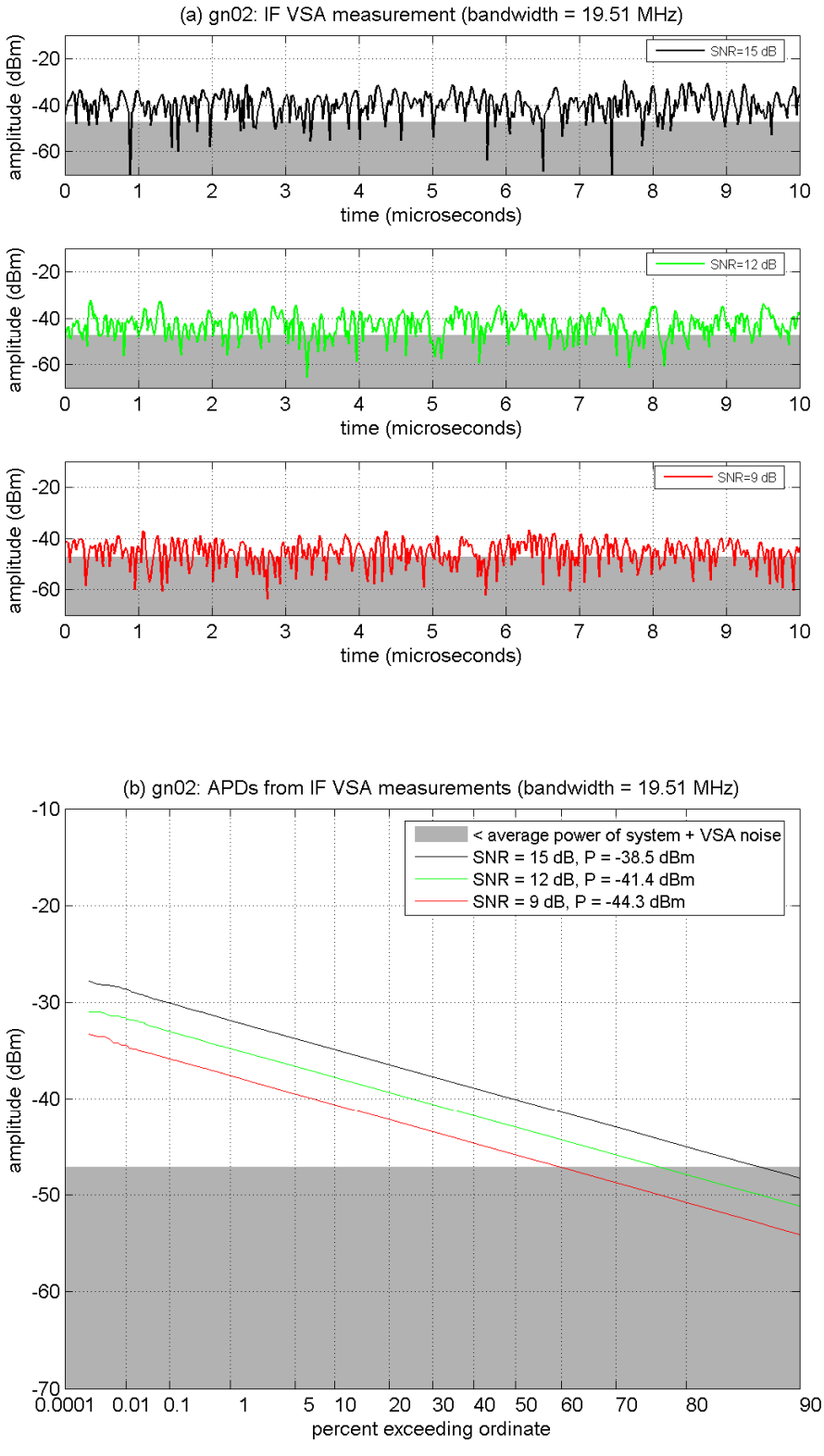

Figure D-6. IF measurements of GN-02 at INR_{TOV}.

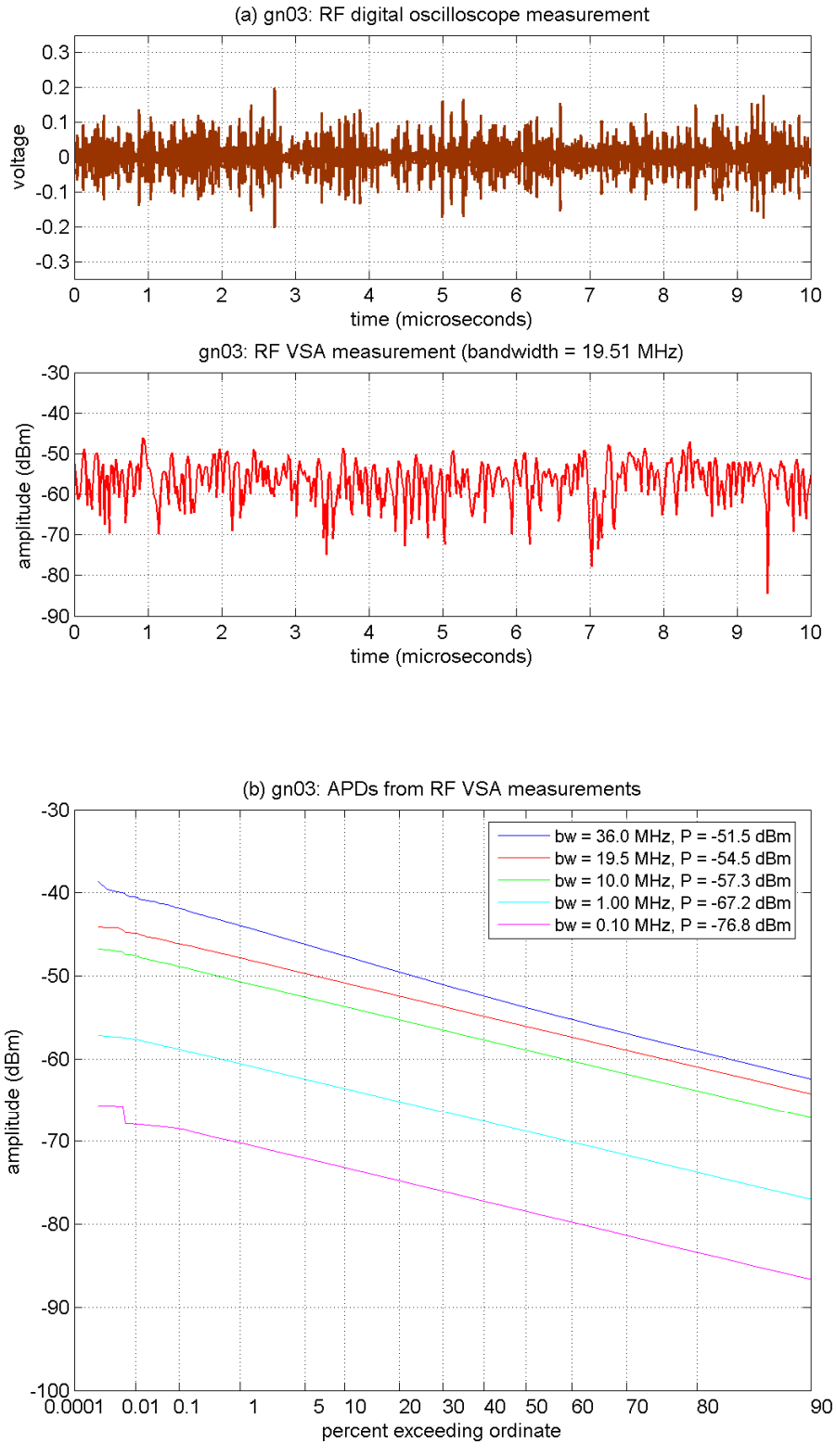

Figure D-7. RF measurements of GN-03 (τ_{on} = 10 ns, ζ = 0.2500).

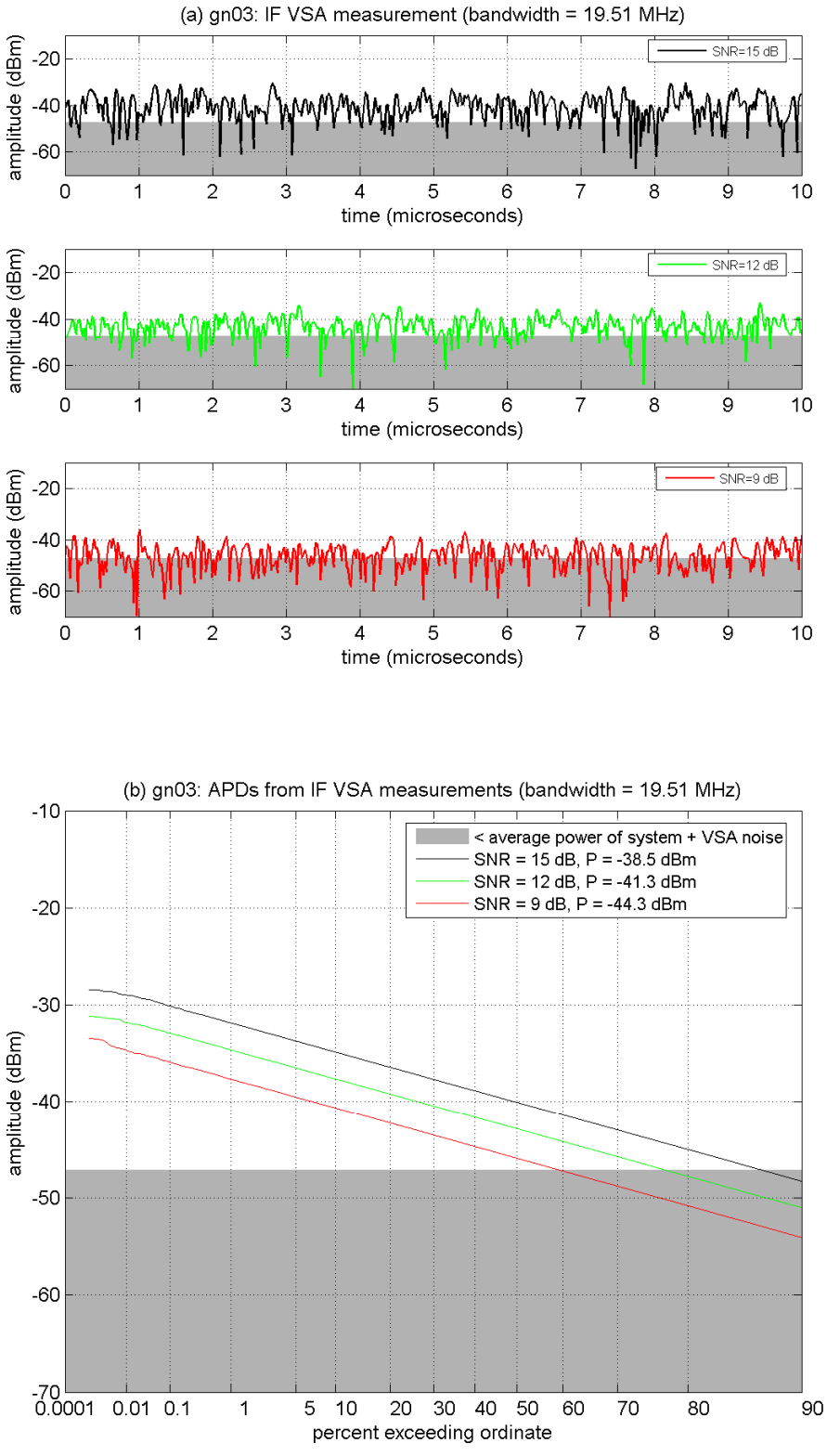

Figure D-8. IF measurements of GN-03 at INR_{TOV}.

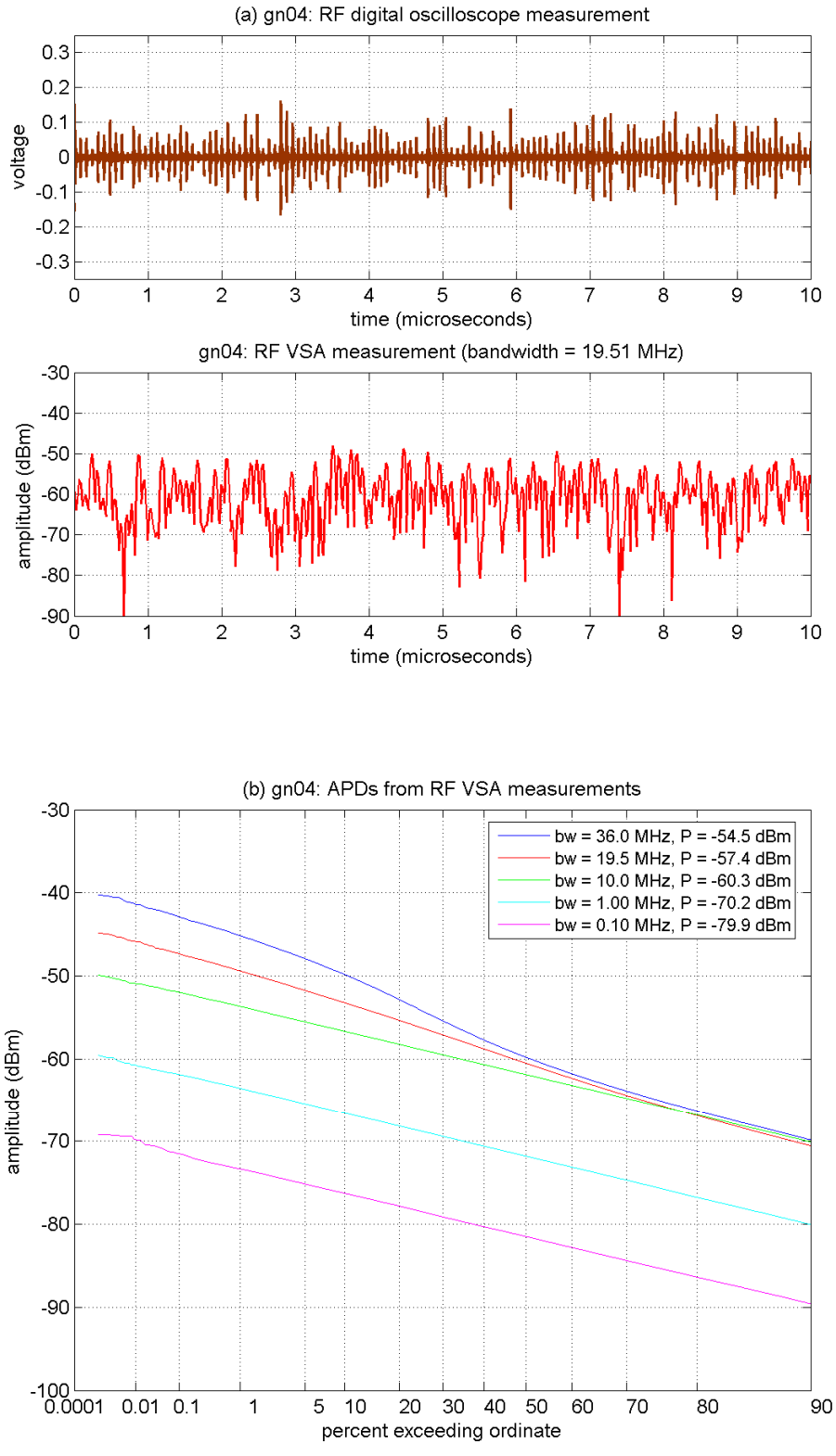

Figure D-9. RF measurements of GN-04 (τ_{on} = 10 ns, ζ = 0.1250).

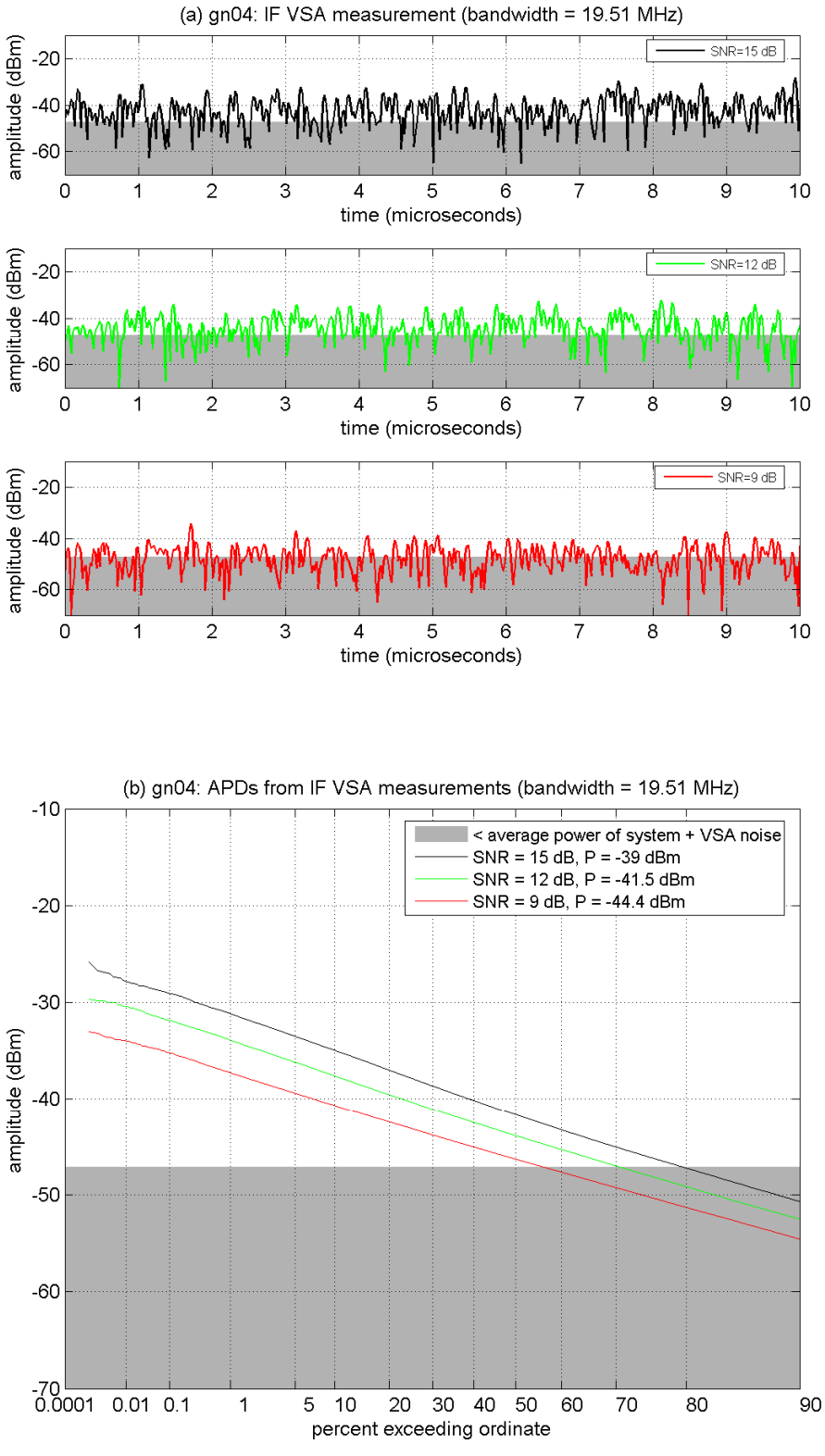

Figure D-10. IF measurements of GN-04 at INR_{TOV}.

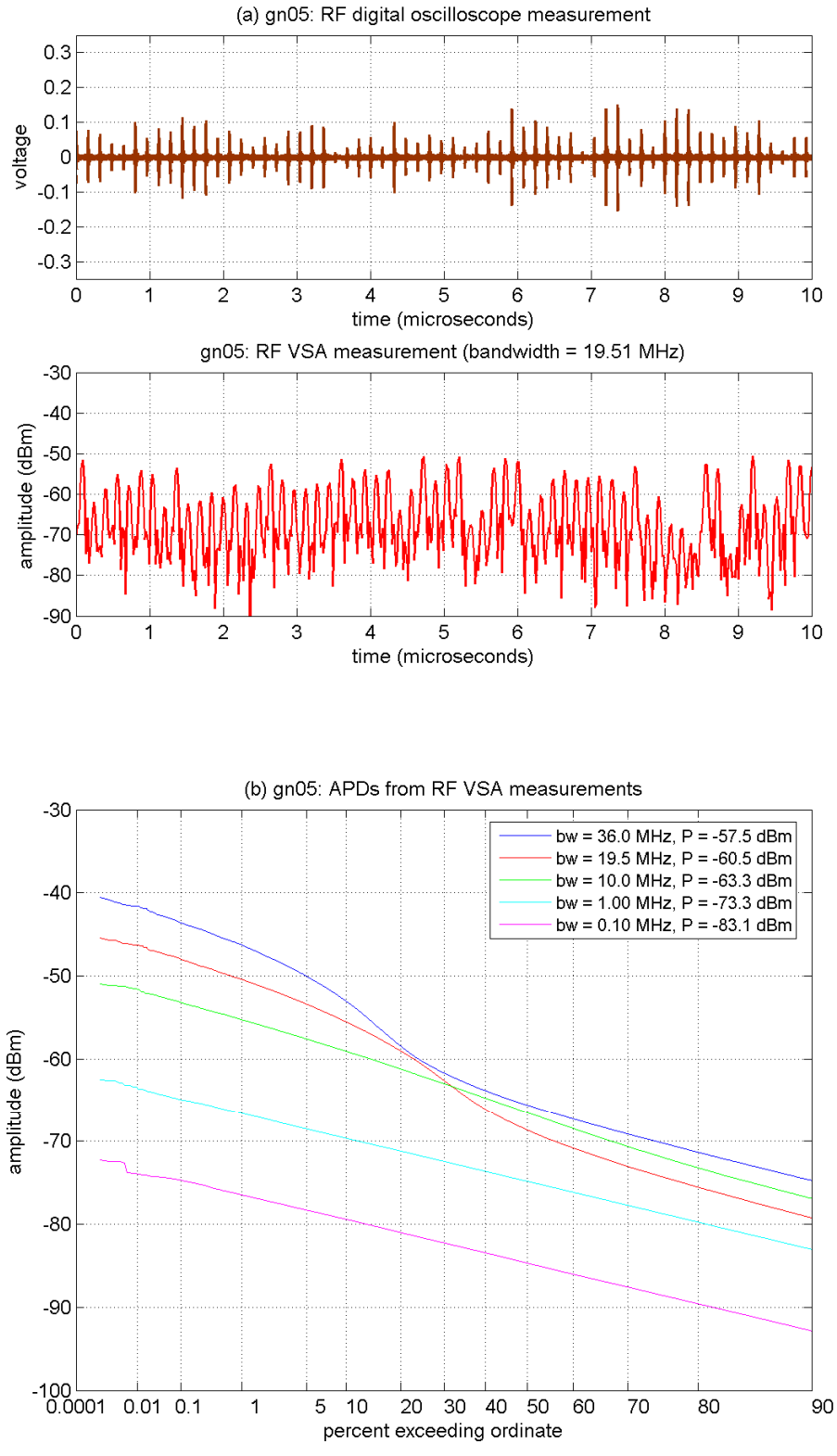

Figure D-11. RF measurements of GN-05 (τ_{on} = 10 ns, ζ = 0.0625).

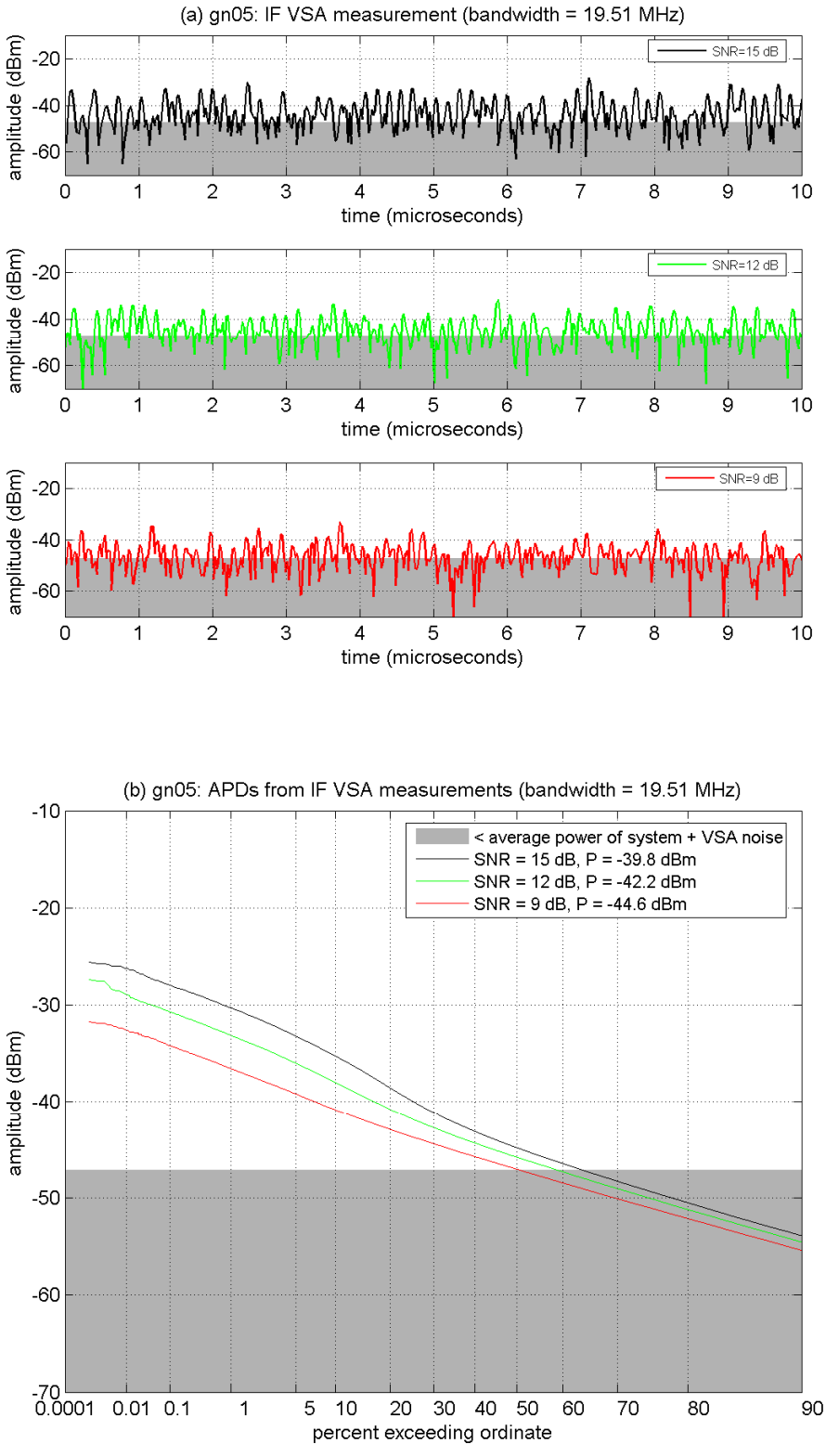

Figure D-12. IF measurements of GN-05 at INR_{TOV}.

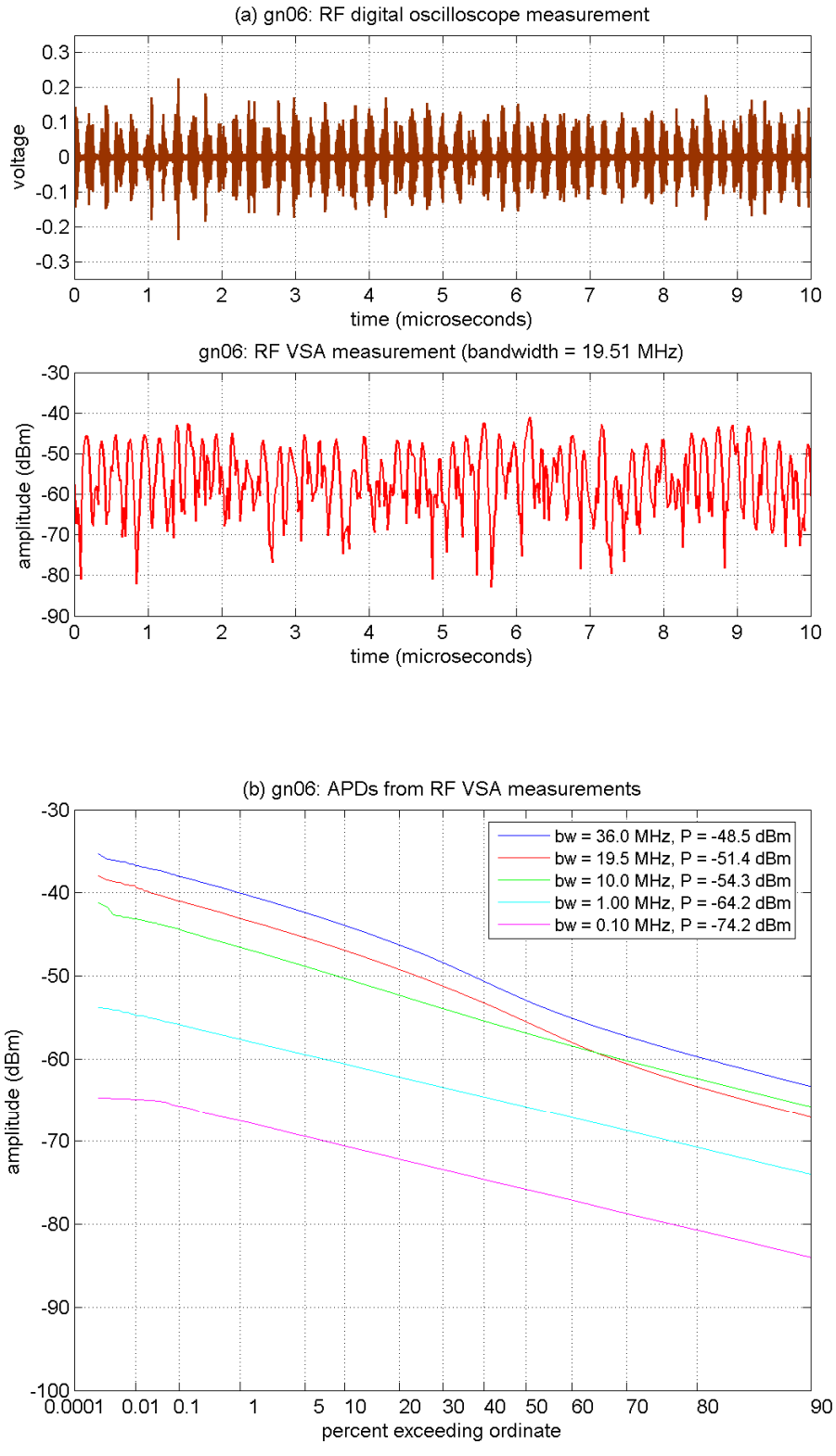

Figure D-13. RF measurements of GN-06 (τ_{on} = 100 ns, ζ = 0.5000).

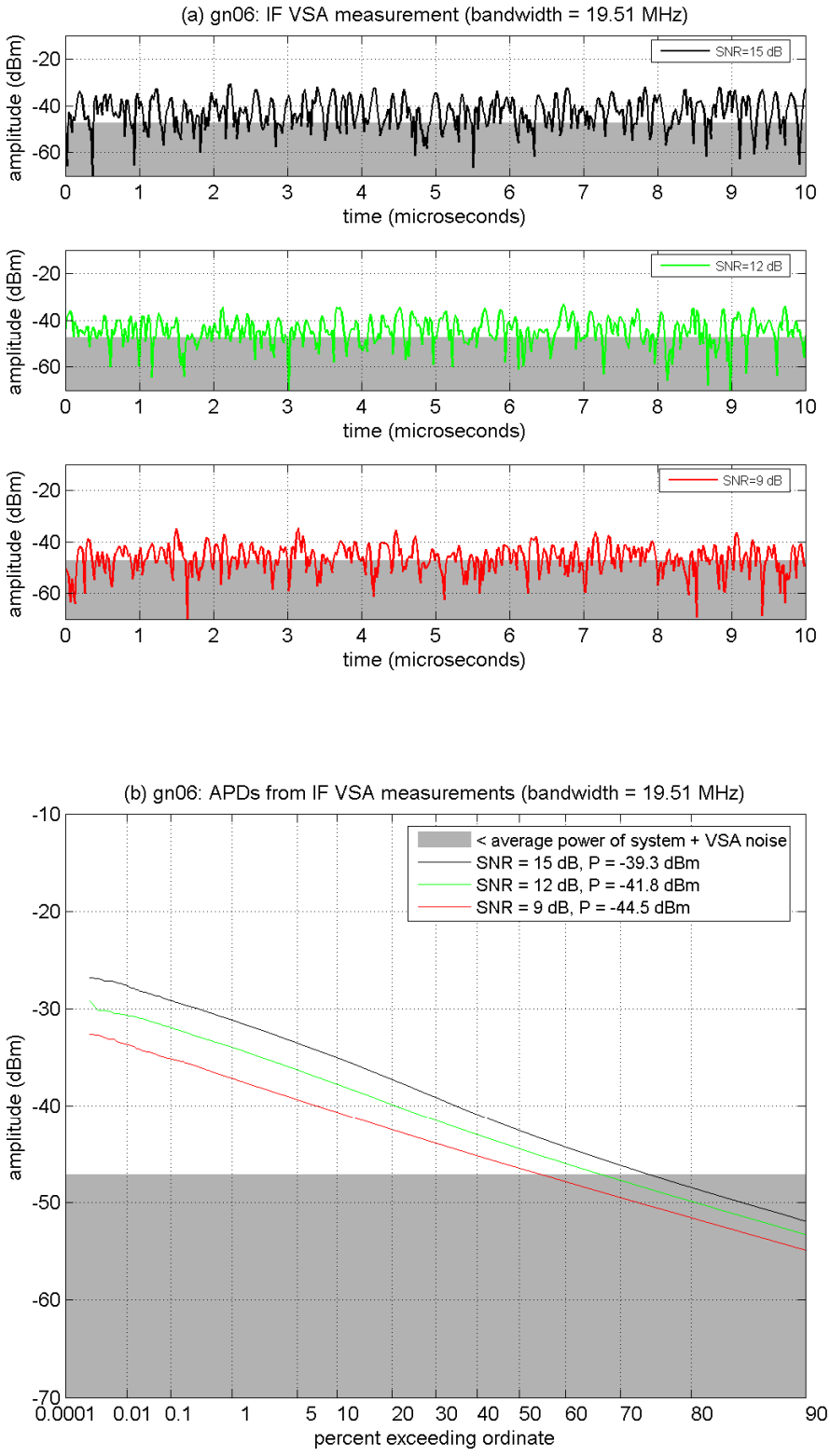

Figure D-14. IF measurements of GN-06 at INR_{TOV}.

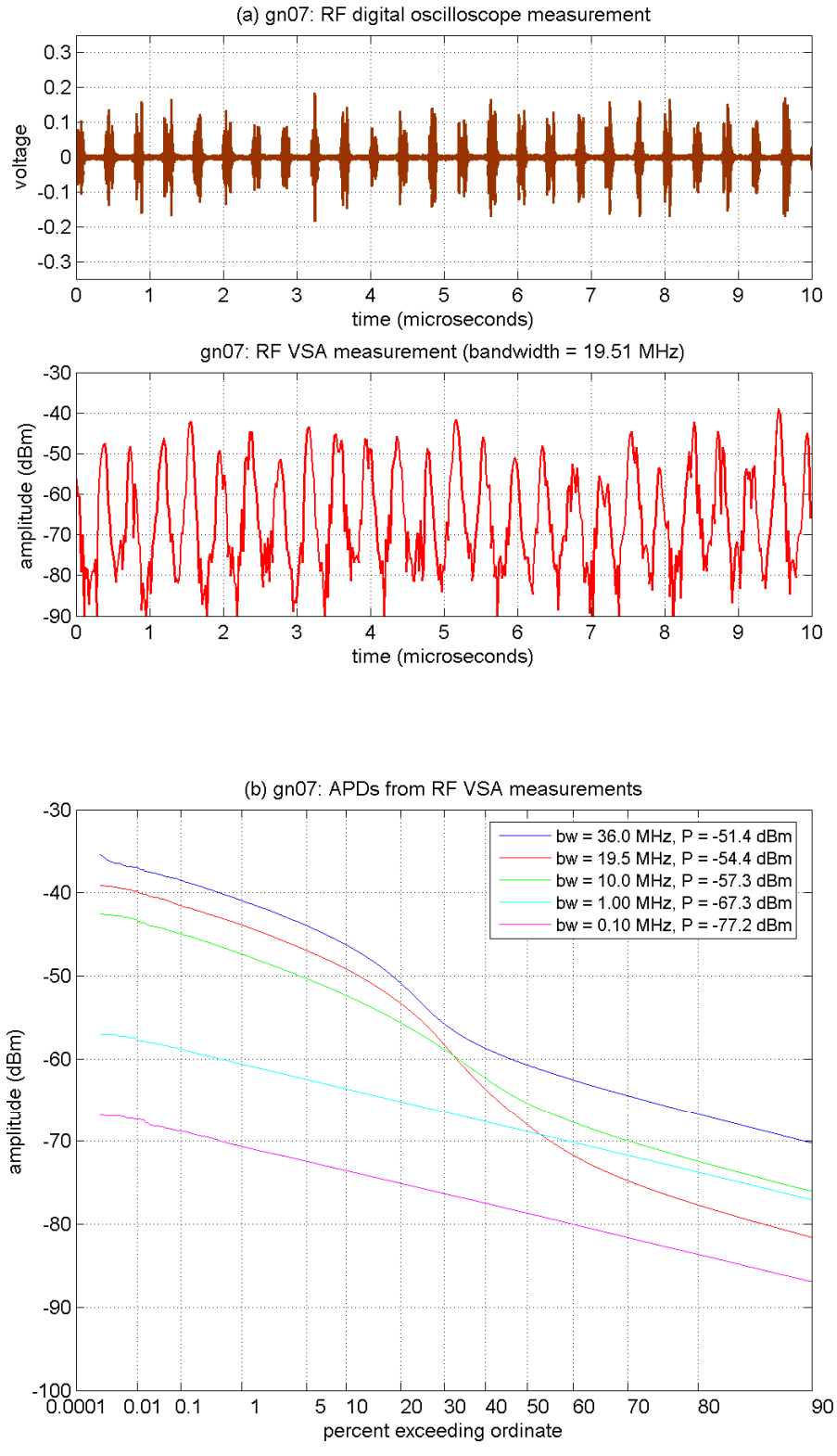

Figure D-15. RF measurements of GN-07 (τ_{on} = 100 ns, ζ = 0.2500).

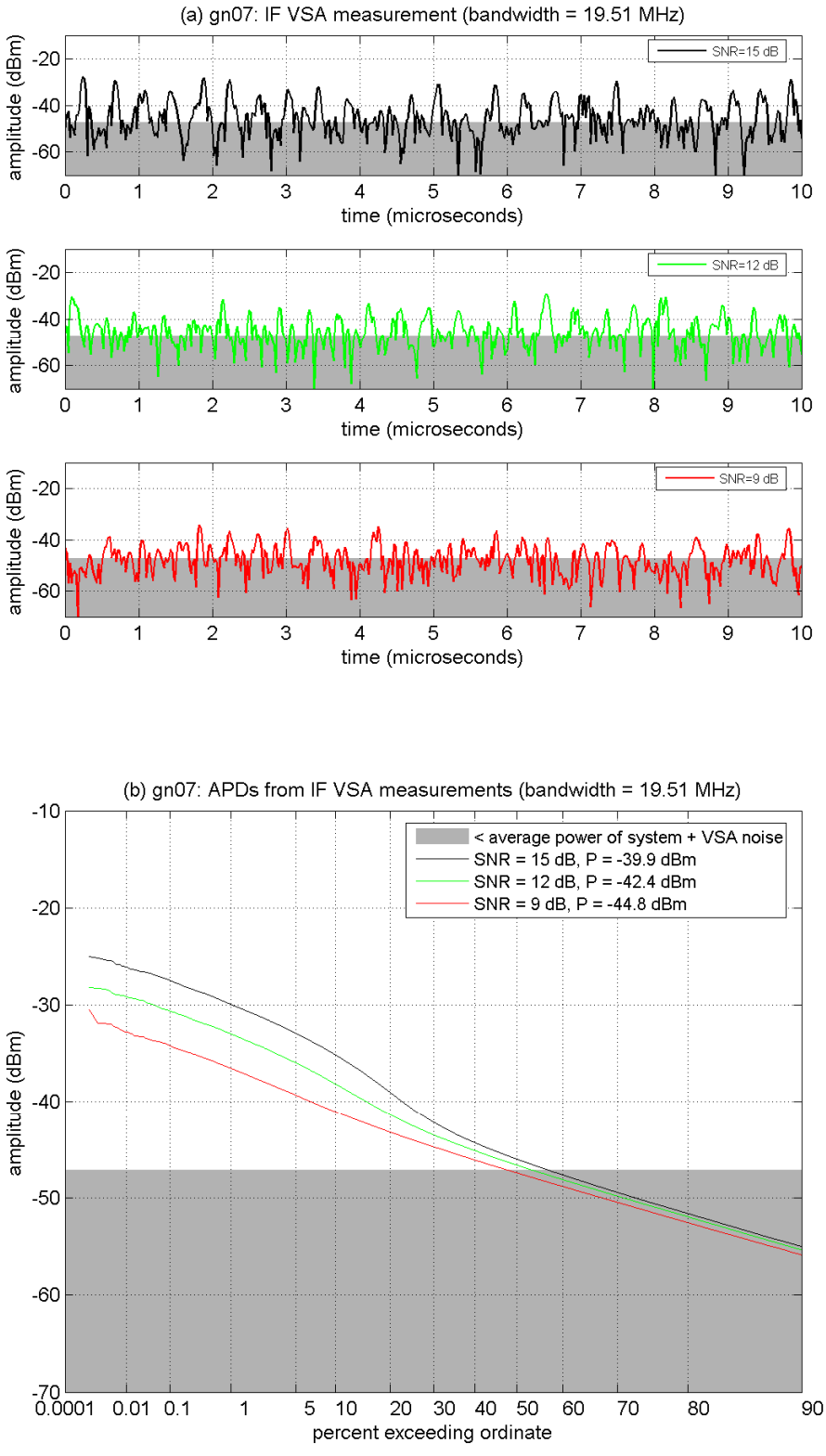

Figure D-16. IF measurements of GN-07 at INR_{TOV}.

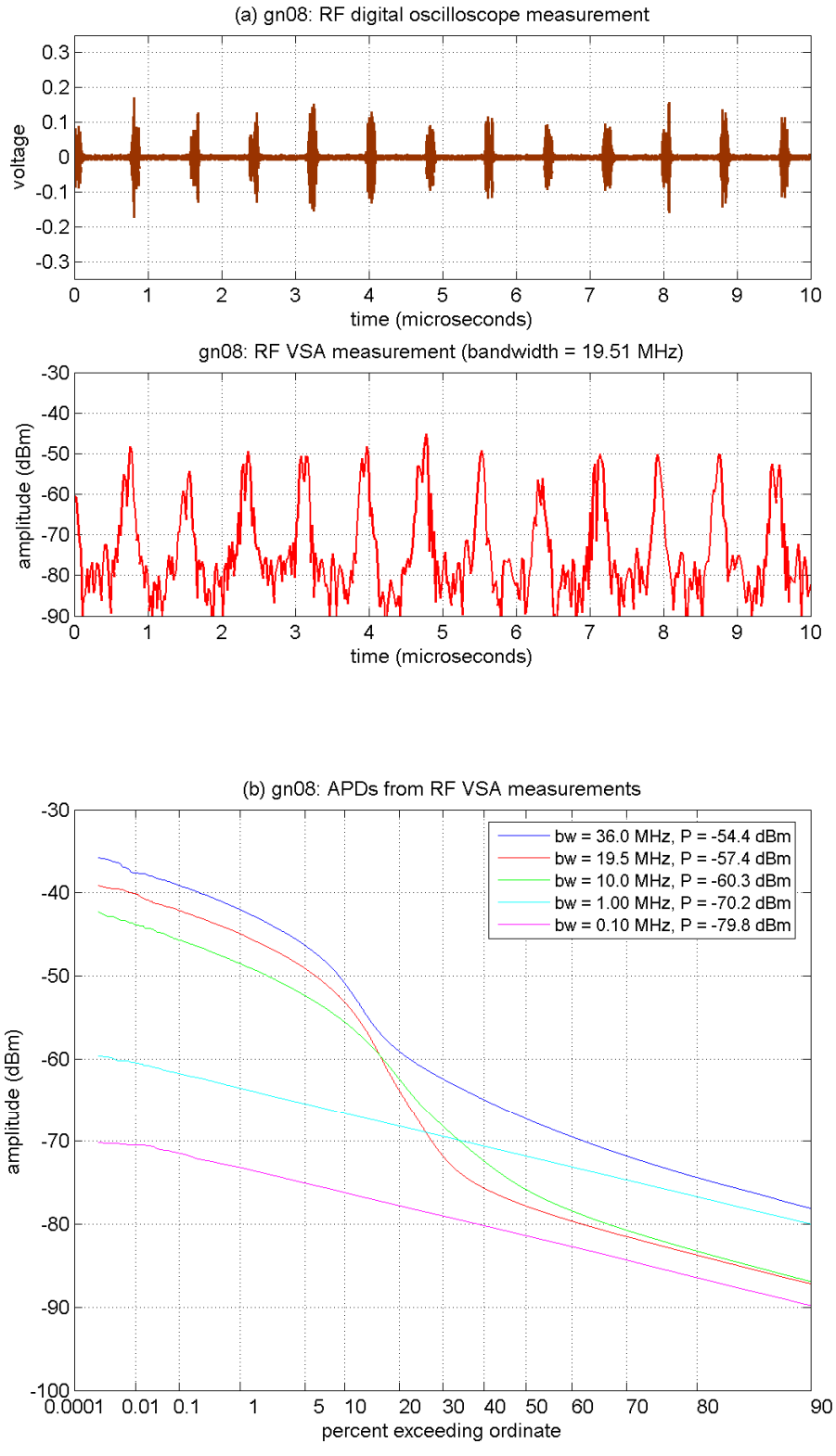

Figure D-17. RF measurements of GN-08 (τ_{on} = 100 ns, ζ = 0.1250).

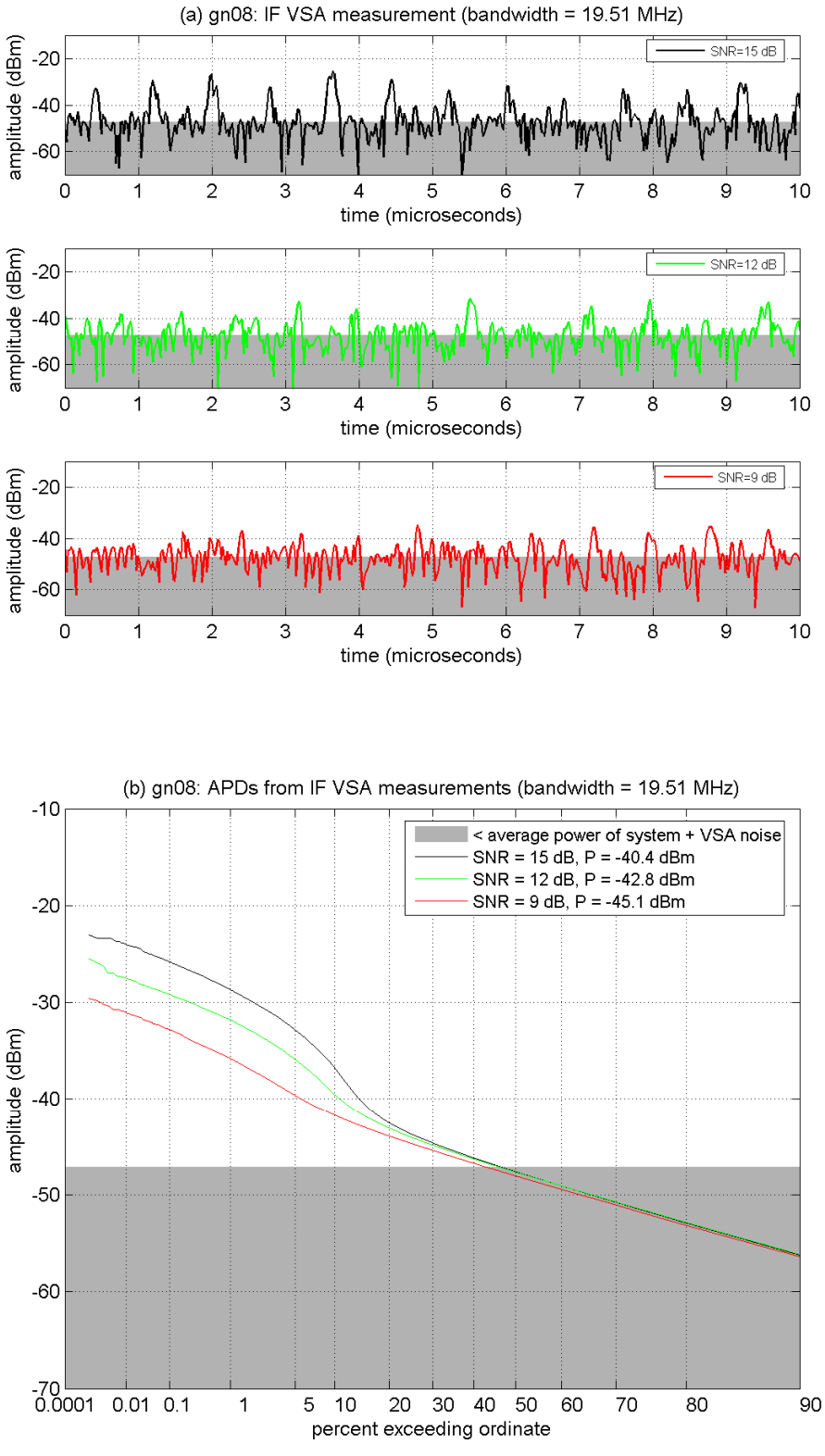

Figure D-18. IF measurements of GN-08 at INR_{TOV}.

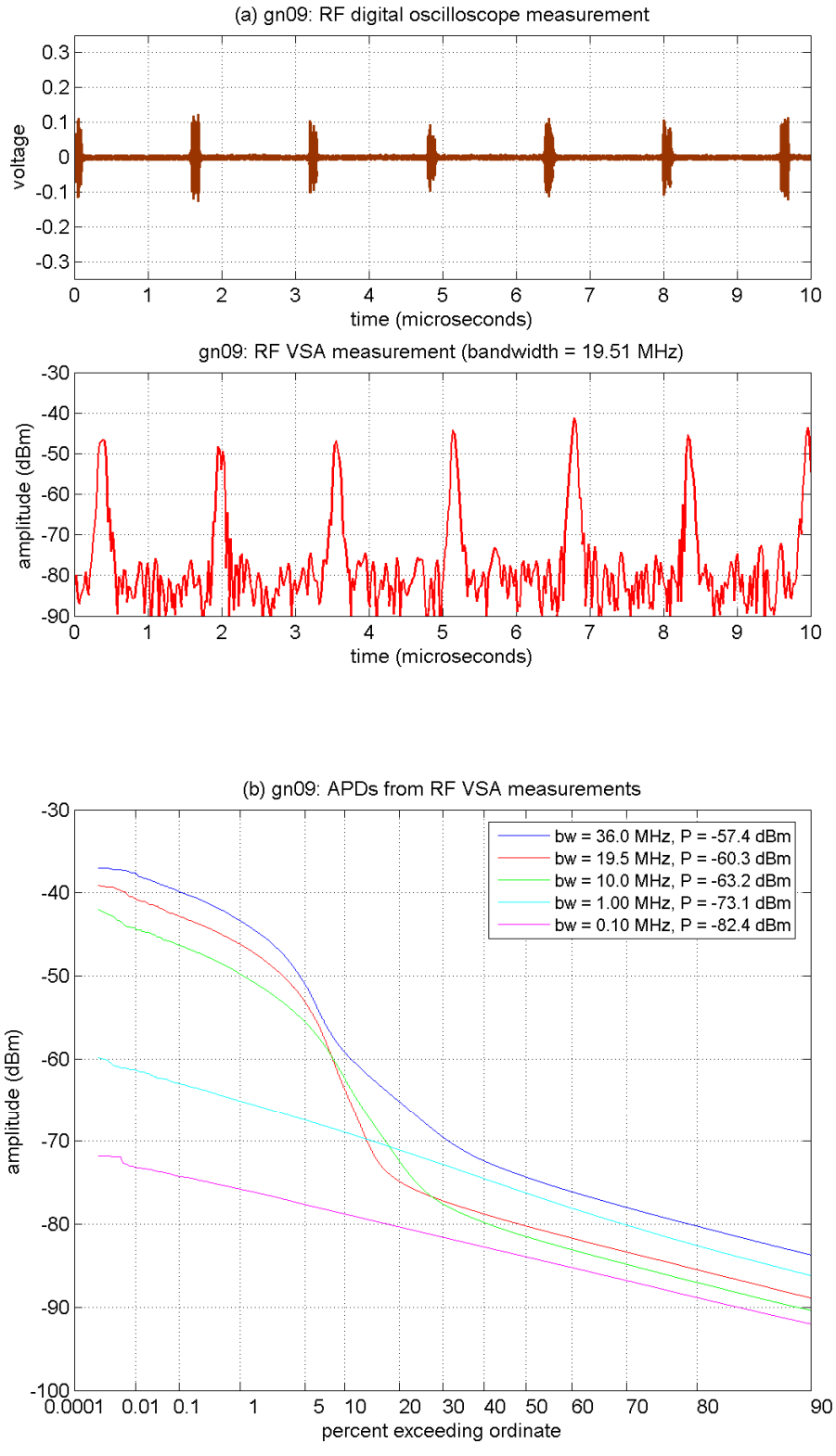

Figure D-19. RF measurements of GN-09 (τ_{on} = 100 ns, ζ = 0.0625).

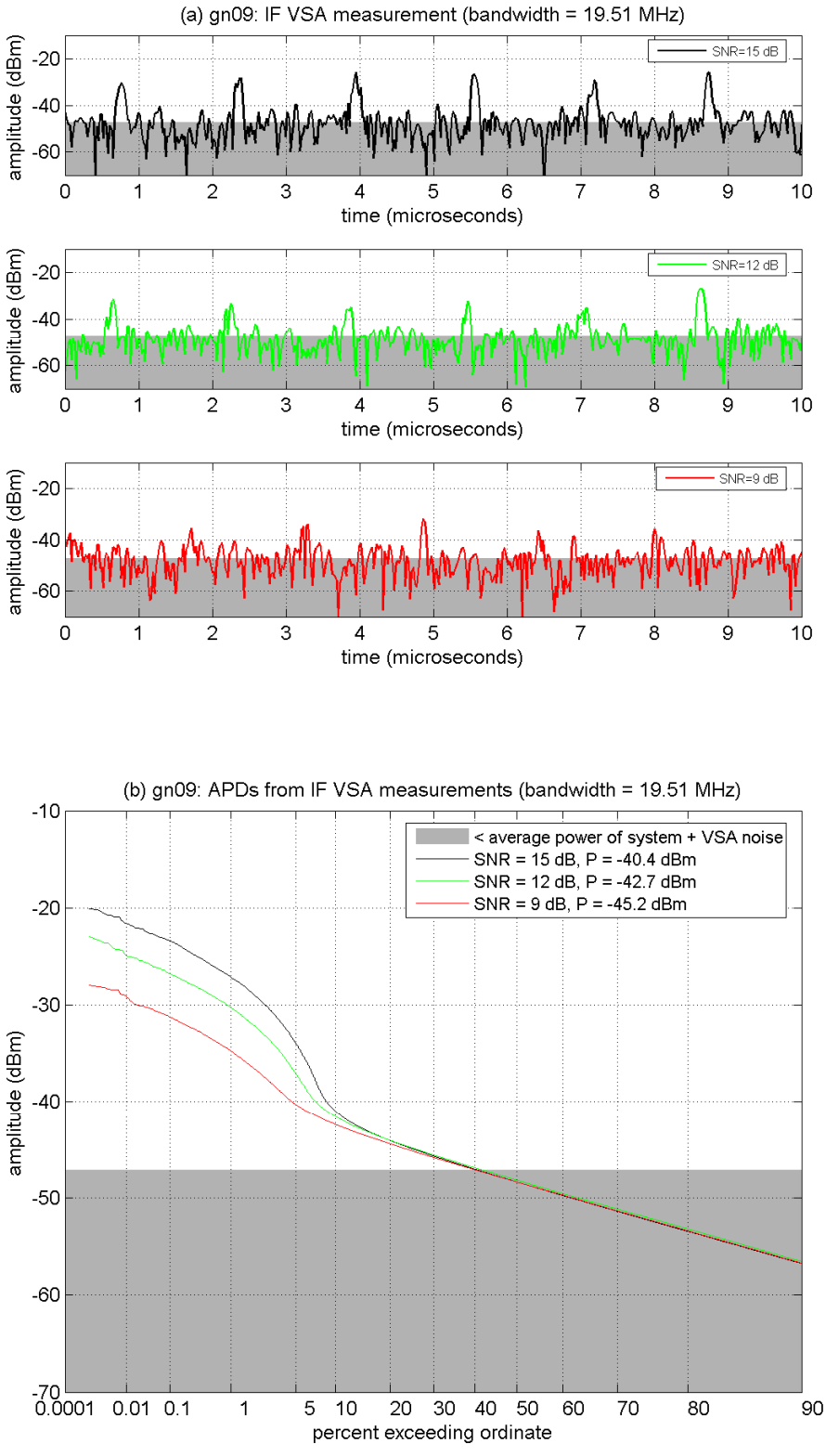

Figure D-20. IF measurements of GN-09 at INR_{TOV}.

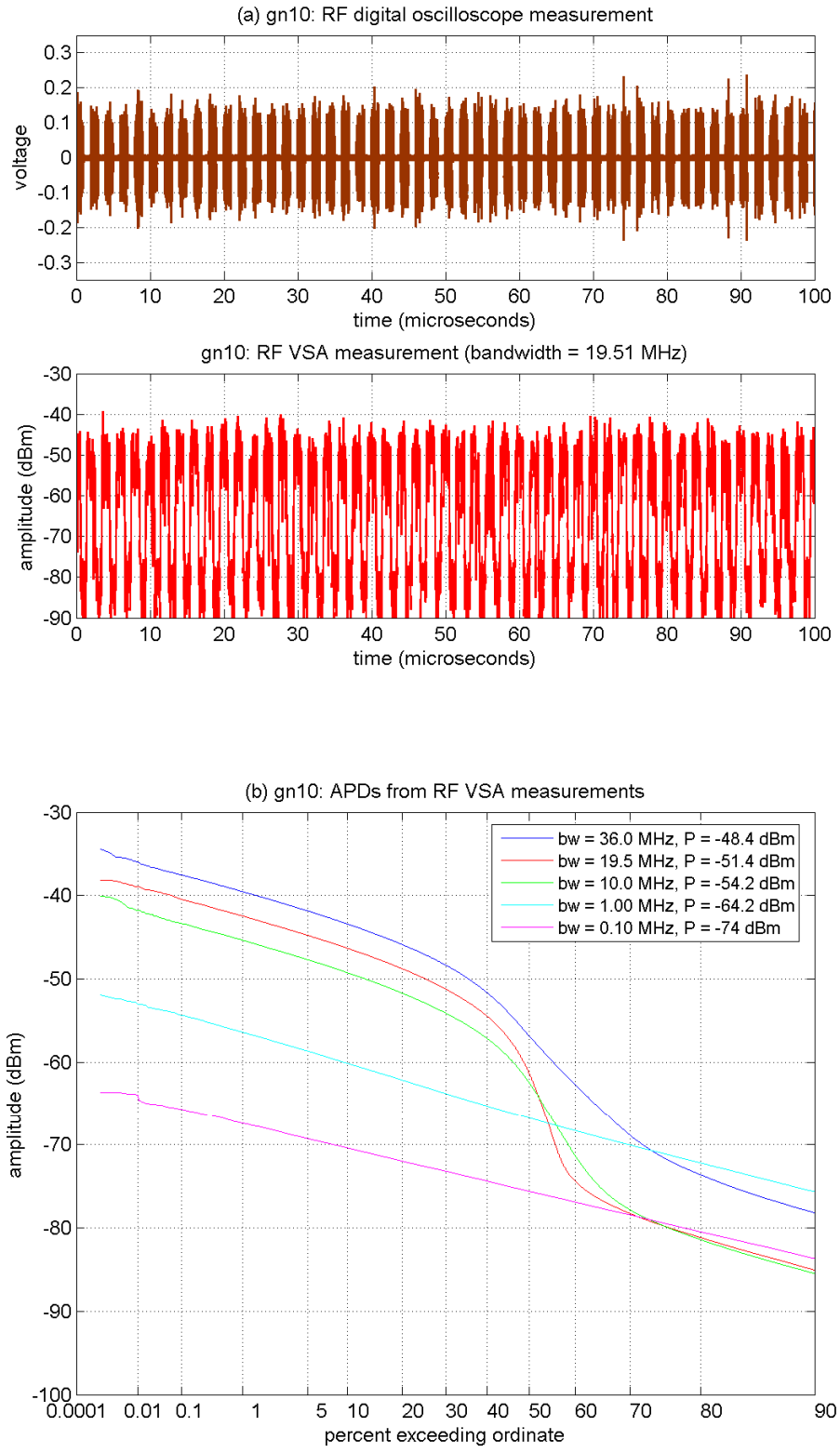

Figure D-21. RF measurements of GN-10 (τ_{on} = 1000 ns, ζ = 0.5000).

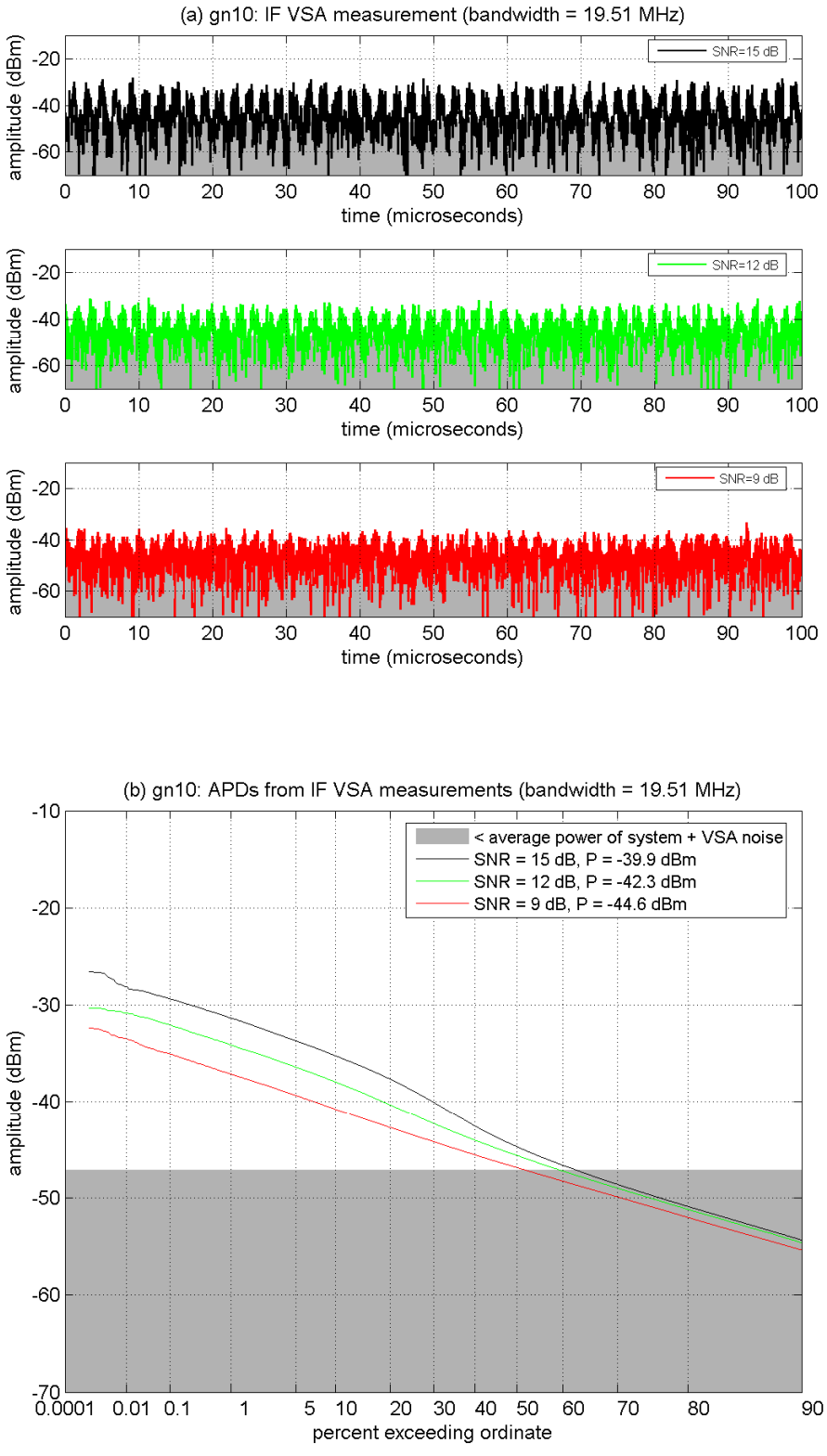

Figure D-22. IF measurements of GN-10 at INR_{TOV}.

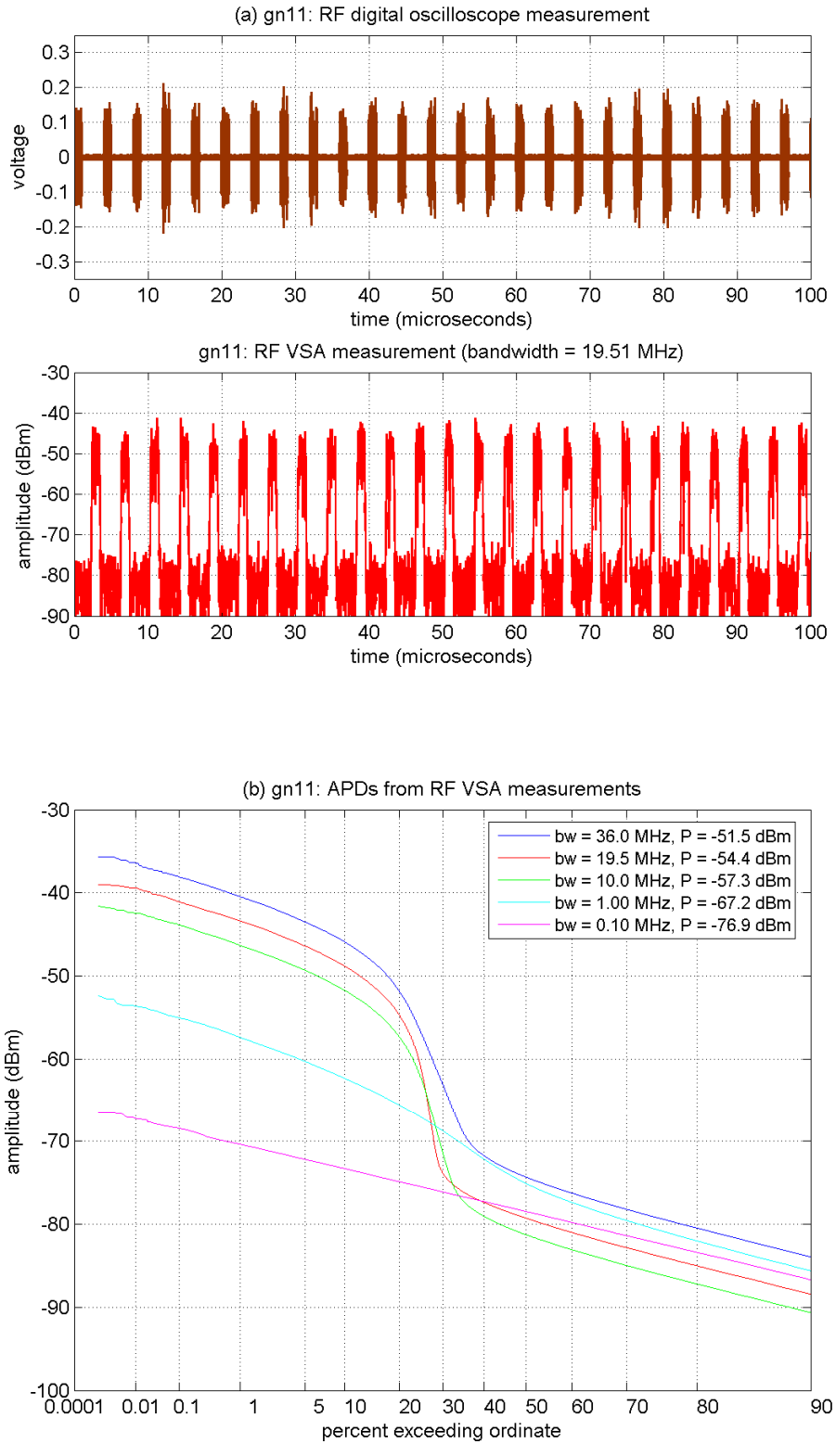

Figure D-23. RF measurements of GN-11 (τ_{on} = 1000 ns, ζ = 0.2500).

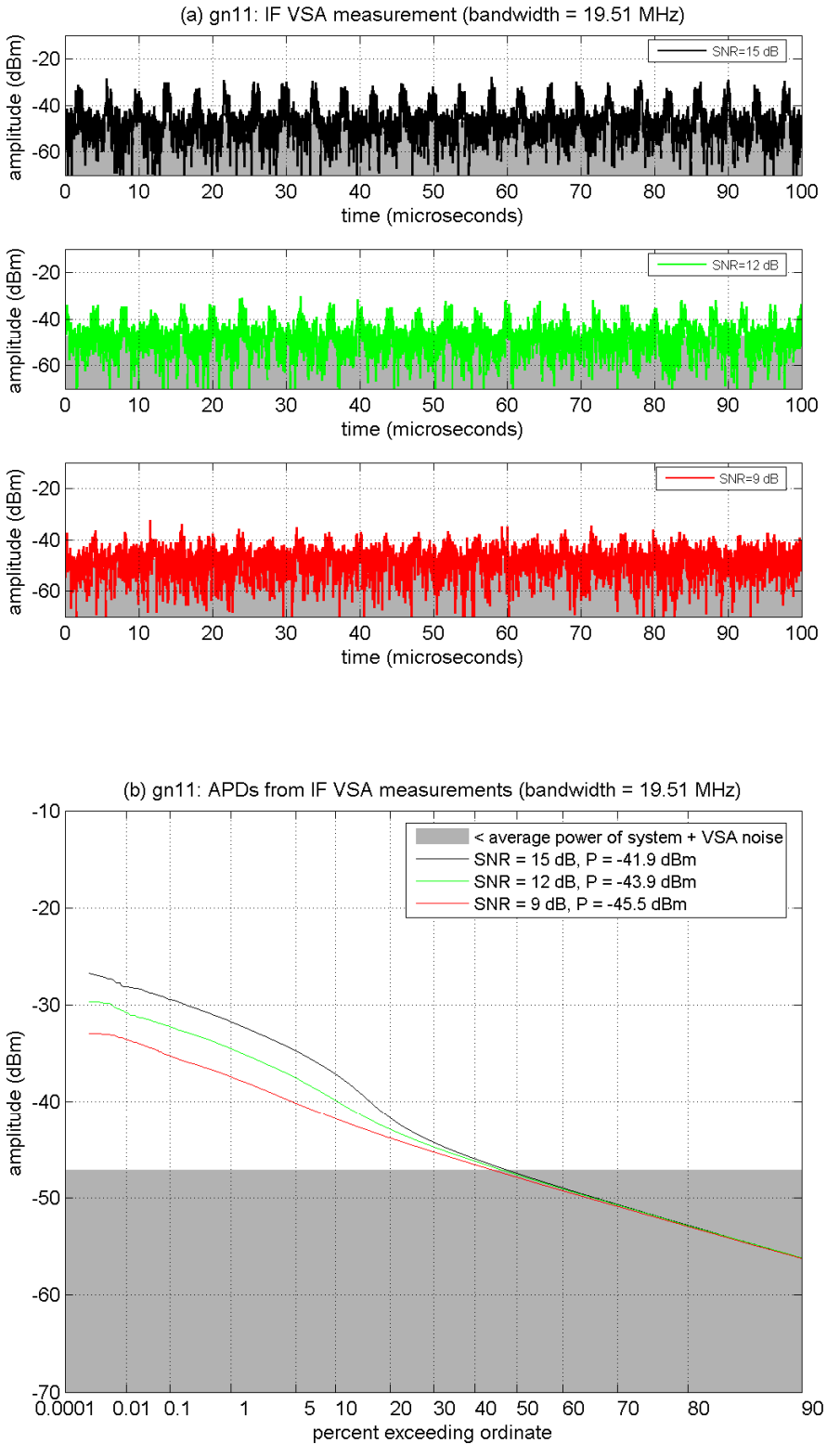

Figure D-24. IF measurements of GN-11 at INR_{TOV}.

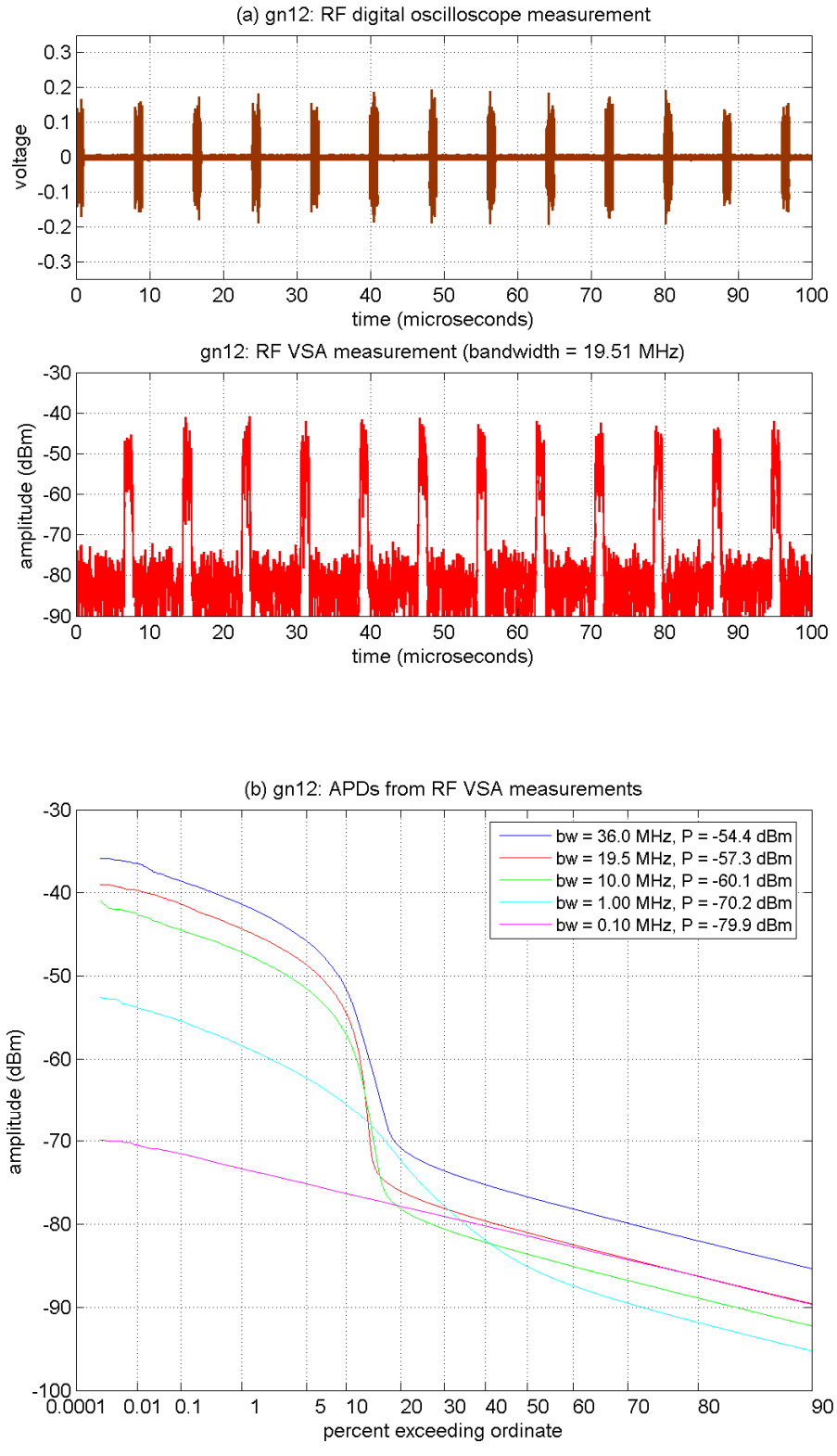

Figure D-25. RF measurements of GN-12 (τ_{on} = 1000 ns, ζ = 0.1250).

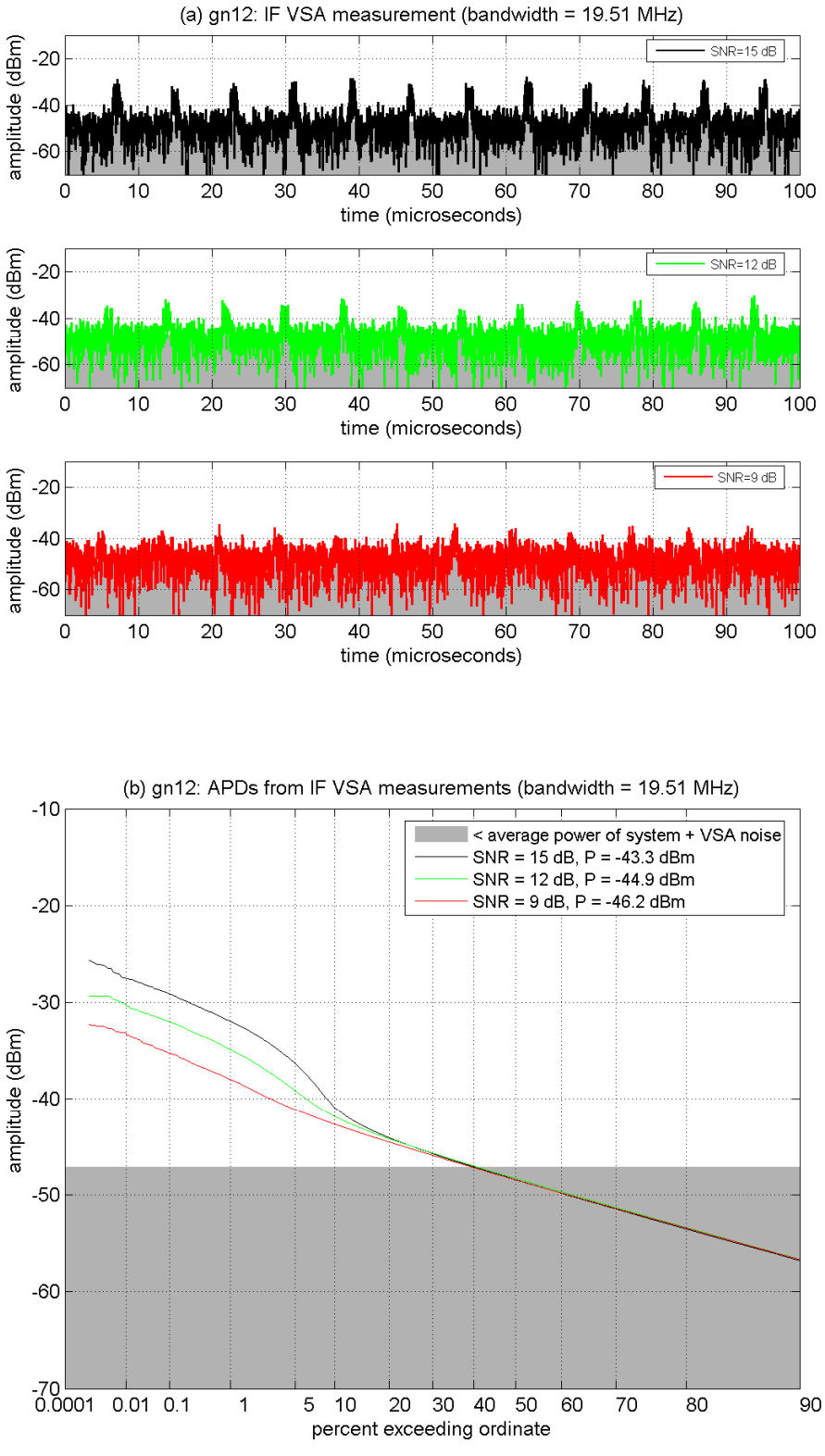

Figure D-26. IF measurements of GN-12 at INR_{TOV}.

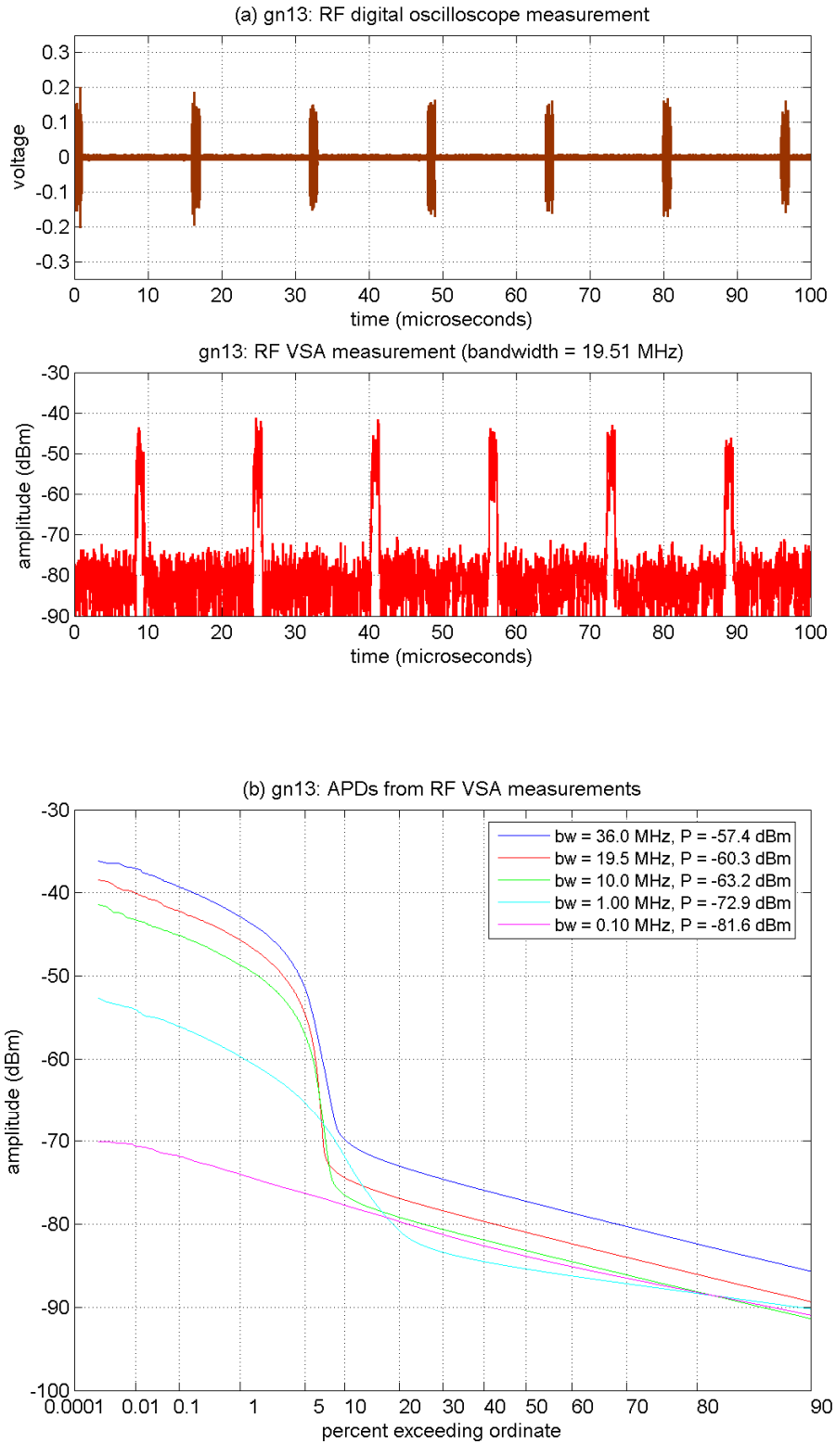

Figure D-27. RF measurements of GN-13 (τ_{on} = 1000 ns, ζ = 0.0625).

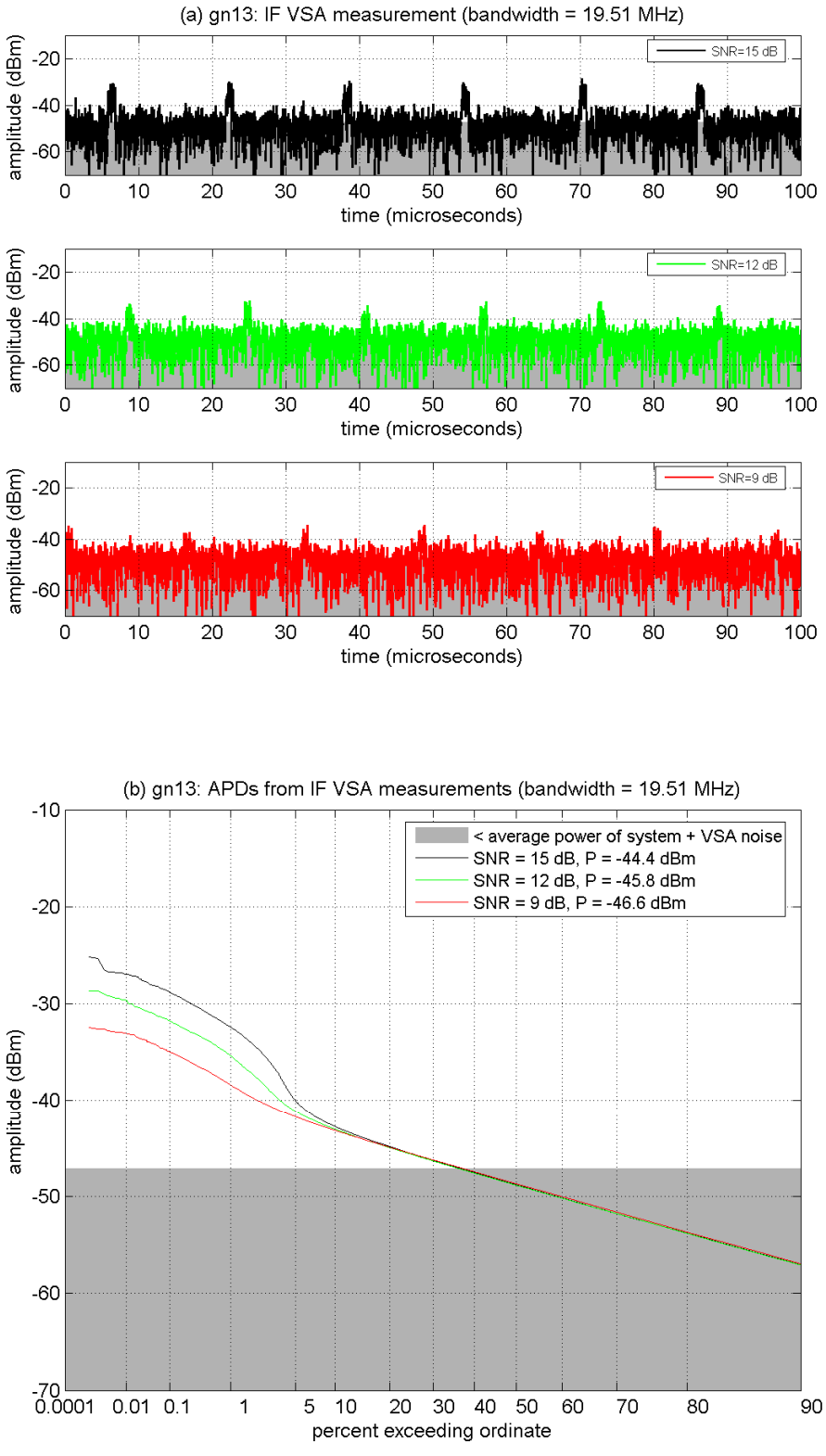

Figure D-28. IF measurements of GN-13 at INR_{TOV}.

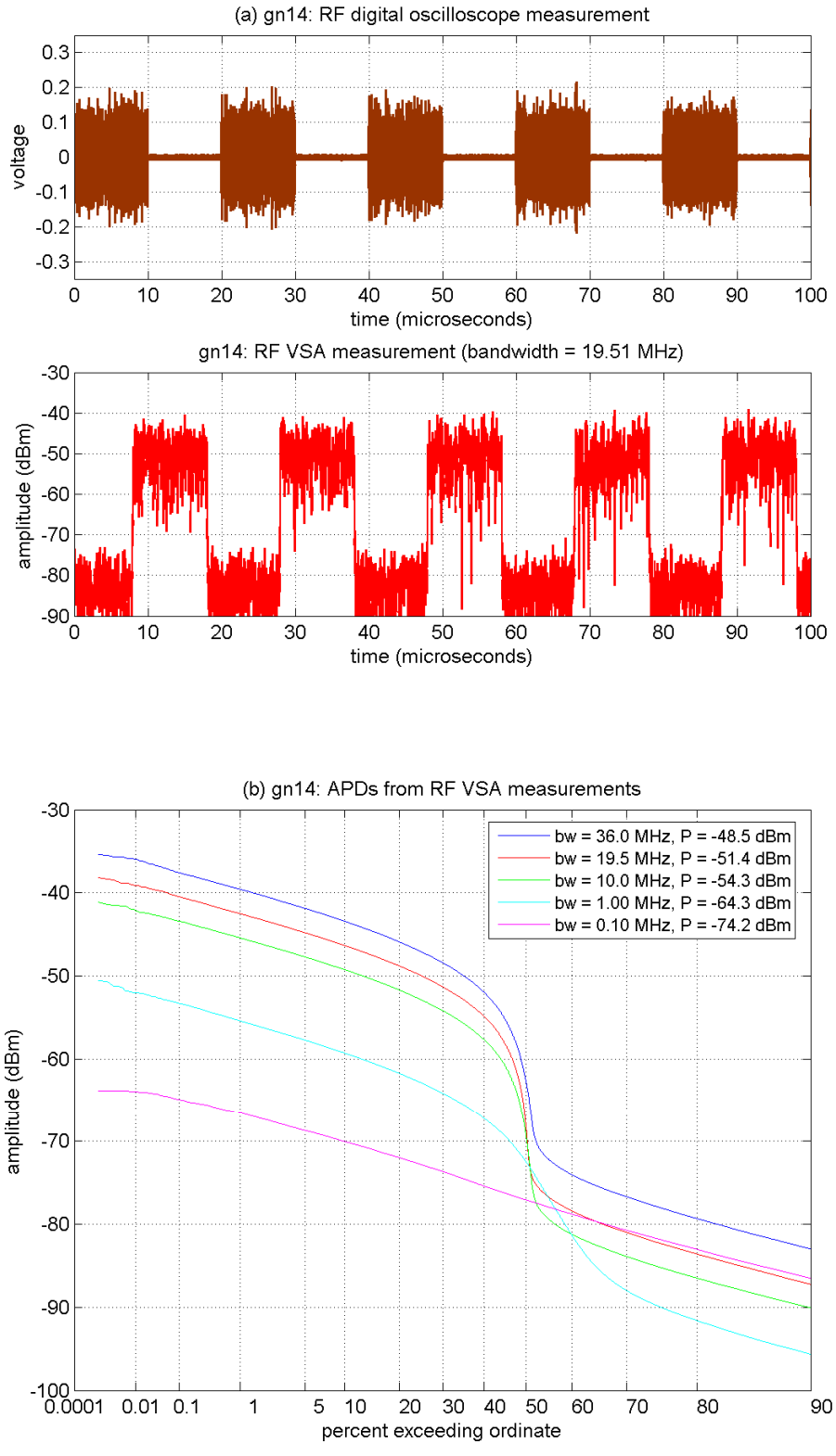

Figure D-29. RF measurements of GN-14 (τ_{on} = 10000 ns, ζ = 0.5000).

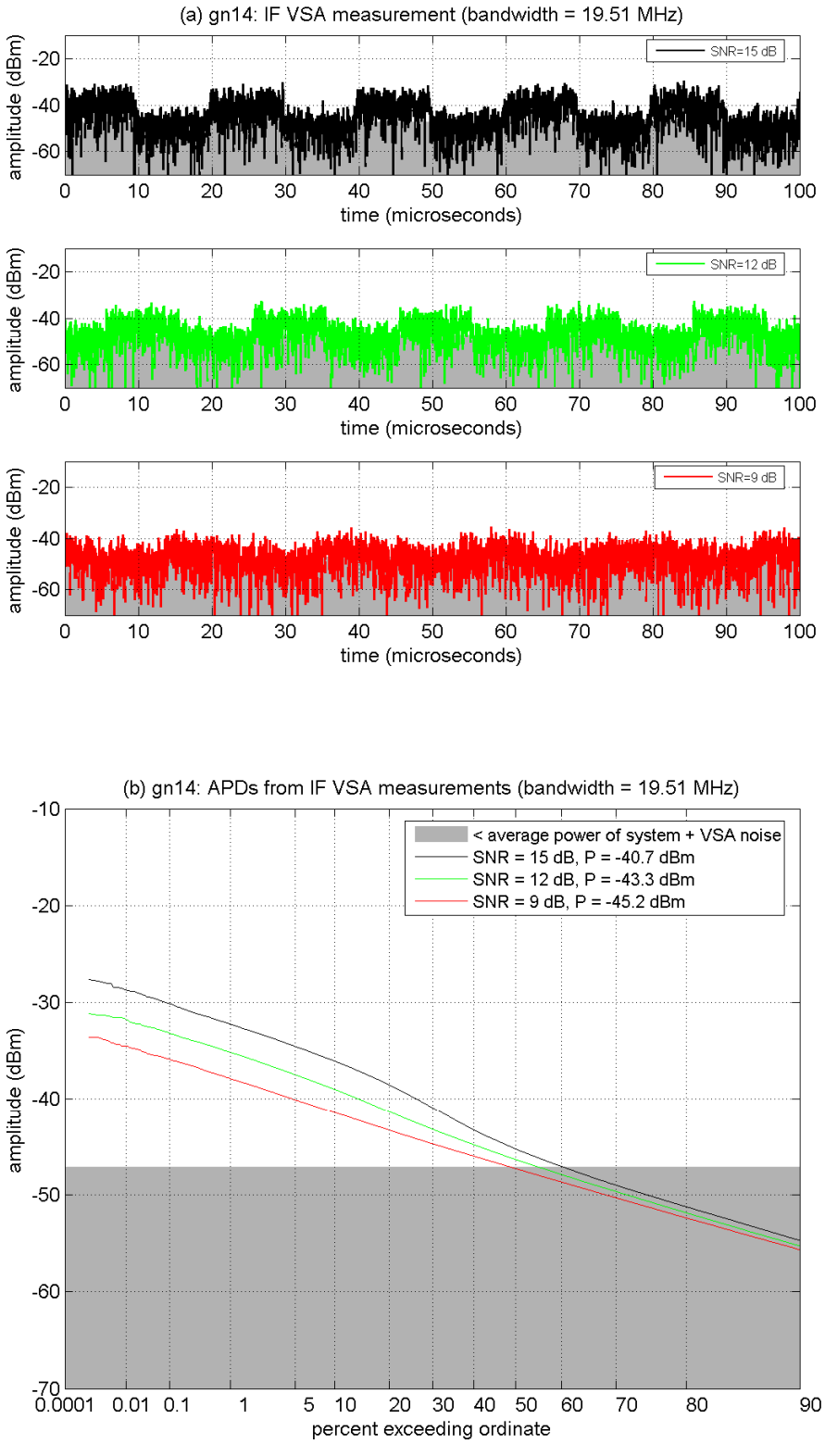

Figure D-30. IF measurements of GN-14 at INR_{TOV}.

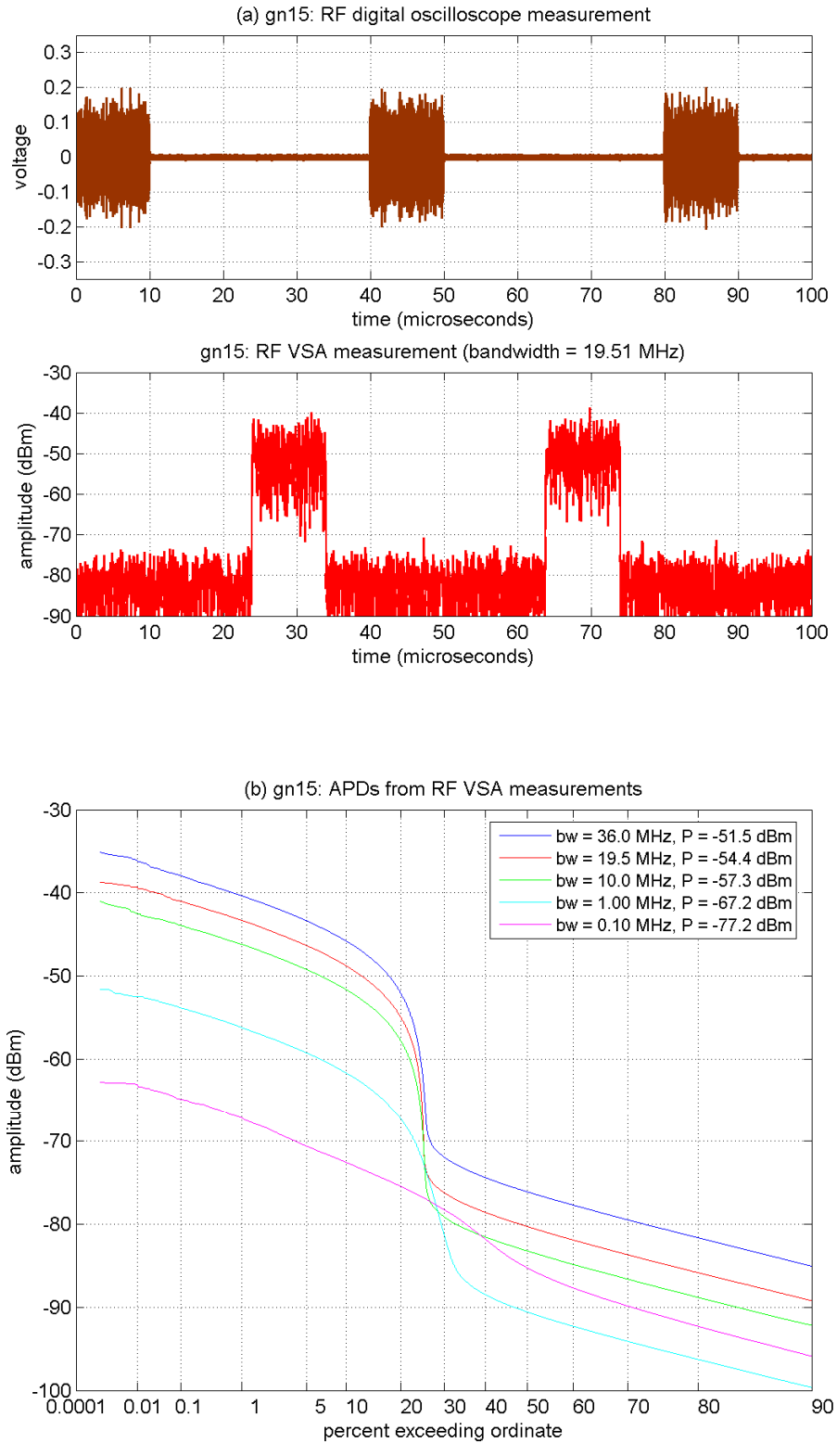

Figure D-31. RF measurements of GN-15 (τ_{on} = 10000 ns, ζ = 0.2500).

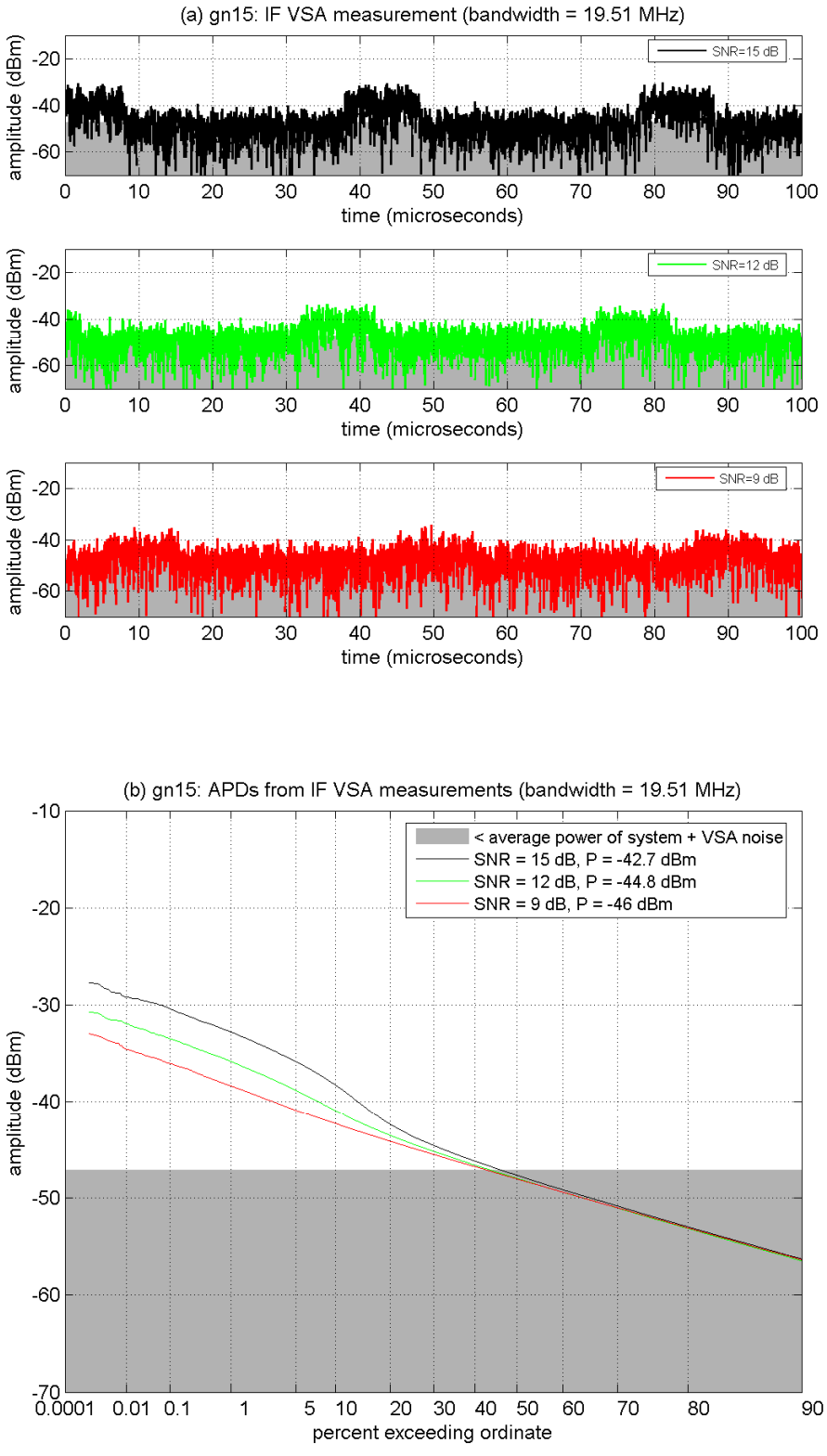

Figure D-32. IF measurements of GN-15 at INR_{TOV}.

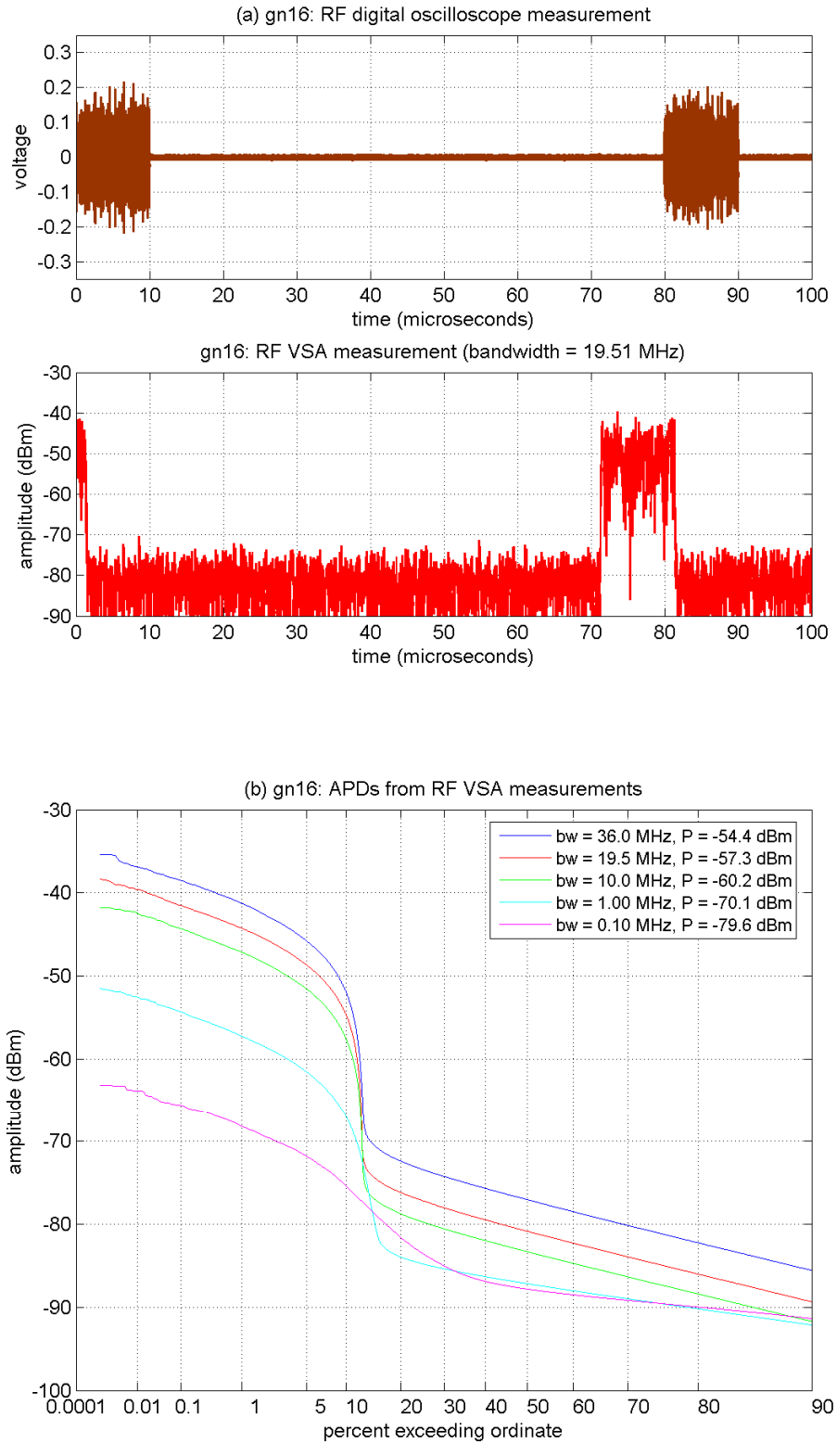

Figure D-33. RF measurements of GN-16 (τ_{on} = 10000 ns, ζ = 0.1250).

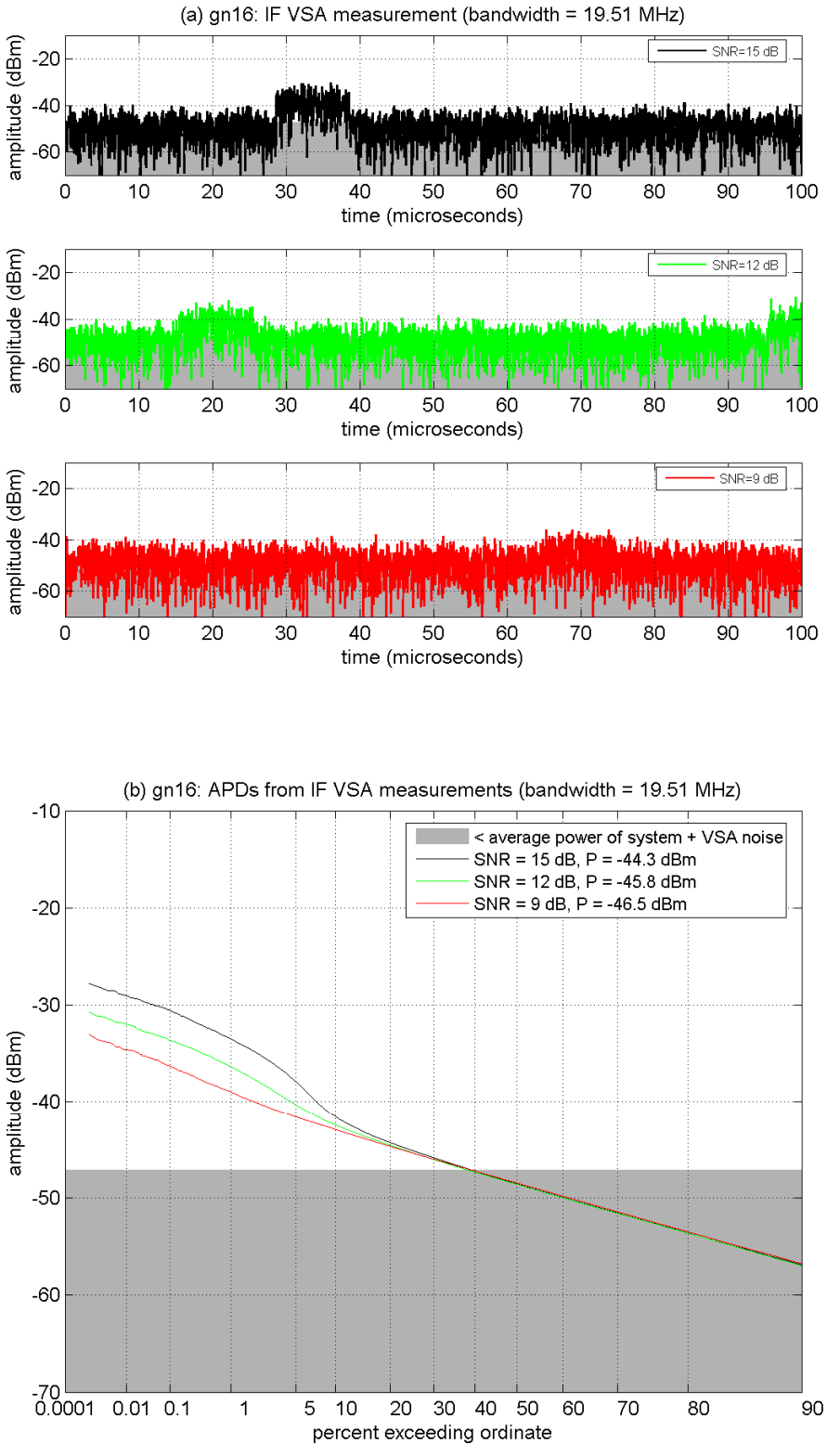

Figure D-34. IF measurements of GN-16 at INR_{TOV}.

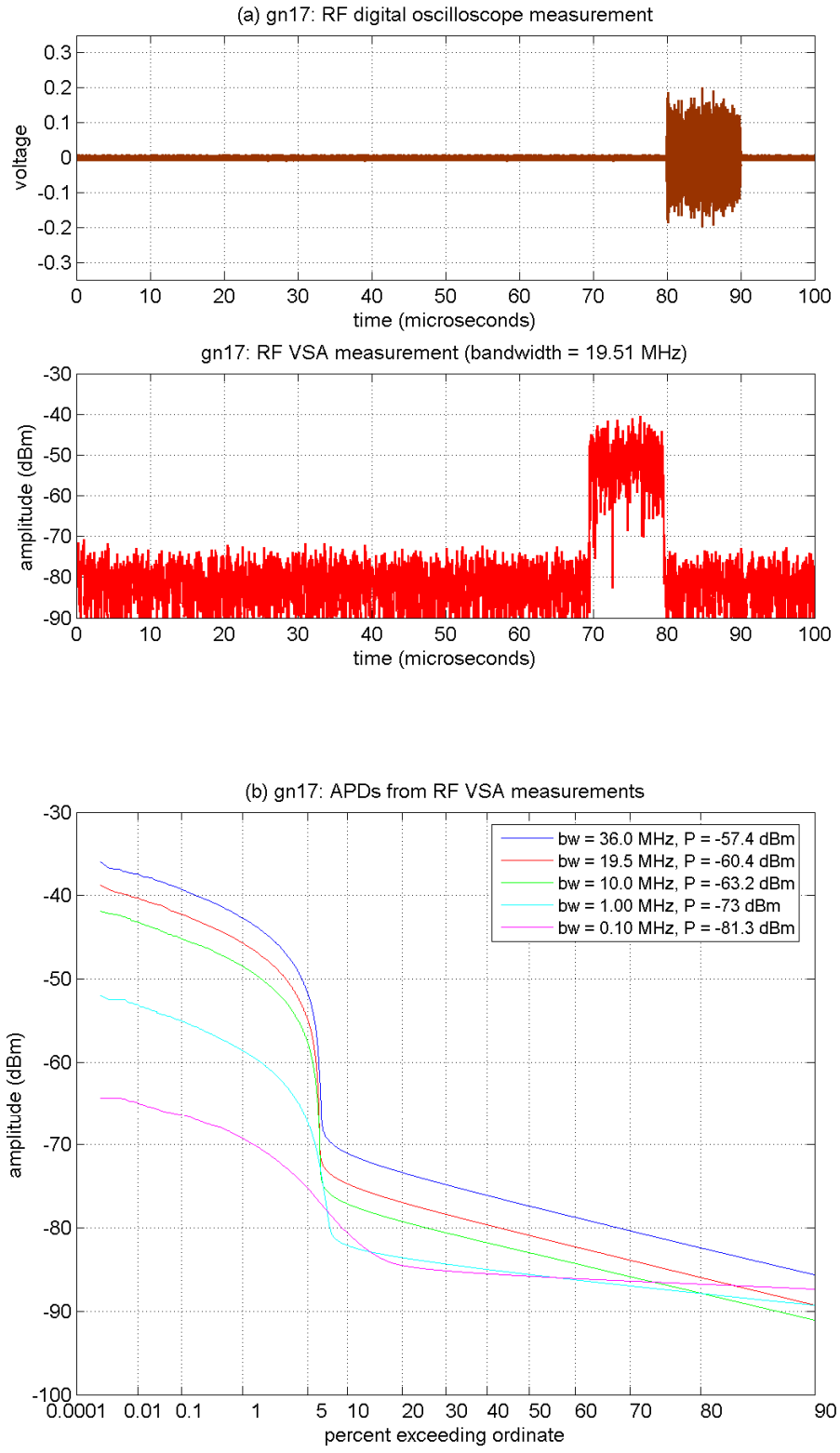

Figure D-35. RF measurements of GN-17 (τ_{on} = 10000 ns, ζ = 0.0625).

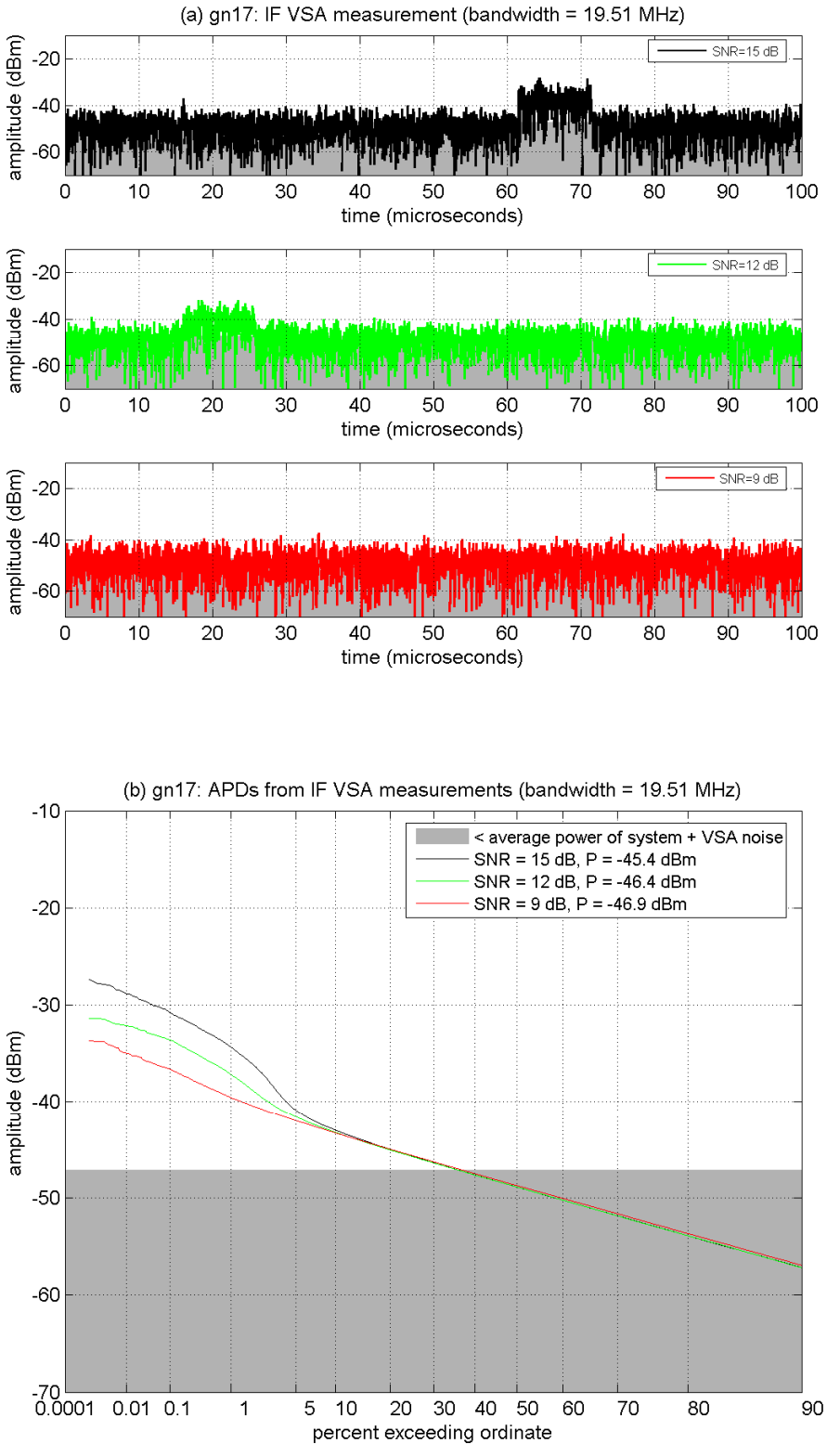

Figure D-36. IF measurements of GN-17 at INR_{TOV}.

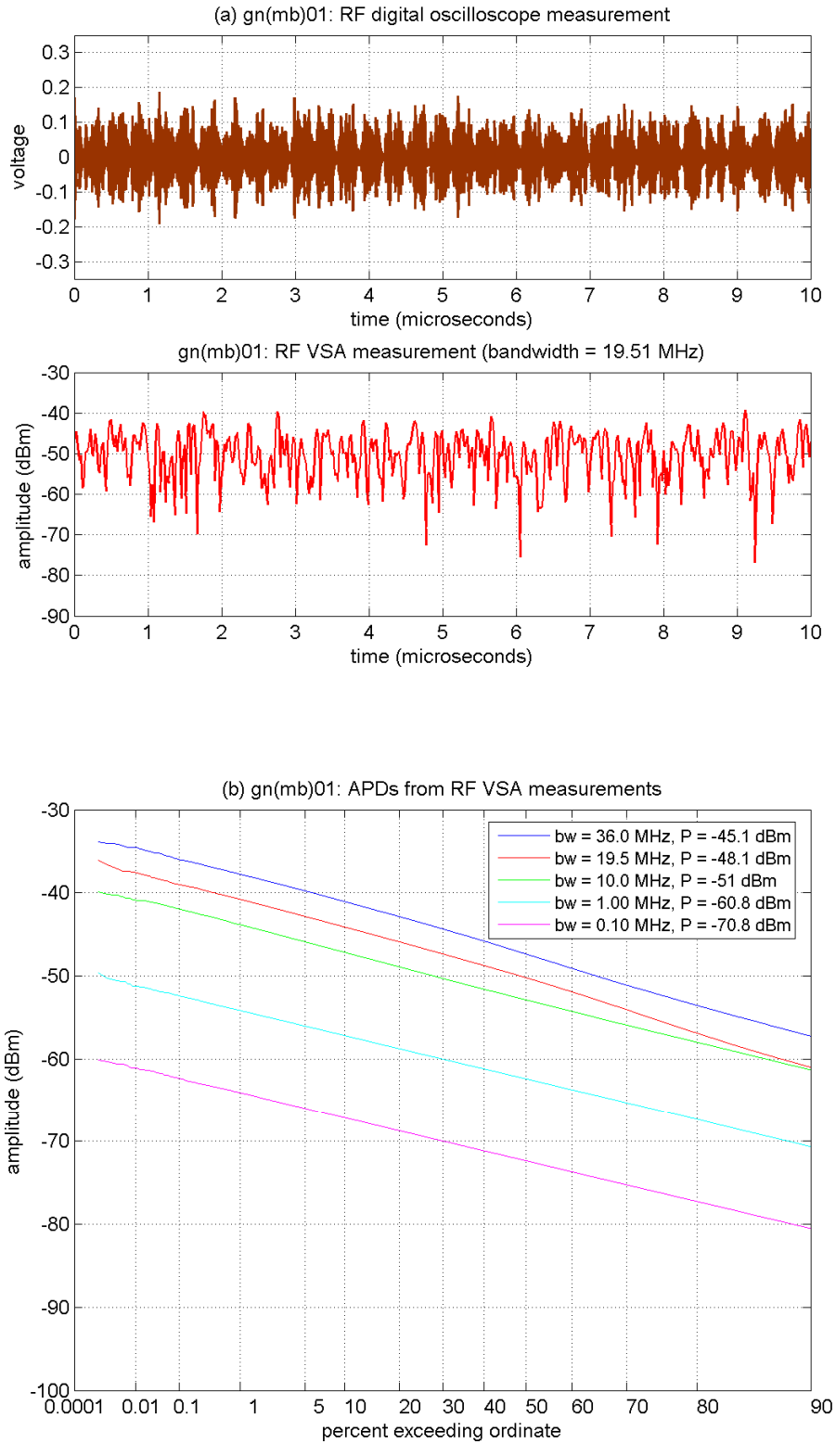

Figure D-37. RF measurements of GN(MB)-01 ($b = 1$, $d = 1$).

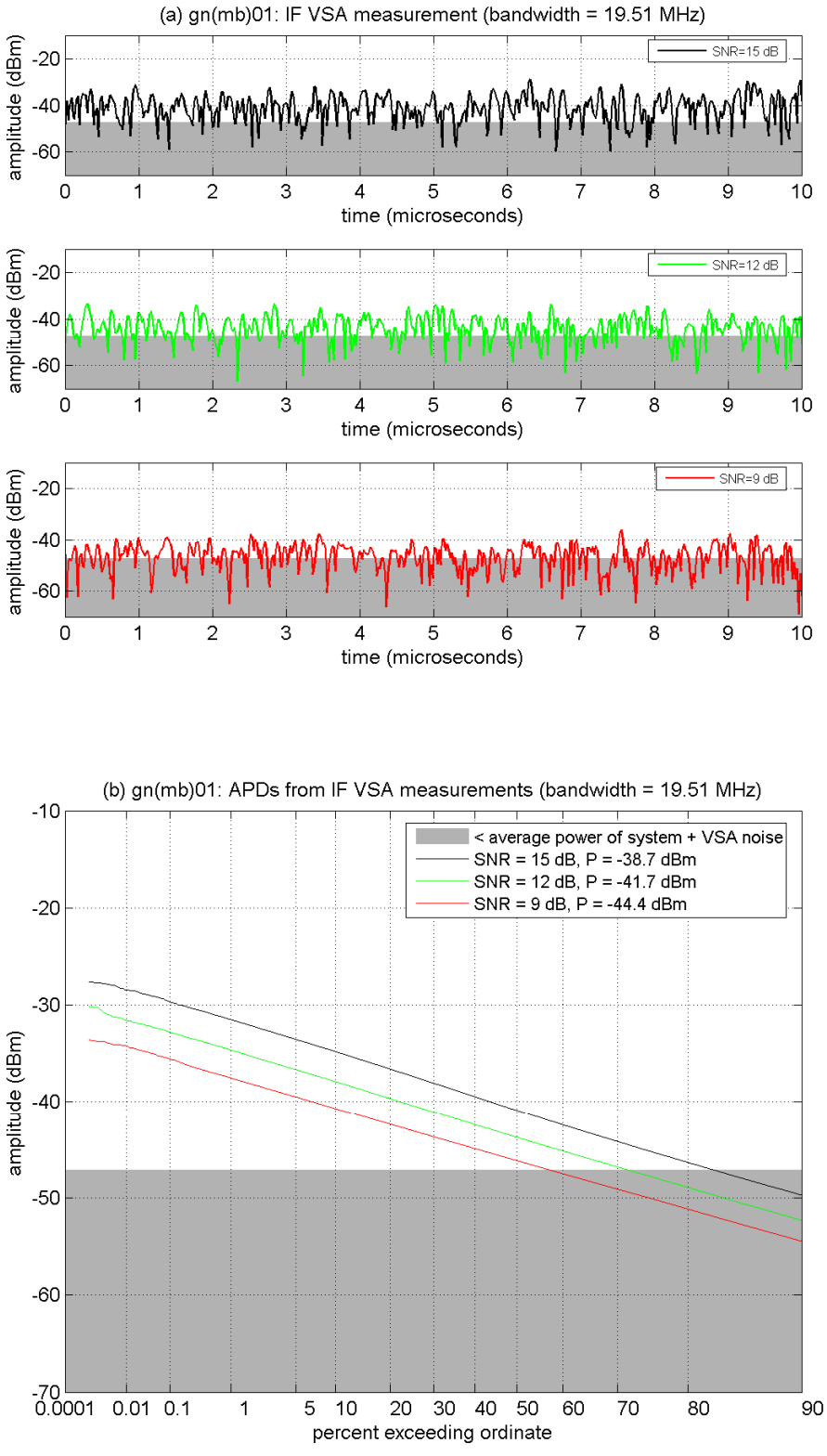

Figure D-38. IF measurements of GN(MB)-01 at INR_{TOV}.

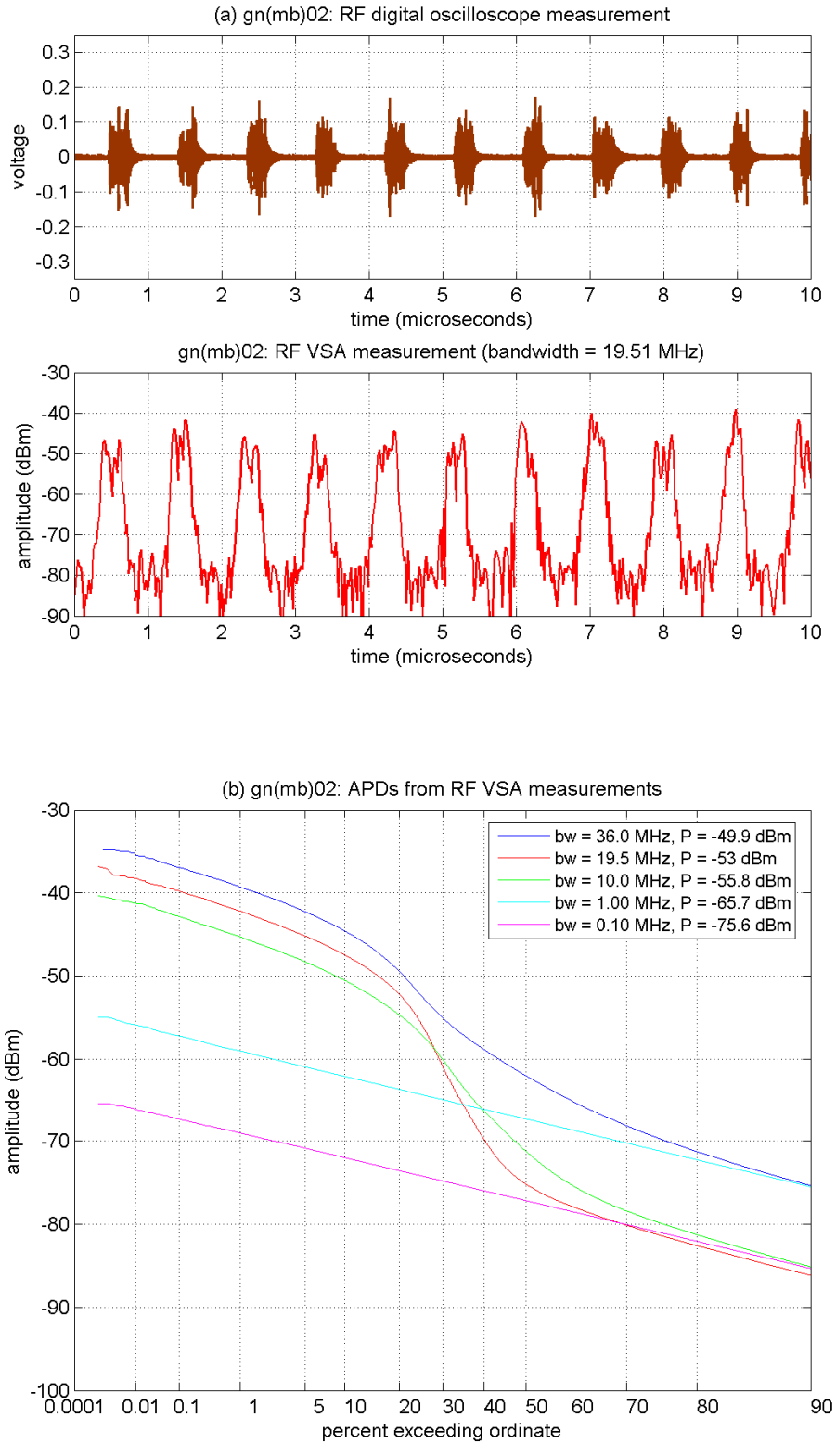

Figure D-39. RF measurements of GN(MB)-02 ($b = 3$, $d = 1$).

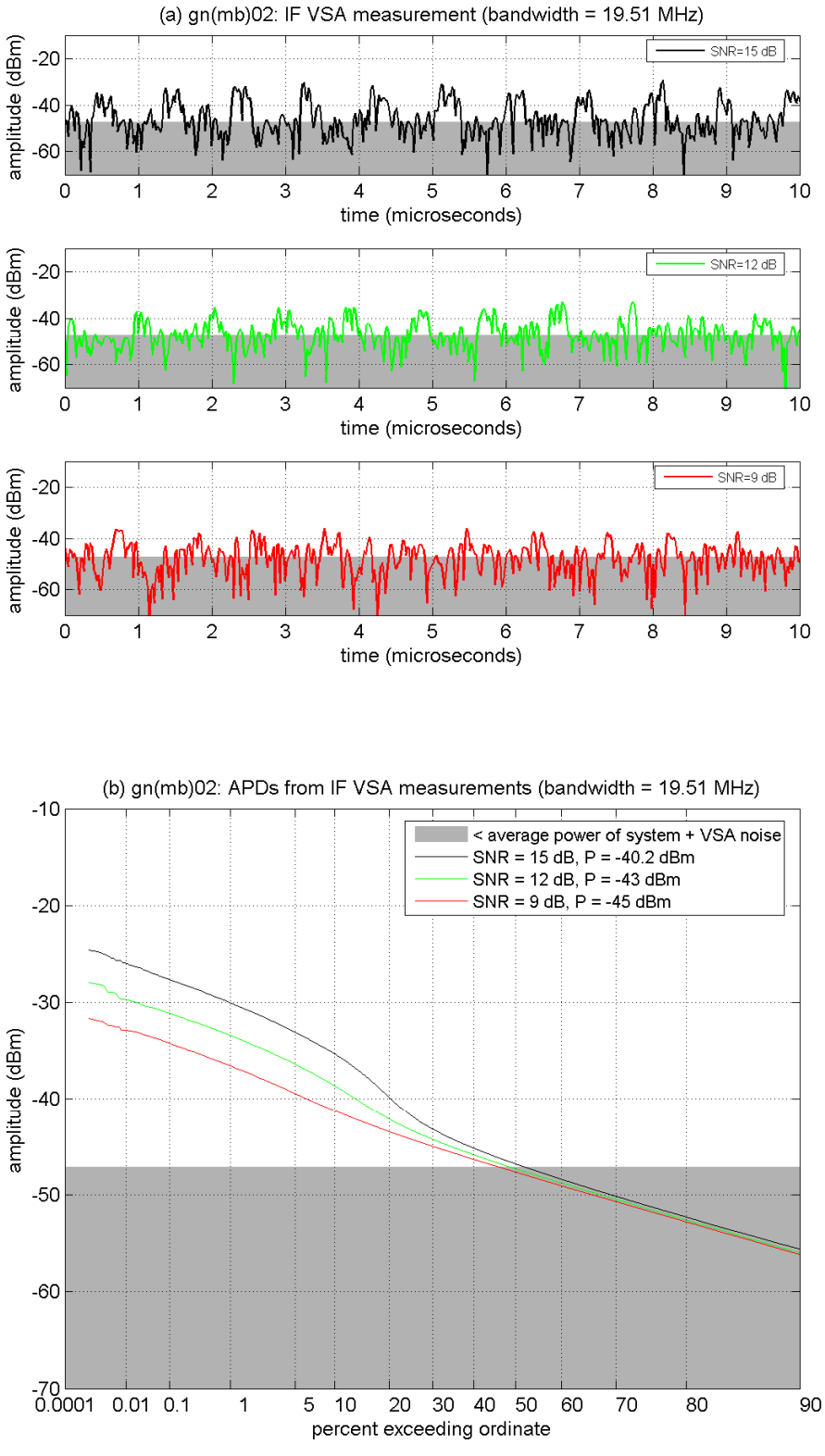

Figure D-40. IF measurements of GN(MB)-02 at INR_{TOV}.

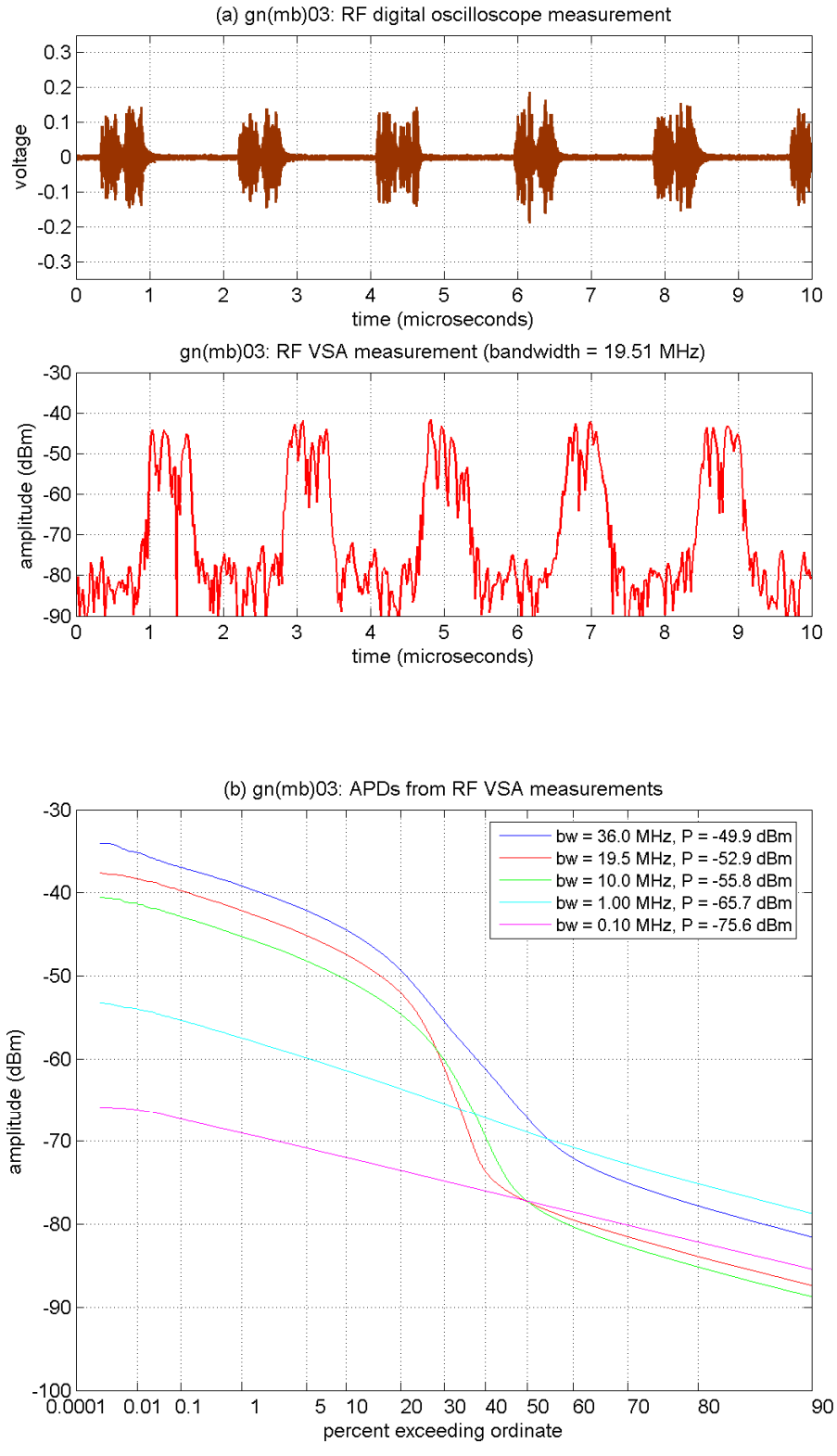

Figure D-41. RF measurements of GN(MB)-03 ($b = 3$, $d = 2$).

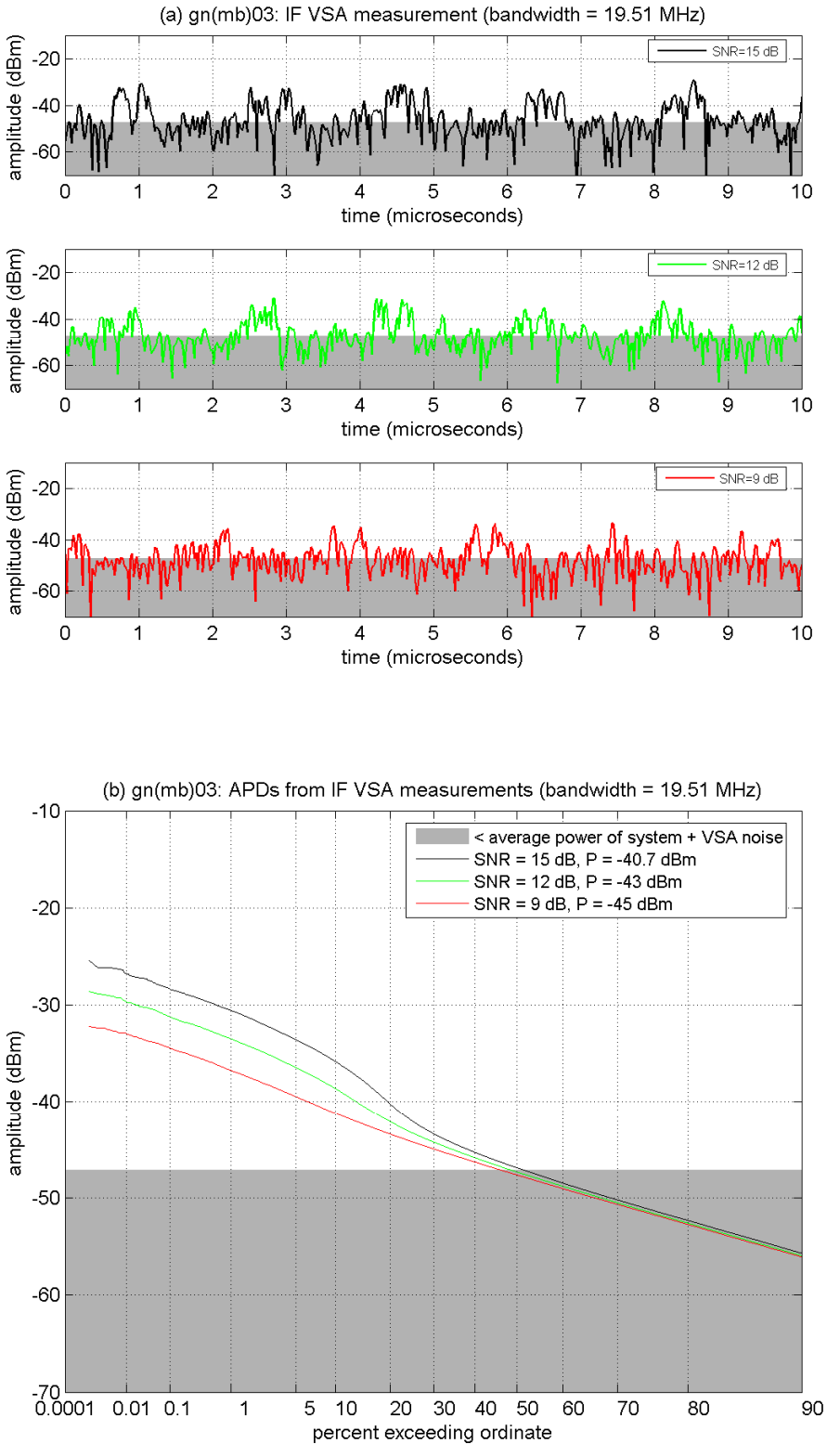

Figure D-42. IF measurements of GN(MB)-03 at INR_{TOV}.

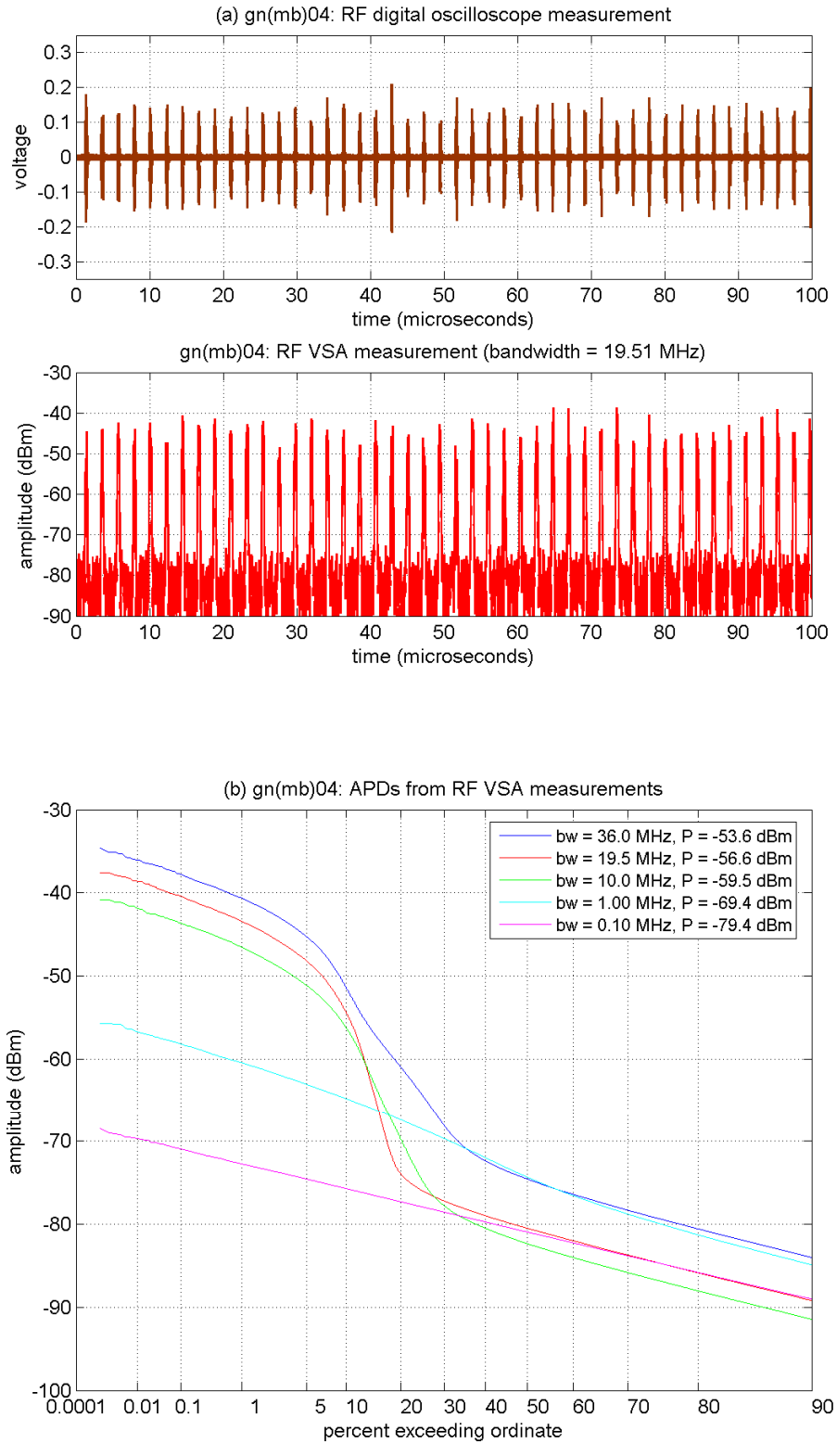

Figure D-43. RF measurements of GN(MB)-04 ($b = 7$, $d = 1$).

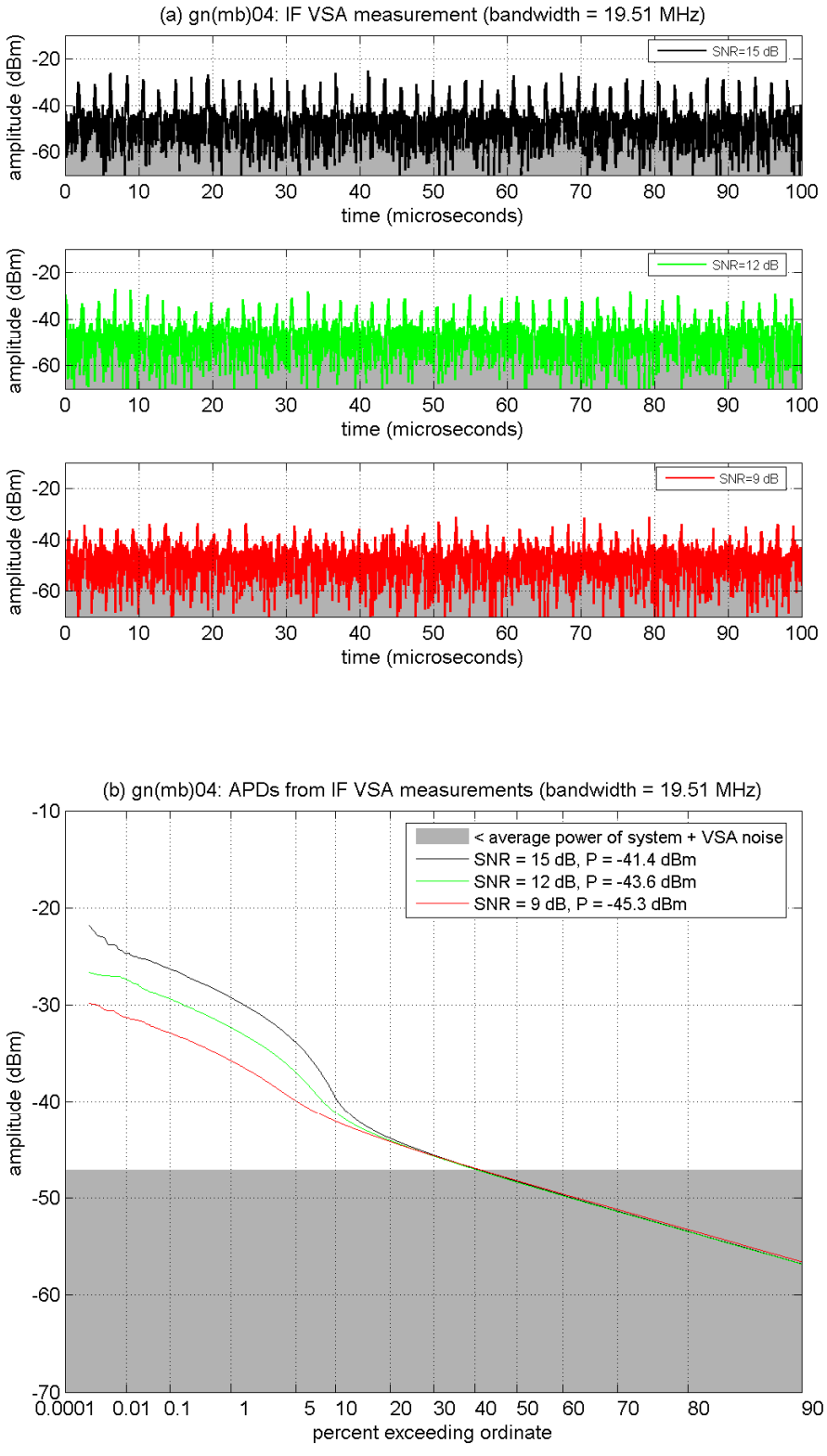

Figure D-44. IF measurements of GN(MB)-04 at INR_{TOV}.

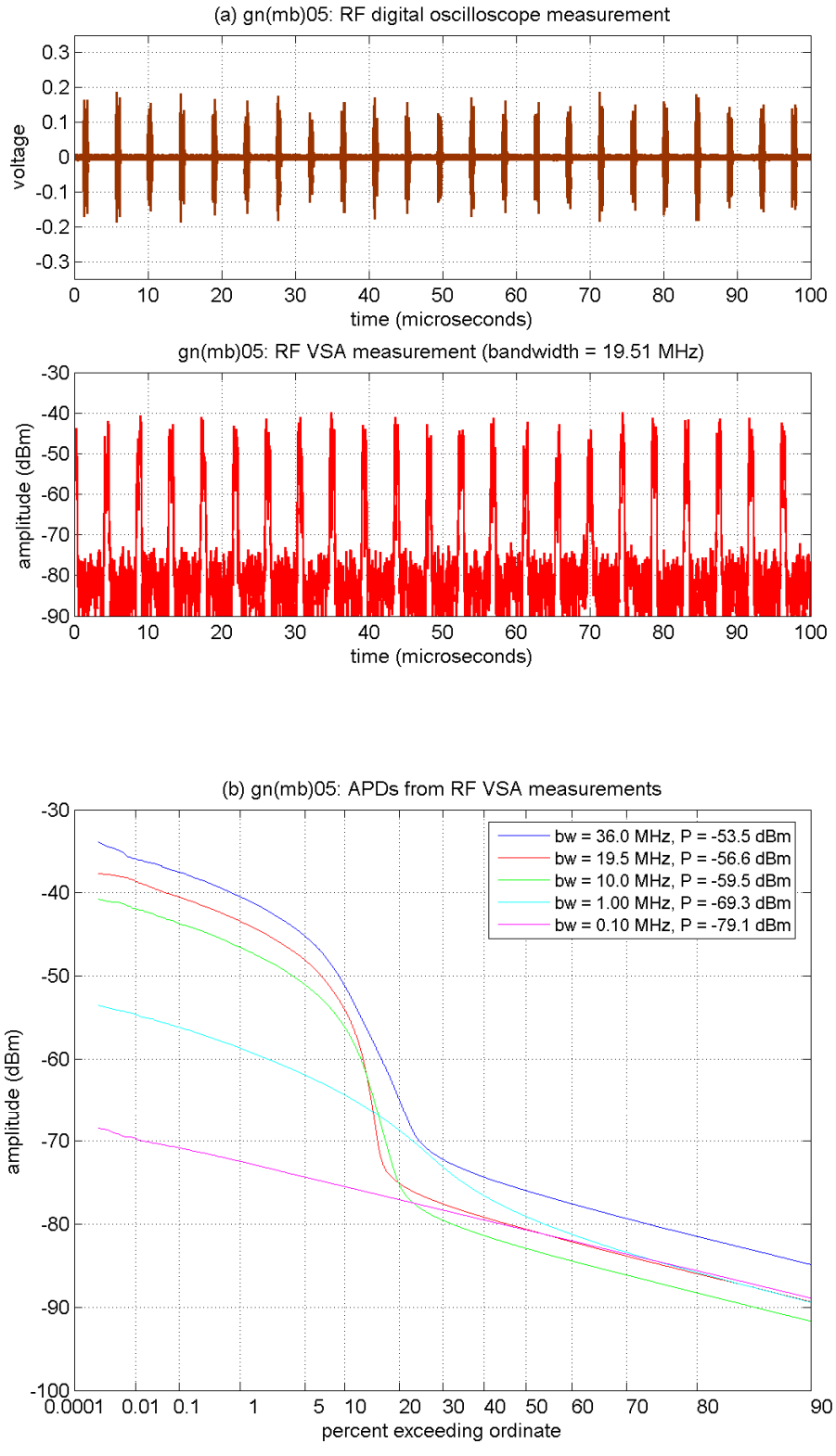

Figure D-45. RF measurements of GN(MB)-05 ($b = 7$, $d = 2$).

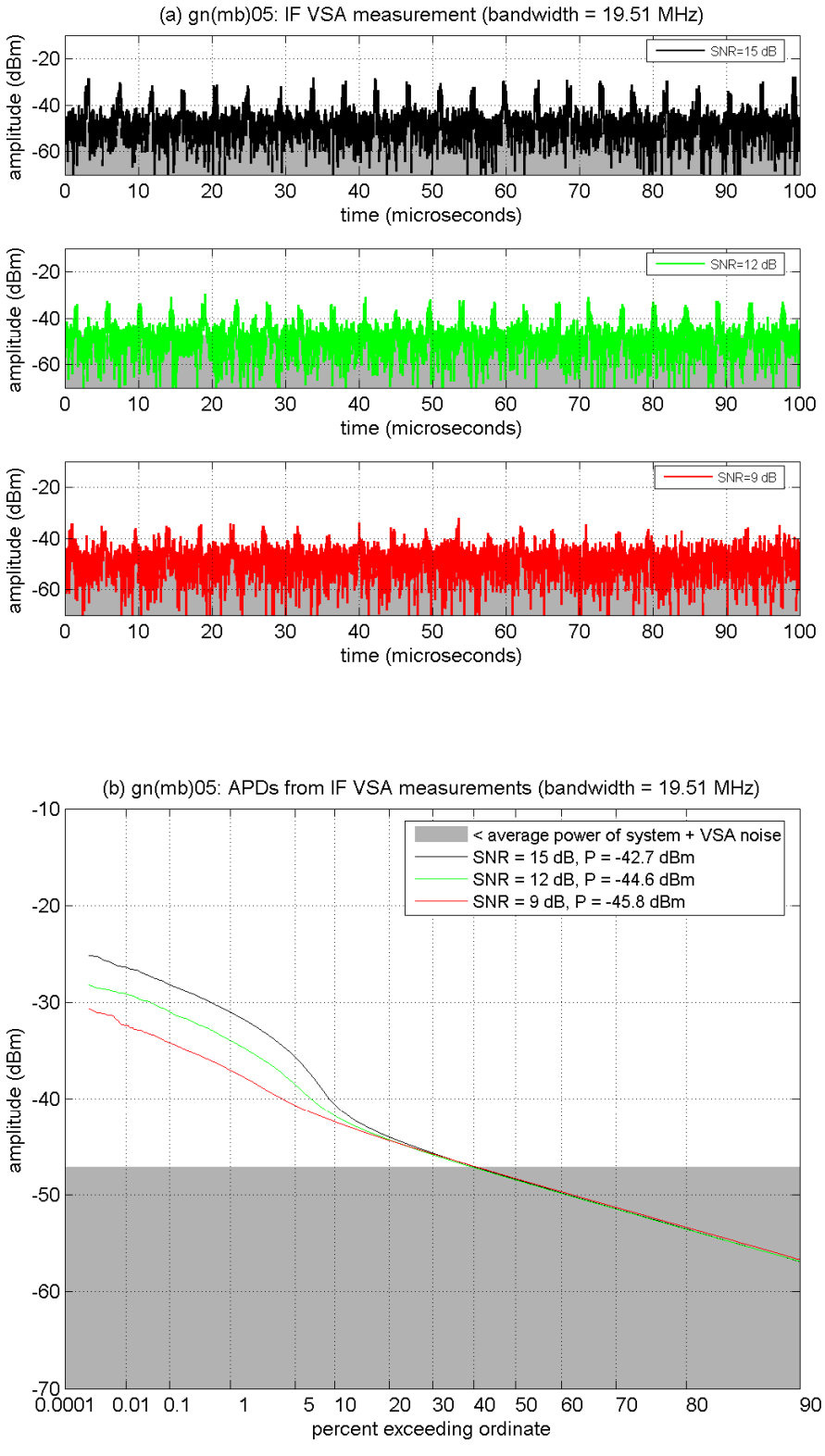

Figure D-46. IF measurements of GN(MB)-05 at INR_{TOV}.

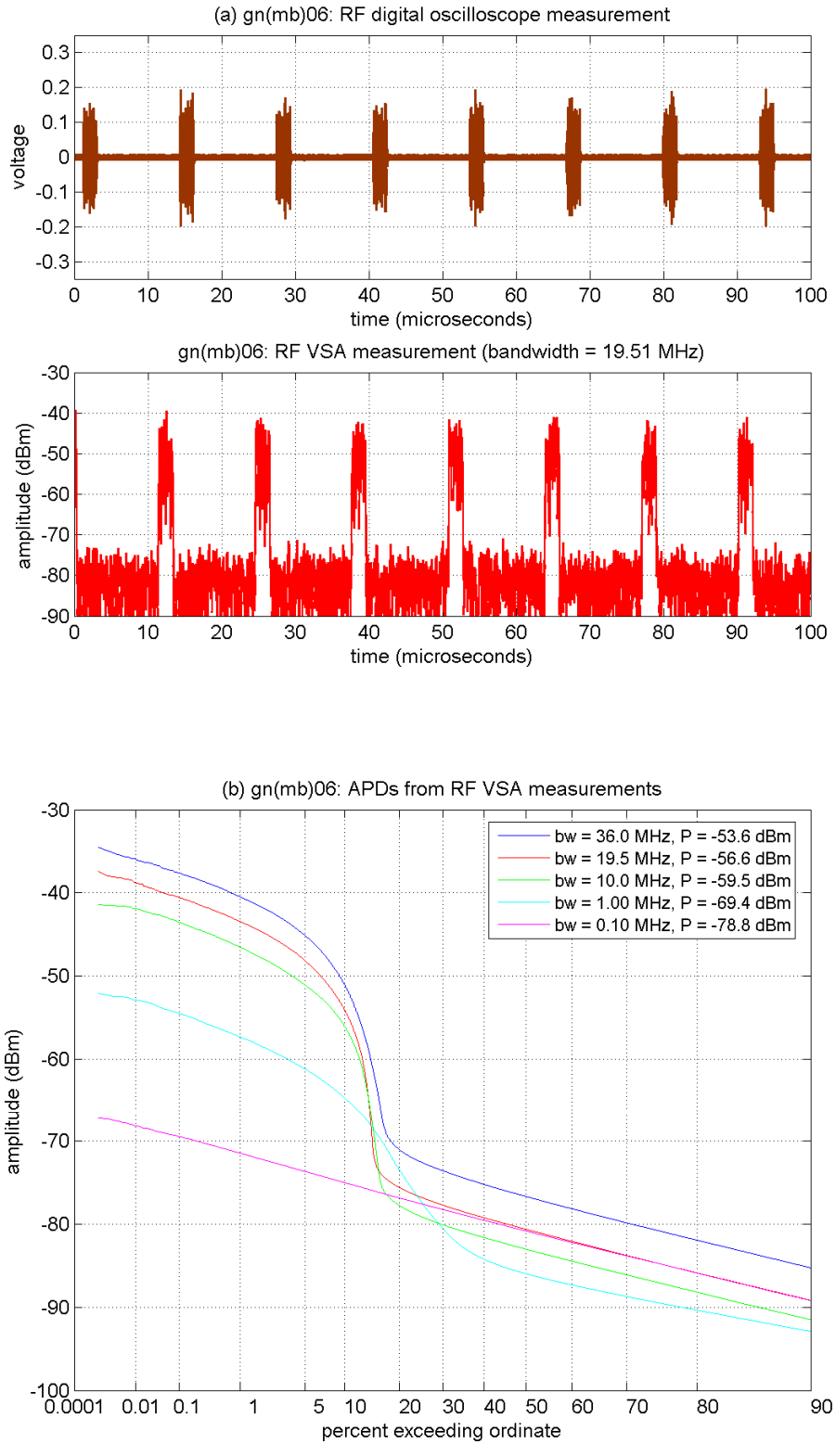

Figure D-47. RF measurements of GN(MB)-06 ($b = 7$, $d = 6$).

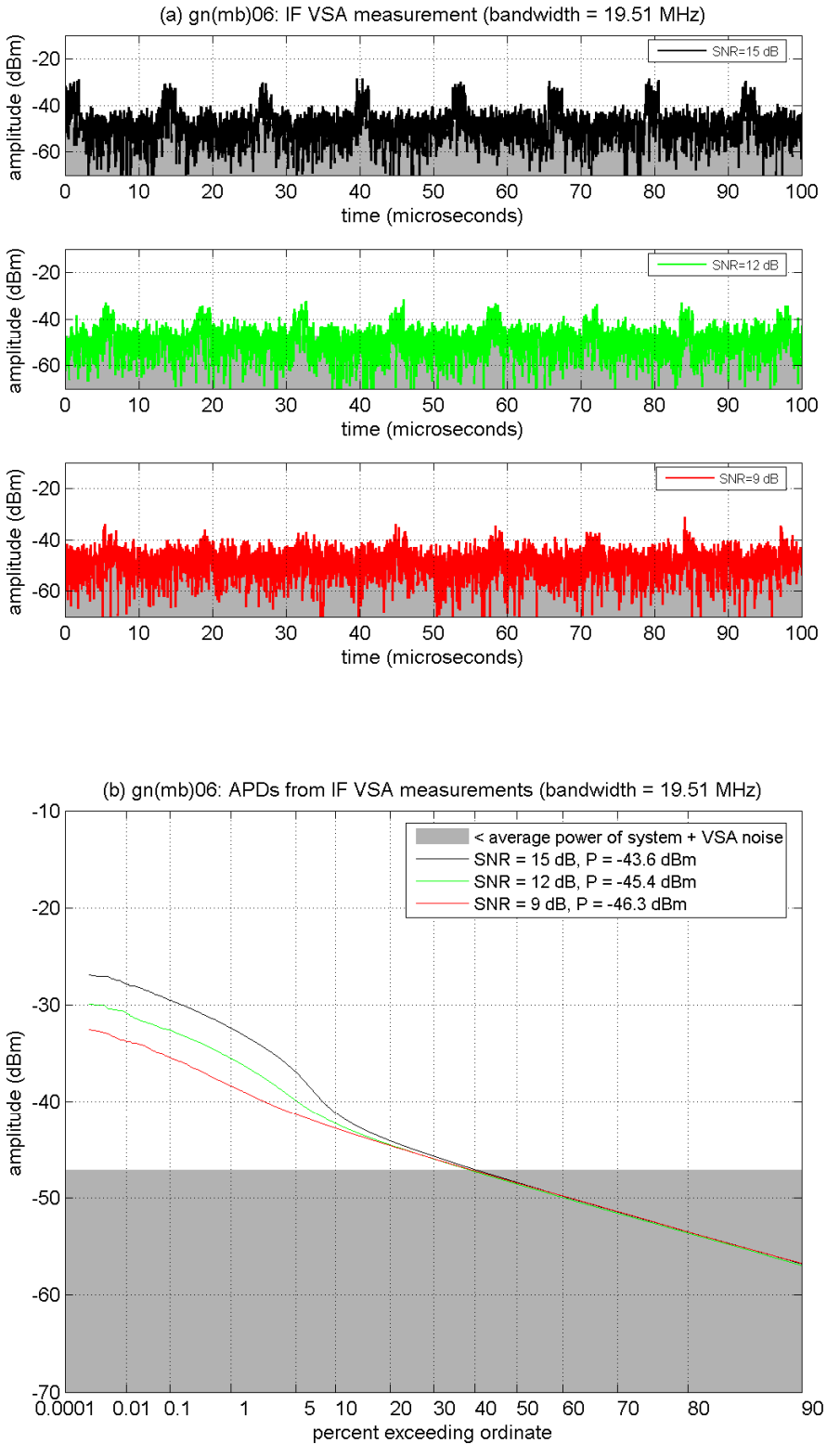

Figure D-48. IF measurements of GN(MB)-06 at INR_{TOV}.

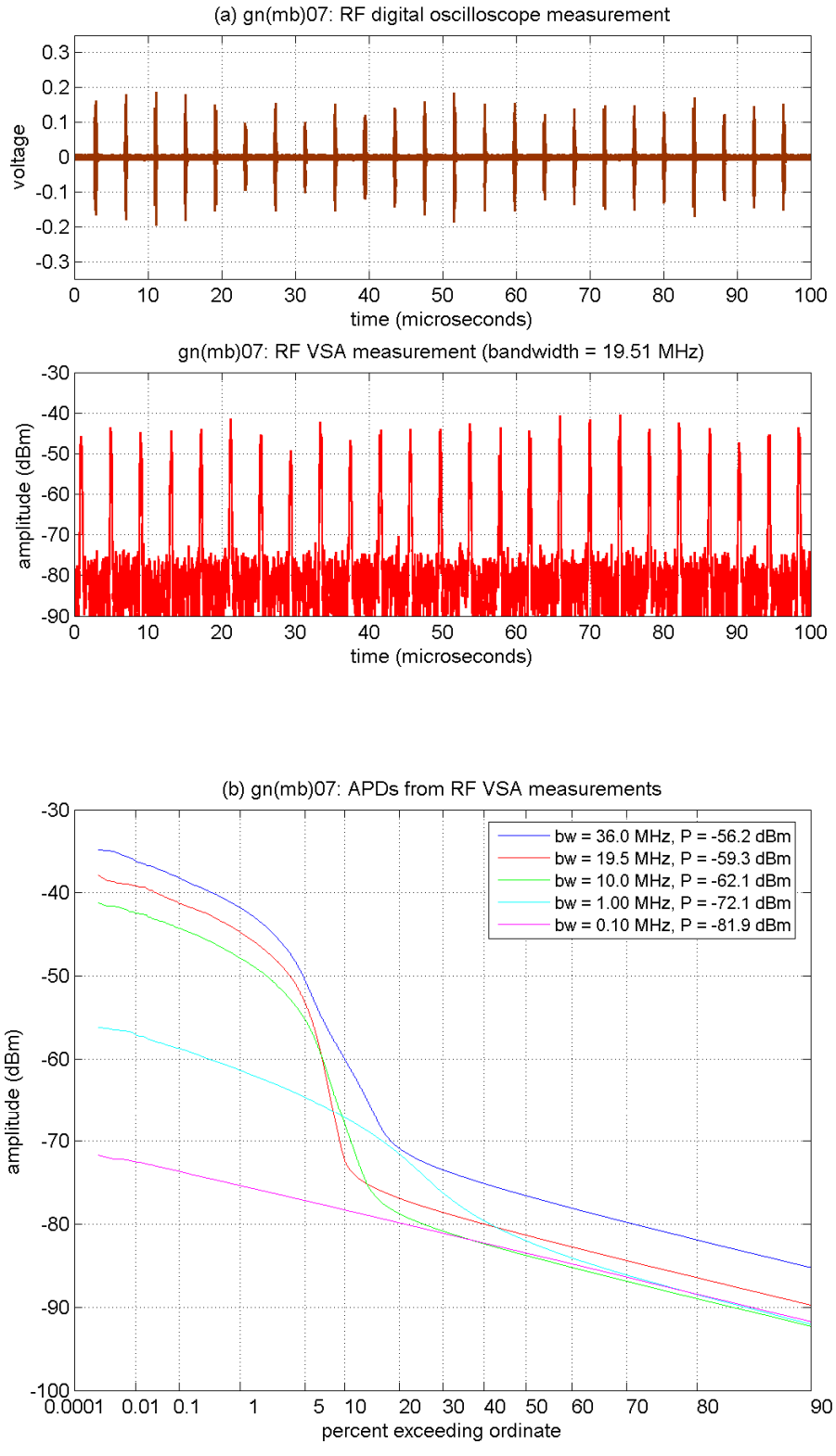

Figure D-49. RF measurements of GN(MB)-07 ($b = 13$, $d = 1$).

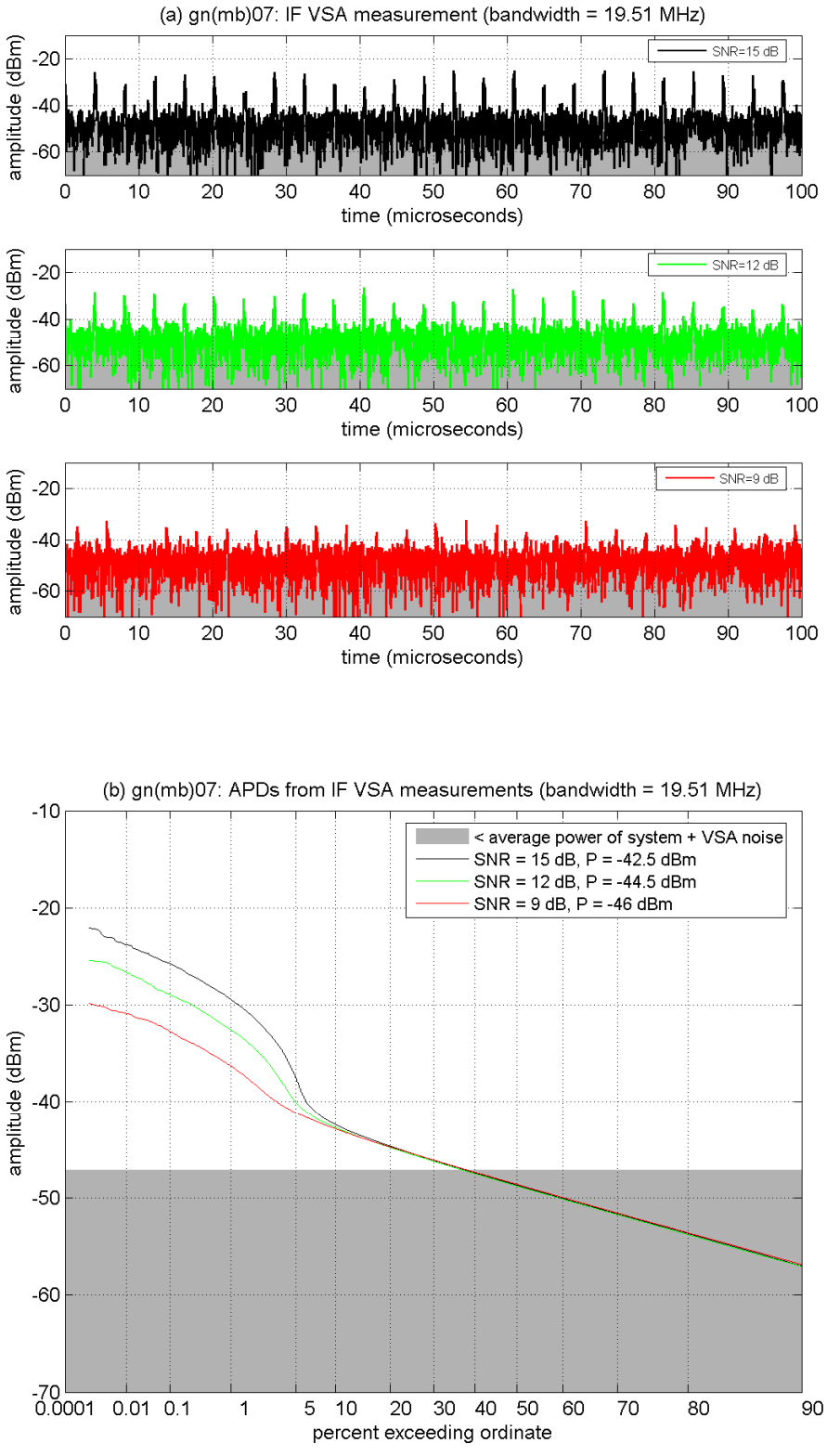

Figure D-50. IF measurements of GN(MB)-07 at INR_{TOV}.

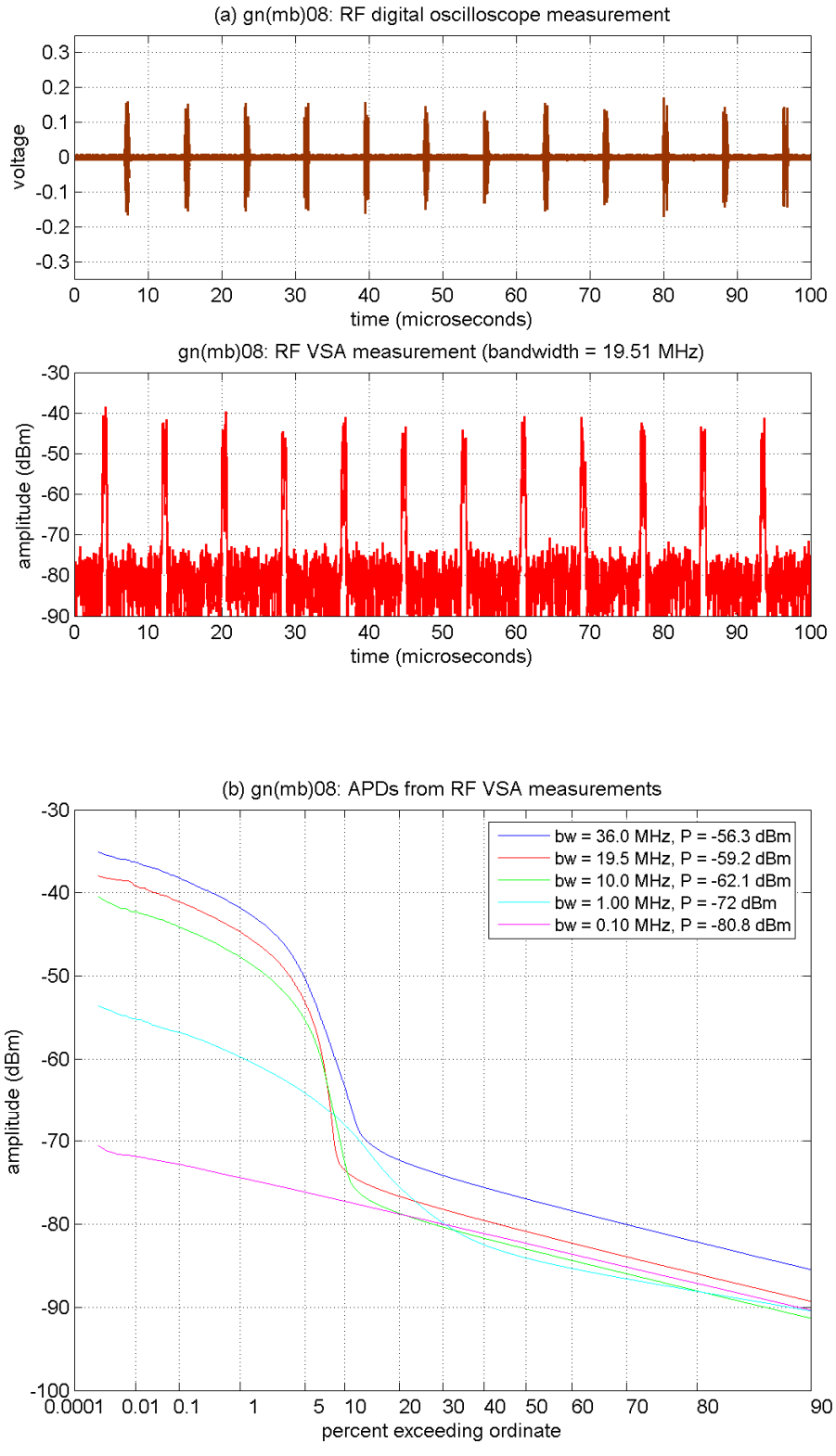

Figure D-51. RF measurements of GN(MB)-08 ($b = 13$, $d = 2$).

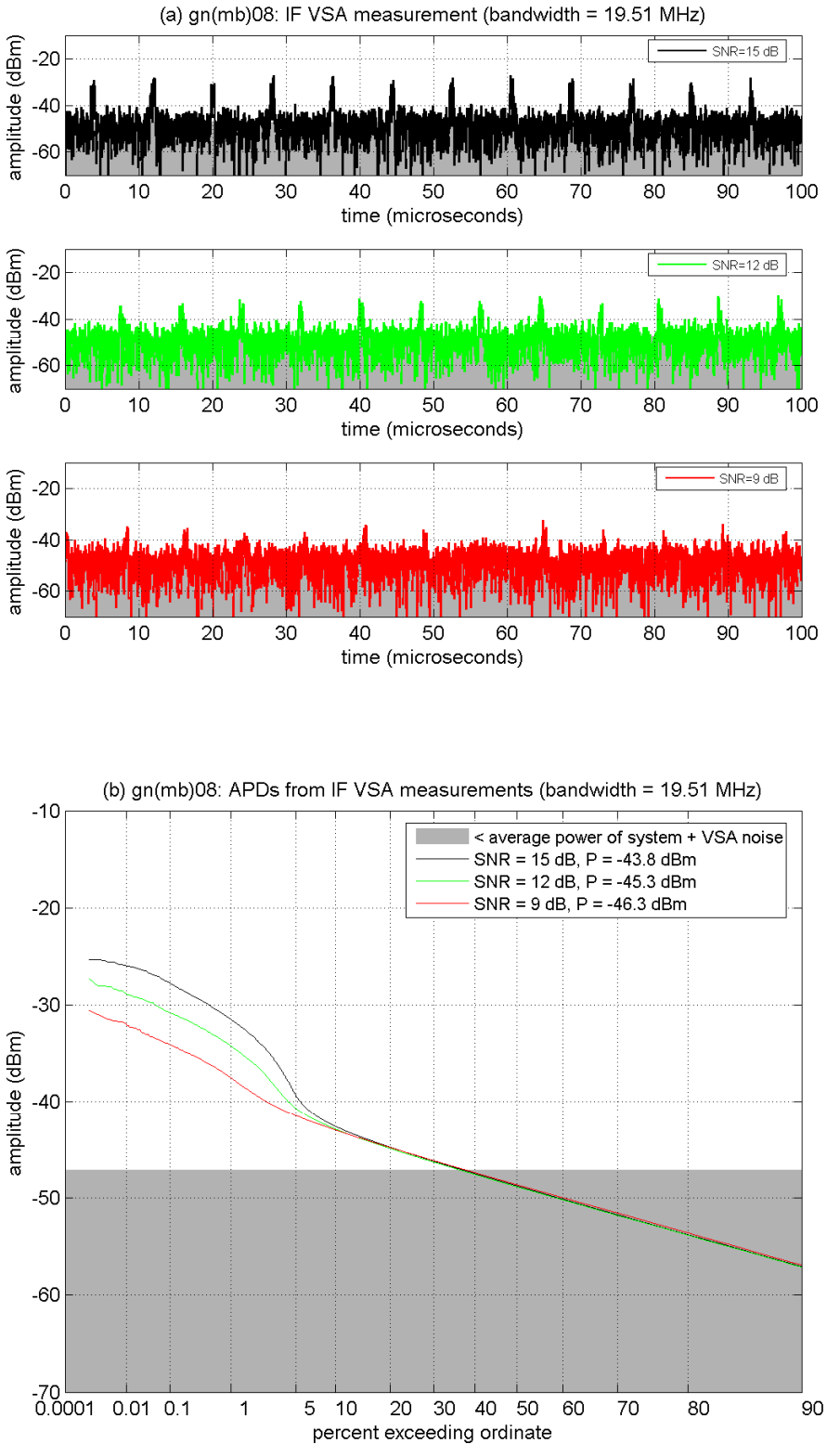

Figure D-52. IF measurements of GN(MB)-08 at INR_{TOV}.

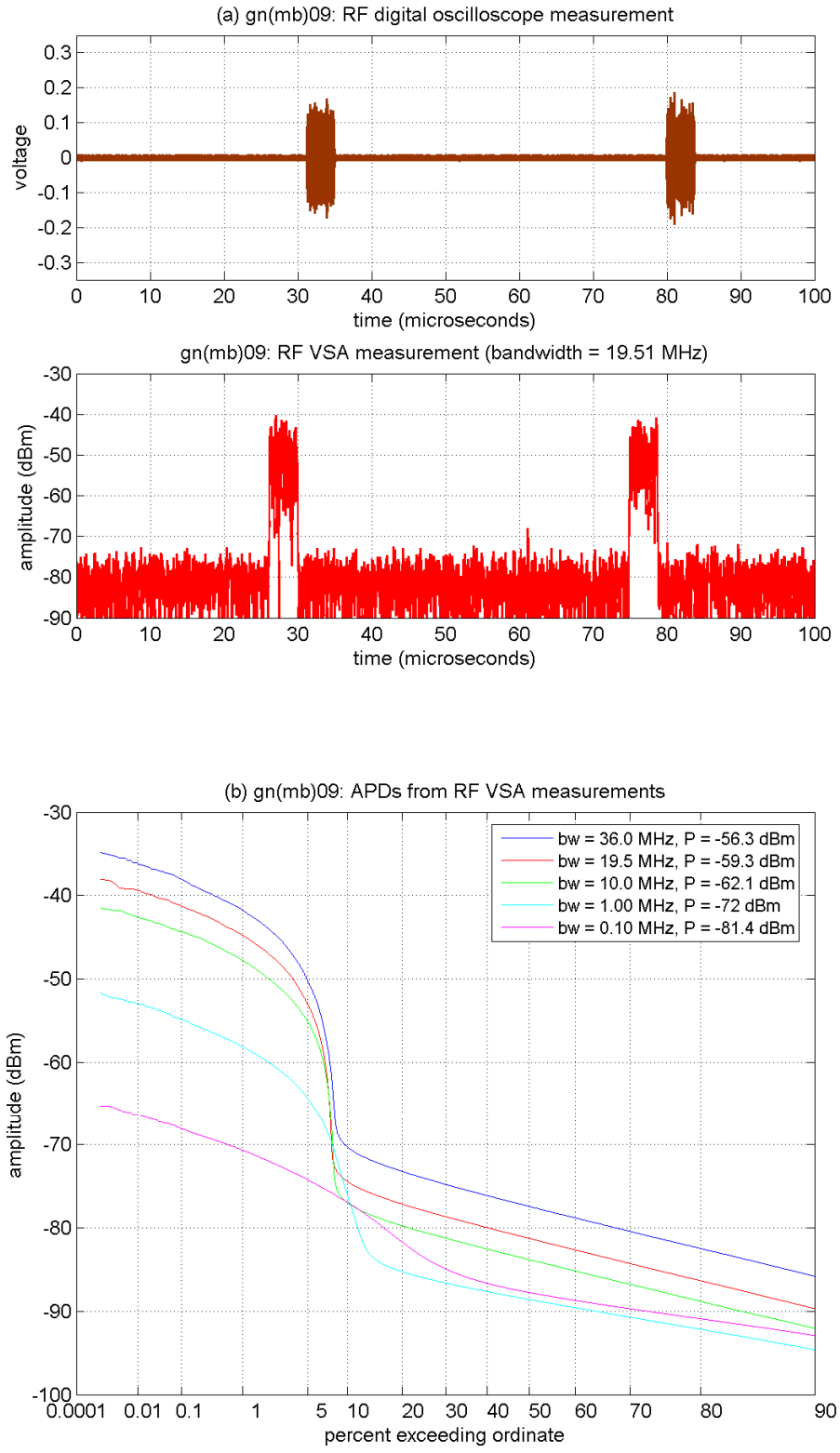

Figure D-53. RF measurements of GN(MB)-09 ($b = 13$, $d = 12$).

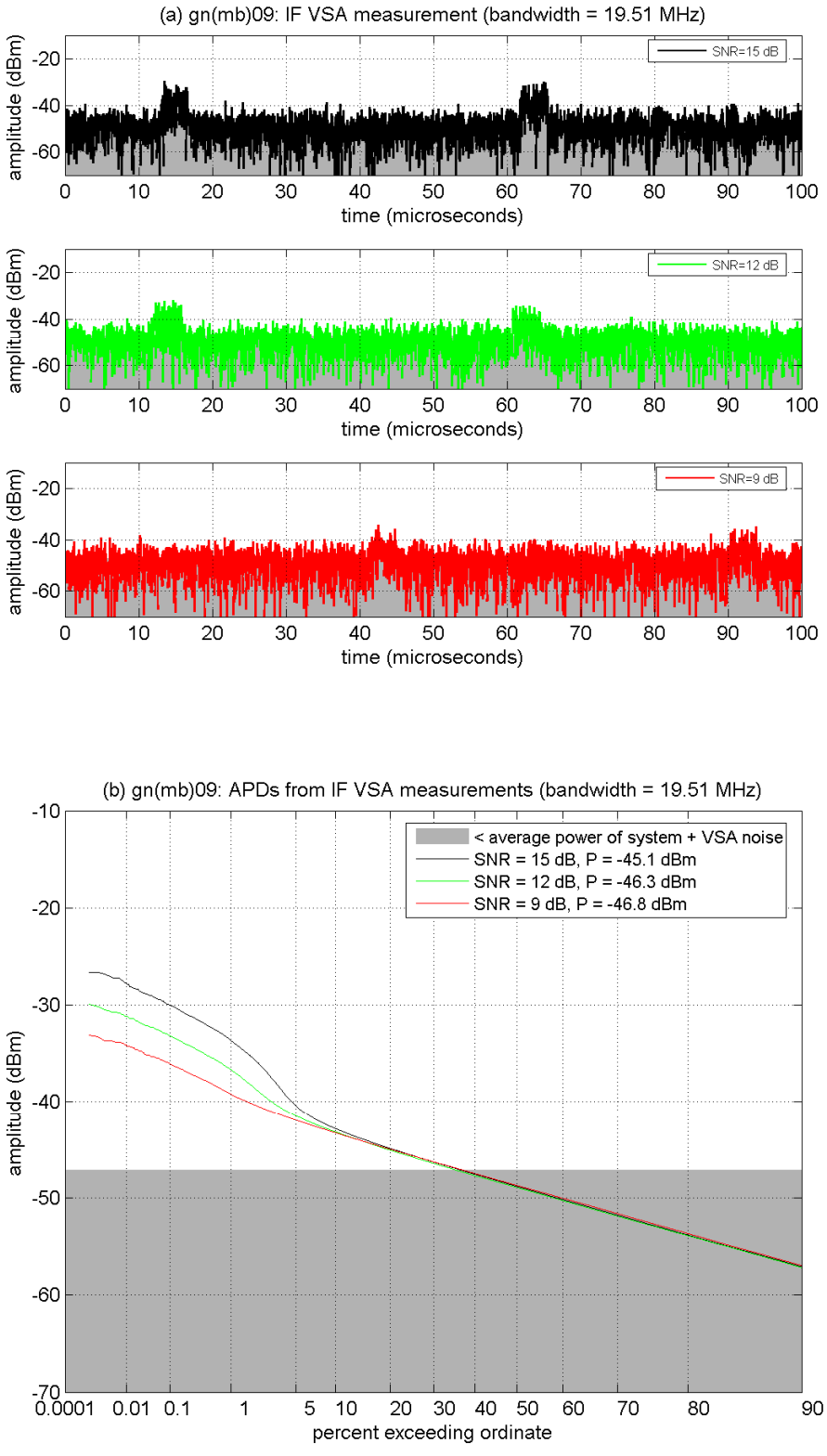

Figure D-54. IF measurements of GN(MB)-09 at INR_{TOV}.